UNIVERSITÀ
DEGLI STUDI
DI PADOVA

Head Office: Università degli Studi di Padova

Department
Physics and Astronomy 'G. Galilei'

Ph.D. COURSE IN: PHYSICS
SERIES XXX

THESIS TITLE:

ENTROPY PRODUCTION IN NON-EQUILIBRIUM SYSTEMS

Supervisor: Prof. Amos Maritan
Co-Supervisor: Dr. Jorge Hidalgo

Ph.D. student : Daniel M. Busiello

Entropy Production in Non-equilibrium Systems

Contents

1 Introduction

"What is the topic of your research?" - this is, probably, the first question a physicist suffers when saying that he's doing a doctorate. Well, maybe after the most floored question: "what do you do in a doctorate?". Skipping the latter is always a hard task, but, at least in this case, let us do this. Unfortunately my answer to the first question is: "stochastic thermodynamics" and an open mouthed reaction is undeniable. So I start again from "how do you know about entropy?", "and thermodynamics?", and so on until I find a positive answer.

Actually, stochastic thermodynamics is more actual and close to reality than expected, as it aims at describing how real biological systems interact and behave, but its fascination comes at the price of an illusory obscurity.

I have experienced this charm by myself at the beginning of my Ph.D., when we decided to focus our attention to the study of non-equilibrium systems, starting with the analysis of one of their characterizing features, the entropy production. If initially the interest was on studying the existence of an extremum principle for systems that operates out of equilibrium, then the entropy production turned out to be an intriguing quantity by itself and also not yet completely understood.

Different frameworks have been used in literature and we aim at analyzing the entropy production, i.e. the fingerprint of non-equilibrium, in some of these, trying to understand differences and analogies between them.

Maybe this thesis will not help me in answering any inexperienced question, since I cannot start from scratch, but I hope it will be of help in spreading the importance of the problems in which we made just a few small steps, that can become giant leaps with the results of future researches.

1.1 Toward the stochastic thermodynamics

Classical thermodynamics studies the transformations of a system from an initial equilibrium state to a final equilibrium one, from a macroscopic perspective [1]. Here we summarize in a nutshell the central results of this field.

It is a matter of fact that an isolated macroscopic system relaxes into a state of thermodynamic equilibrium, characterized by a set of macroscopic state variables, for example the total energy E, the volume V and the number of particles N. Such a system can interact with its surroundings in reaching its final state, leading to a change in the energy E due to macroscopic

controllable forces (accounted in the definition of work) and to microscopic processes (heat Q). To better understand the physical nature of the mechanisms under consideration, we introduce another state variable called entropy and denoted by S. A macroscopic system is thermodynamically characterized by the way the entropy depends on its state, $S = S(E, V, N, ...)$ [2].

First introduced by Clausius as a measure of the energy exchanged with the medium in the form of heat [3], then Boltzmann gave a definition of this quantity as a measure of the disorder of a system in terms of the number of accessible microstates which correspond to the same macrostate [4].

This macroscopic description has its microscopic counterpart in the equilibrium statistical mechanics. In this context arises the description in terms of ensembles, being the latter the collection of all the possible microstates in which the system can be found. All the thermodynamics properties can be recovered and the entropy S gets a statistical interpretation:

$$S = -\sum_i p_i \log(p_i) \tag{1}$$

where p_i is the probability of finding the system in the specific microstate i. This expression, known as Gibbs entropy, is intimately related to the definition given by Boltzmann and these two are equal at equilibrium in all the known ensembles [2, 5, 6]. Moreover it has been found to be a quantification of the uncertainty of a randomly generated message, providing the starting point for the development of the information theory [7, 8].

The celebrated maximum entropy principle evidences the leading role of the entropy in thermodynamics, representing a link between equilibrium statistical mechanics and information theory. This principle states that, given a set of conserved quantities, the most probable macroscopic state is determined by the maximization of the expression in Eq. (1) [5, 6].

So far we have summarized all the results concerning systems at thermodynamic equilibrium. However, many of the interesting non-biological and biological systems are constantly maintained away from equilibrium. Just to cite as examples, a colloidal particle driven by external fields [9, 10, 11] as well as actively moving micro-swimmers [12, 13, 14] or molecular machines [15, 16].

Although the mechanisms to keep a system out of equilibrium are very different [17, 18], e.g. electrical fields for colloids, ATP for molecular motors and pressure gradients in rheological experiments, the stochastic thermodynamics provide a very successful framework to describe all these processes.

The name "stochastic" comes from the fact that, besides the macroscopic effect of a driving force, small (mesoscopic) systems are also subject to random fluctuations due to the coupling with the external environment. These kinds of erratic effect is negligible for macroscopic systems, being of the order of $k_B T$ in the energy scale. Indeed, the stochastic thermodynamics describes systems at a mesoscopic level, considering thermodynamic quantities also for a single stochastic trajectory, instead as only macroscopic observables [19, 20, 21, 22, 23].

The mathematical background of this theory is represented by stochastic processes, which provide a modelization of a physical system in terms of random variables and probabilities. Until now we have used the word "mesoscopic" without questioning the meaning of this definition. In what follows we are going to talk about "macroscopic" dynamics as the one governed by deterministic and (in general) irreversible evolution, whereas we will name "mesoscopic" a dynamics based on stochastic models. The latter provides a less coarse-grained level of description respect to the macroscopic one, even if not yet microscopic, i.e. reversible in time.

The degree of resolution in space is of fundamental importance, but also the timescales involved need a brief discussion. The Markovian postulate represents an important connection between statistical mechanics and stochastic thermodynamics [24]. This can be considered as a consequence of the local equilibrium assumption [25]. It states that, on the mesoscopic timescale, the unobserved degrees of freedom follow an equilibrium distribution, which act as a long-time limit attractor of a non-driven dynamics. As a consequence, the random forces have to be sampled from an equilibrium distribution, being thus uncorrelated with the history of the system.

We have seen so far the main theoretical reasons which reveal the need of the introduction of the stochastic thermodynamics, evidencing the differences between a classical, statistical and stochastic description of a system. In the next section we will briefly expose some of the main results in this field of interest, just to have an idea of the area in which we are going to move.

1.2 The frameworks of non-equilibrium

Differently from the classical thermodynamics, a unified set of laws describing all non-equilibrium phenomena is still lacking. However, in recent years, several different approaches have been used in order to characterize systems that operate out of equilibrium.

One of the main lines of research concerns the investigation of systems experiencing small deviations from the equilibrium condition. In this context, the so-called linear response theory allows to express the desired quantities in terms of equilibrium correlation function [26, 27]. This paradigm lies on the hypothesis that the macroscopic relaxation of a system back to its equilibrium state is governed by the same physics as the spontaneous relaxation of fluctuations around equilibrium. Fluctuation-dissipation relations at and out of equilibrium, the Johnson-Nyquist formula for electronic white noise [28, 29] and the Onsager reciprocity for linear response coefficients [30] are some of the results along this way of thinking.

Another important approach consists in studying the dynamical properties of non-equilibrium systems at the level of a single stochastic trajectory. This led to the celebrated fluctuation theorems, which express universal properties of the probability distribution of thermodynamic functionals such as heat, work or entropy change. Although each theorem has been derived case by case, a unified theory has been recently proposed [31, 32, 18].

Besides these two frameworks, a lot of important results have been found aiming at "scaling down" to the mesoscopic level the framework of the macroscopic thermodynamics. Non-equilibrium steady states, the effects of a time-dependent driving and systems strongly coupled to the environment are just few examples over the myriad of paradigms studied and, nowadays, still under investigation [33].

A slightly different but, nevertheless, interesting direction of research, proposed by Jaynes, is based on the interpretation of the statistical physics as a theory of statistical inference [5, 6]. This idea lies on the deduction that Eq. (1) represents the entropy from the point of view of statistical mechanics and information theory as well, as stated above. The maximum entropy principle takes place in this more general context as a paradigmatic fundamental law to derive and interpret the thermodynamic properties of a system. Although this approach has been developed by Landauer and Bennett to find a quantification of the information loss [34, 35, 36] and a physical explanation of the Maxwell's demon [37], it appears to be quite far from being applicable to the area of non-equilibrium systems.

In what follows we will consider the entropy production in some of these lines of research, evidencing its leading role and its importance in the whole panorama of the stochastic thermodynamics.

1.3 Entropy production in stochastic thermodynamics

System out of equilibrium are characterized by a continuous exchange of energy and matter with the environment via different mechanisms, thus producing entropy at the macroscopic level [38]. We have already introduced the concept of entropy, S, as a state variable. If the state of a system changes during its own evolution, the entropy will change and its variation dS accounts for all the irreversible phenomena involved. Naively speaking, the entropy production, here defined as the variation of entropy for unit time dS/dt, is a specific feature of systems out of equilibrium, which evolve toward a stationary (equilibrium) state. In this sense the entropy production can be considered as a fingerprint of a genuine non-equilibrium condition and then it will be very interesting to analyze the properties of this quantity in all the different frameworks of the stochastic thermodynamics.

An integral fluctuation theorem and the Hatano-Sasa relation put in evidence some of the statistical features of the entropy production at the level of a single trajectory [23, 39, 40, 41]. Another fluctuation theorem can be derived for systems in a non-equilibrium steady state, a paradigm commonly used to describe biological molecular motors, which states that the probability to find a microscopic trajectory with a negative entropy production is exponentially decreasing as the time or the system size increases [42, 20, 21]. Moreover, several works have discovered and studied universal properties (infima and passage probabilities) and system-dependent characteristics (mean, variance, large deviation function), both at a mesoscopic and a macroscopic level of description [43, 44, 45, 46, 47].

Concerning the modelization of biological systems, systems with an external time-periodic driving has been studied to mimic the dynamics of artificial molecular motors. In this context the entropy production can always be interpreted as a "cost" of performing a given task [33, 48, 49]. Some of the points here arisen will be discussed extensively in the next chapters and will be subjects of investigation.

An important problem underlying to the plethora of different paradigms deals with the foundations of the stochastic thermodynamics and concerns the space and time resolution to describe the system of interest. Given a particular mesoscopic (stochastic) dynamics, we can ask ourselves how many microscopic details we are ignoring. Moreover, depending on the specific (mesoscopic) dynamics, it is possible to cast a different definition of the entropy production. The question that naturally arises is: how the entropy

production is related to the level of coarse-graining adopted in our description? In the literature it has been found that the coarse-graining procedure (both spatial and temporal) reduces the quantification of the entropy production, as less information about the system is accessible [50, 51, 52, 53]. Further details on this topic will be discussed later on in this thesis, but, for the moment, the message is that this problem is not completely solved, in particular when different dynamical description (related to a different level of coarse-graining) are compared.

Some others open problems about the entropy production come from the Jaynes approach to statistical physics. Several attempts have been made recently to develop an extremum principle for non-equilibrium systems, which could play a similar role as the maximum entropy principle for equilibrium ones. In 1947 Prigogine derived the so-called minimum entropy production principle, but its applications are narrow and it is believed not to be a general law [1]. On the other hand, both experimental observations and mathematical derivations (or justifications) have tried to propose a maximum entropy production principle as a general optimization approach for systems out of equilibrium [54, 55, 56, 57]. However, part of the scientific community is very skeptic about this approach and rose many counter examples [58]. In general, we would say that an exhaustive answer for an extremum principle in this context is far from being found and in this thesis we will try to address also this problem, even if not systematically, but only as a stimulus for future discussions.

1.4 Organization of the thesis

In this section the structure of this thesis is explained, trying to put in evidence the essential technical points, the main results and the take-home message of each single work here contained.

In Chapter 2 we will start with a particular stochastic model, the so-called Master Equation, aiming at describing discrete-state Markovian systems. After a brief review of the idea behind this modelization, we will derive the formula for the entropy production for this class of systems that is known from the seminal work of Schnakenberg. To do this we first will pass through some previous and well-known statements on entropy and entropy production in general, just to introduce a quantity that will be of fundamental relevance throughout this thesis. Moreover a small digression on networks will be presented, since discrete-state systems can be described as a network

of transitions, where each node represents a state and each link a transition rate between two different states. In this chapter we will try to understand how topological features of the underlying transition network influence the value of the entropy production. Interestingly, for systems driven out of equilibrium both by asymmetric transition rates and an external probability current, close to equilibrium, the stationary entropy production is composed by two contributions. The first one is related to the Joule's law for the heat dissipated by a classical electrical circuit properly introduced, whereas the second contribution has a Gaussian distribution with an extensive mean and a finite variance that does not depend on the microscopic details of the system.

This result is interesting by itself, finding a thermodynamic validation of the Schankenberg's formula by comparison with the well-known Joule's law and a universal distribution of the contribution that stems from the asymmetry of the transition rates. Another important consequence is that the entropy production depends just on two parameters, the first one accounting for the symmetric part of the transition rates and the second one related to the asymmetry. In other words the statistical properties of the entropy production of a system close to equilibrium can be inferred from its network of transitions between accessible states. Moreover, these results shed some light on the meaning of an extremum principle for systems out of equilibrium, since it becomes possible to compare real-world interaction topologies with the ones that maximize/minimize the entropy production to tackle this challenging problem from a novel perspective.

The Appendix A is dedicated on this side aspect. We used a realistic dynamical model to understand why the topologies of most of the interaction matrices of living systems exhibit the so-called property of sparsity (the percentage of active interactions scales inversely proportional to the system size). Although this section is manifestly different from the topic of the thesis, it can be somehow related to the general problem of understanding how a living system can adapt to cope to external changes.

In Chapter 3 we will introduce a different framework of stochastic processes: the Fokker-Planck equation, describing systems that continuously diffuse in a medium. We will point out why this new modelization can be seen as a coarse-grained version of the Master Equation and we will derive the formula of the entropy production for this particular case, as obtained by Seifert. After this technical part we will present in a nutshell a review of some interesting results in the literature on the effects of coarse-graining in

stochastic thermodynamics. The question we will try to answer in this chapter concerns how neglecting information in describing a system can influence the value of its entropy production. In this case we aim at comparing two different forms of the dynamics, lying at different level of coarse-graining: Fokker-Planck equation (FPE) and Master Equation (ME). We will find a new formula for the entropy production of a system governed by a FPE which, surprisingly enough, is not independent on the microscopic details (the ones that appear in the ME). This new expression can be reduced to the well-known Seifert's formula when we have no information about the ME description, but, in general, we will show that it is greater than the latter. A simple pedagogical example will be carried out to clearly explain and interpret the latter result as a consequence of the presence of extra contributions of microscopic currents that make inroads in the system, which are neglected during the coarse-graining procedure.

This work is very promising, since it is associated to some previous results of the same topic, also connecting two different dynamical models. This study provides a quite novel and simple interpretation of how the details we neglect can change an essential non-equilibrium quantity as the entropy production, at the same time undermining the basic notion of equilibrium at a mesoscopic level of description.

Chapter 4 is dedicated to the problem of comparing two different frameworks of the stochastic thermodynamics: non-equilibrium steady states and time-periodic driving. Such a comparison is stimulated by similar features that these two paradigms exhibit, e.g. a probability distribution that significantly deviates from equilibrium, a constant (time-averaged) flux and a non-vanishing entropy production in the environment. First we will recap a previous result: a time-periodic driving can always mimic a non-equilibrium steady states (NESS) and viceversa, in terms of probability distribution, flux and entropy production, for discrete-state systems. Here we will try to derive a similar mapping for diffusive systems described by a Fokker-Planck equation. The main results of this chapter is that both the probability distribution and the flux can be mimicked, but the entropy production follows an inequality stating that the time-dependent driving always produce more entropy than a NESS.

Reminding that these two frameworks are used to describe natural (NESS) and artificial (time-periodic driving) molecular machines, this result states that building a device to mimic a biological diffusive system is easier from an engeneering point of view but costs more than the original natural one in

terms of production of entropy in the surroundings.

Finally, in the last chapter we will contextualize all our results in the general field of stochastic thermodynamics, providing some ideas for future research on the role of the entropy production in non-equilibrium systems.

2 Entropy production in systems with random transition rates

In this chapter the entropy production of a system with a finite number of states connected by transition rates is studied. We will use tools from stochastic processes and network theory that will be briefly introduced in what follows.

2.1 Master Equation and discrete-state systems

Let us consider a system with a finite number of states, say N, such that the probability to be in the state i is p_i. Suppose now that such a system follows a continuous time Markov process via discrete jumps between states. Naively speaking this means that the system can continuously jump from one state to another with a certain probability per unit time. The Markov condition formally requires that the time ordered conditional probability depends just on the most recent event or, in other words, that each state at time t depends just on the state at time $t - dt$ [59, 60].

As outlined before, for a Markov process to be a reasonable model, the memory time has to be very small respect to the observation time. In general Markov processes can have a continuous or discontinuous sample path; in this context we will consider just the latter case, as we are dealing with systems that perform jumps between states in time. If all these basic assumptions are valid, we can write the dynamics of the system under investigation as the so-called Master Equation:

$$\partial_t p_i(t) = \sum_{j=1}^{N} \left(w_{ij} p_j(t) - w_{ji} p_i(t) \right) \tag{2}$$

where $w_{ij} > 0$ is the transition rate, i.e. the transition probability per unit time, to pass from the state j to the state i. In the simple setting we will consider in this section the transition rates does not depend on time. An intuitive interpretation of Eq. (2) can be provided by discretizing the time derivative:

$$p_i(t + dt) = p_i(t) + \sum_{j=1}^{N} \left(w_{ij} p_j(t) - w_{ji} p_i(t) \right) dt \tag{3}$$

Thus the probability to be in the state i at time $t + dt$ is equal to the probability to stay in the state i at time t, $p_i(t)$, plus the probability to be in the state $j = 1, ...N$ performing a jump (to the state i) between t and $t + dt$ with probability $w_{ij}dt$, minus the probability to be in the state i jumping away from this state in the time interval $[t, t + dt]$.

The justification of Eq. (2) here presented stems from intuitive argumentations, although a more formal derivation exists and it will be briefly presented in the next section.

In what follows, we will consider systems for which, if $w_{i\to j} \neq 0$ also $w_{j\to i} \neq 0$. We will justify this constraint when talking about entropy production.

A lot of systems in Nature are amenable to be modeled via a Master Equation. Some examples are the ATP hydrolysis, the kinetic proofreading, the model of ions permeating a membrane through a pore and, in general, most of the chemical and biochemical reactions [61].

Once we have defined the dynamics governing our discrete-state system, we recall some essential features of a Master Equation. It's worth noting that we are only interested in the physical region, i.e. where

$$0 \leq p_i \leq 1 \qquad \forall i = 1, ...N \qquad \sum_{i=1}^{N} p_i = 1 \tag{4}$$

since $(p_i)_{i=1,...N}$ is a set of probabilities.

We can rewrite Eq. (2) in a more compact form as:

$$\partial_t p_i(t) = \sum_j W_{ij} p_j(t) \tag{5}$$

where W_{ij} is the following $N \times N$ transition matrix:

$$W_{ij}(t) = w_{ij}(t) - \delta_{ij} \sum_{k=1}^{N} w_{ki}(t) \tag{6}$$

For the system to be ergodic, we need that if $W_{ij} \neq 0$, also $W_{ji} \neq 0$ and that all the N states of the system are dynamically accessible [33]. This ergodic requirement will be useful in what follows.

Given the Eq. (6), it is easy to see that $\det(W_{ij}) = 0$ such that at least one stationary solution exists in the physical region. Moreover, by making use of a stability theorem proposed by Schlogl [62], it is possible to demonstrate

that any solution that starts in the physical region will stay in the physical region and eventually will converge asymptotically to a stable steady state. As a by-product we get that the stationary solution is unique, since a solution cannot be asymptotically stable respect to two different states [61].

2.1.1 Derivation from the Chapman-Kolgomorov equation

This section enlighten a technical derivation of the Master Equation [60]. Let us start from the Chapman-Kolmogorov equation, that is nothing but a rearrangement of a probability axiom stated for Markov processes.

$$p(x_1t_1|x_3t_3) = \int\int dx_2dt_2 p(x_1t_1|x_2t_2)p(x_2t_2|x_3t_3) \tag{7}$$

where $t_1 > t_2 > t_3$ and $p(x_1t_1|x_3t_3)$ is the probability to be in state x_1 at time t_1 given that at time t_3 the system was in the state x_3. Eq. (7) is qualitatively equivalent of saying that summing over all mutually exclusive events of one kind in a joint probability will eliminate that variable, i.e.

$$\sum_B P\left(A \cap B \cap C \cap ...\right) = P\left(A \cap C \cap ...\right) \tag{8}$$

adopting the standard notation of probability theory.

For all $\epsilon > 0$ we require that

$$\lim_{\Delta t \to 0} \frac{p\left(x, t + \Delta t|z, t\right)}{\Delta t} = W\left(x|z, t\right) > 0 \tag{9}$$

uniformly in x, z and t for $|x - z| \geq \epsilon$. This condition implies that the probability of having a jump of size greater than ϵ in a time interval $[t, t+\Delta t]$, for $\Delta t \to 0$, is positive, so that indicating that the system is experiencing a discontinuous stochastic process.

We have to add two additional conditions:

$$\begin{aligned}
\lim_{\Delta t \to 0} \frac{1}{\Delta t} \int_{|x-z|<\epsilon} p\left(x, t + \Delta t|z, t\right)\left(x_i - z_i\right) d^n x &= A_i\left(z, t\right) + \mathcal{O}(\epsilon) \\
\lim_{\Delta t \to 0} \frac{1}{\Delta t} \int_{|x-z|<\epsilon} p\left(x, t + \Delta t|z, t\right)\left(x_i - z_i\right)\left(x_j - z_j\right) d^n x &= B_{ij}\left(z, t\right) + \mathcal{O}(\epsilon)
\end{aligned} \tag{10}$$

uniformly in z, ϵ and t, where n is the dimensionality of the state space. Since a general process can exhibit a mixed behaviour between jumps and a continuous sample path, these two conditions are related to the first and the second moment of the continuous part of the process. In fact, if $W(x|z,t) = 0$ the Lindeberg condition is fulfilled and the process is purely continuous. Conversely, if $A_i(z,t) = 0$ and $B_{ij}(z,t) = 0$ the process has a discontinuous trajectory. In what follows we will carry on the derivation in this particular case, showing that the contribution from the discontinuous part is equivalent to a Master Equation, Eq. (2).

Let us consider an arbitrary function $f(z)$ that has the following expansion:

$$f(x) = f(z) + \sum_i (x_i - z_i)\partial_i f(x)|_z + \frac{1}{2}\sum_{ij}(x_i - z_i)(x_j - z_j)\partial_{ij} f(x)|_z + |x-z|^2 R(x,z) \tag{11}$$

where $R(x,z) \to 0$ when $x \to z$, i.e. when $\epsilon \to 0$. Then we can write the following evolution equation for $p(x,t|y,t')$:

$$\partial_t \int f(x) p(x,t|y,t')\, = \lim_{\Delta t \to 0} \frac{1}{\Delta t} \int f(x) \left[p(x,t+\Delta t|y,t') - p(x,t|y,t')\right] d^n x \tag{12}$$

The right hand side can be rewritten as:

$$\lim_{\Delta t \to 0} \frac{1}{\Delta t} \int d^n x \int d^n z f(x) \left[p(x,t+\Delta t|z,t) p(z,t|y,t') - \int d^n z p(z,t|y,t') f(z) \right] \tag{13}$$

where we have inserted the so-called *short-time propagator* $p(x,t+\Delta t|z,t)$ and made use of the Chapman Kolmogorov equation, Eq. (7).

Splitting the integrals in the two regions $|x-z| < \epsilon$ and $|x-z| \geq \epsilon$, inserting the expansion of $f(x)$, Eq. (12), using the conditions (9) and (10), and taking to zero the contribution from the continuous path of the process, from Eq. (13) we get the following equation:

$$\partial_t \int f(z) p(z,t|y,t') d^n z = $$
$$= \int d^n z f(z) \int_{|x-z|\geq\epsilon} d^n x \left[W(z|x,t) p(x,t|y,t') - W(x|z,t) p(z,t|y,t') \right] \tag{14}$$

Then, we suppose that the process is confined in a region R. Integrating by parts and choosing $f(z)$ to be arbitrary but non-vanishing only in a subregion R' of R, Eq. (14) becomes:

$$\partial_t p(z,t|y,t') = \int d^n x \left[W(z|x,t) p(x,t|y,t') - W(x|z,t) p(z,t|y,t') \right] \qquad (15)$$

where, in the limit of vanishing ϵ (this is done to get rid of the reminder term in Eq. (12)), we are ignoring the singular cases in which it is necessary to consider the integral in Eq. (15) as a principal value. Note that Eq. (15) is nothing but the continuous version of the Master Equation presented in Eq. (2). When the state space consists in a finite number of states N, we recover exactly the same equation.

2.1.2 Detailed balance and equilibrium

The detailed balance condition, roughly speaking, requires that, in the stationary state p_i^*, each possible transition is balanced by the reversed one. This general criterion can be formulated for the Chapman-Kolmogorov equation and, hence, for a Master Equation describing a discrete-state dynamics, leading to the following condition:

$$w_{ij} p_j^* = w_{ji} p_i^* \qquad (16)$$

Inserting Eq. (16) in (2) it is easy to see that this condition implies that around any closed cycle of states, at stationarity, there is no net flow of probability. A necessary and sufficient condition to have detailed balance in a discrete-state Markov process is the Kolmogorov's criterion, which demands that, for each loop, the product of the associated transition rates in the forward direction must be equal to the product for the reverse direction [63].

The most important physical consequence of detailed balance is that, when this holds, the stationary distribution coincides with the equilibrium distribution. This can be understood since the "no net flow" condition coicides with the definition of equilibrium in statistical physics.

2.2 Entropy and entropy production: technical background

In this section we will present a review of the concepts of entropy and entropy production, deepening the notions given in the introduction. This will be useful to the reader to better understand the content of this section and of this thesis in general.

2.2.1 Classical thermodynamics

We have already defined the entropy of a system as a measure of the heat that a system exchange with a medium. In formulas, Clausius introduced the variation of entropy in a thermodynamic system as [3]:

$$\Delta S_s = \int \frac{\delta Q}{T} \tag{17}$$

where δQ is the infinitesimal heat flow from the medium in a reversible process and T is the instantaneous absolute temperature. For a reversible process the variation of entropy depends just on the initial and final state of the system, thus, according to Clausius equality, for a reversible cyclic process, the integral in Eq. (17) is

$$\Delta S_{\text{cycle}} = \oint \frac{\delta Q}{T} = 0 \tag{18}$$

indipendently on the specific details of the process [64]. This means that, as said in the introduction, the entropy is a state function of a thermodynamic system, being indipendent on the particular reversible path along which we perform the integration.

On the contrary, if we consider an irreversible process, it can be shown that the variation of entropy along its path is no longer a function of the state of the system and the following inequality holds:

$$\Delta S^{\text{irr}}_{\text{cycle}} = \oint \frac{\delta Q^{\text{irr}}}{T} \leq 0 \tag{19}$$

It is worth noting that the entropy variation is defined just for reversible process and Eq. (19) contitutes just a mathematical inequality. Thus, combining this result with Eq. (18), we get a formulation of the second law of thermodynamics:

$$\Delta S_s \geq \int \frac{\delta Q^{\text{irr}}}{T} = -\Delta S^{\text{med}} \rightarrow \Delta S_{\text{total}} \geq 0 \tag{20}$$

where ΔS^{med} has the opposite sign since we have to consider the heat flowing from the system to the medium [2]. Summarizing, the entropy of an isolated system (thermodynamic open system plus its surrounding medium) cannot decrease and the equality in Eq. (20) is fulfilled if only reversible process are present. Reminding that the entropy production heuristically quantifies the amount of irreversible dissipation during the evolution of a system, Eq. (20) can be stated in terms of this quantity, saying that it has to be always non-negative.

2.2.2 Irreversible thermodynamics

Now we try to go beyond the classical thermodynamics, being interested in relating the entropy production to the irreversible phenomena which may occur inside the system of interest [38].

First we rewrite the second law of thermodynamics for infinitesimally small parts of a system, assuming that the same laws holds as in the macroscopic description. This assumption lies on the current interpretation that local macroscopic measuements are actually measurements of the properties of small parts of a system, which still contains a large number of particles. Let us write:

$$dS_{\text{total}} = dS_s + dS_{\text{med}} \geq 0 \tag{21}$$

Now we shall rewrite this equation for a system in which the densities of extensive quantities (e.g. mass and energy) are continous function of the space coordinates. Let us write

$$S_s = \int \rho s dV \tag{22}$$

$$\frac{dS_{\text{med}}}{dt} = \int J_{\text{s,tot}} d\Omega \tag{23}$$

$$\frac{dS_{\text{total}}}{dt} = \int \sigma_t dV \tag{24}$$

where ρ is the total density, s the entropy per unit mass, $J_{\mathrm{s,tot}}$ the total entropy flow per unit are and unit time and σ_t the entropy production per unit volume and unit time.

Rewriting Eq. (21) in this case, also using Gauss' theorem, we get:

$$\int \left(\frac{\partial \rho s}{\partial t} + \nabla J_{\mathrm{s,tot}} - \sigma_t \right) = 0 \tag{25}$$

Since this holds for an arbitrary volume, it follows:

$$\begin{aligned} \frac{\partial \rho s}{\partial t} &= -\nabla J_{\mathrm{s,tot}} + \sigma_t \\ \sigma_t &\geq 0 \end{aligned} \tag{26}$$

Without going into details, in order to relate the variations in the physical properties of the systems to the entropy production, we remind that the entropy can be expressed as a function of parameters that are necessary to determine the macroscopic state of the system, say the internal energy u, the specific volume v and the mass fractions c_k: $s(u, v, c_k)$.

Then, using the Gibbs' relation:

$$Tds = du + pdv + \sum_k \mu_k dc_k, \tag{27}$$

assuming that it holds for a mass element followed along its center of gravity motion, and expliciting the expression for du and dc_k, we can derive the following general form for the entropy production:

$$\sigma_t = \sum_k J_k F_k \tag{28}$$

Eq. (28) is a bilinear form, where the first factor is a flow quantity (e.g. heat flow, diffusion flow) and the second one is related to an external force as a gradient of an intensive variable (e.g. temperature, chemical potential). These quantities that multiply the fluxes are called "thermodynamic forces".

Note that in this section we are using the name $\dot{S}_{\mathrm{total}}$ for the total entropy production, whereas in the other sections the notation $\dot{S}$ has been used. In what follows, unless otherwise specified, the two notation must be considered as equivalent.

2.2.3 Statistical mechanics and information theory

Let us start from Eq. (1). This formula is equivalent to the Boltzmann entropy [4], as we said in the introduction, and it measures the amount of uncertainty of a probabilistic source of data. Here we try to derive and understand the functional form and the meaning of this expression.

Consider a random variable X that can take a finite set of values ω, each one with probability p_ω. The uncertainty $S(X)$ (or entropy) of X has to satisfy the following axioms [8]:

- $S(X)$ has to depend just on p_ω;
- $S(X)$ is maximum when the uncertainty is maximum, i.e. for a uniform distribution;
- Let Y be a random variable that can take values on a larger set than X, such that the probabilities are the same for the subspace of X, then $S(Y) = S(X)$;
- Let X and Y be two random variables, then:

$$S(X,Y) = S(X) + \sum_\omega S\left(Y|X=\omega\right) \tag{29}$$

  where $S(X,Y)$ is the joint entropy and $S(Y|X=\omega)$ is the entropy of Y conditioned on $X=\omega$.

The only functional form of $S(X)$ for which all these axioms are satisfied is the following [65]:

$$S = -\sum_\omega p_\omega \log(p_\omega) \tag{30}$$

The formula in Eq. (30) is equivalent to the one in Eq. (1), introduced in the first chapter as the Gibbs entropy (or Shannon entropy in the area of information theory). It is easy to understand that this quantity can be related to the uncertainty of a distribution. The first axiom states that we can compare any random variable with each other, the second one is of immediate interpretation, the third imposes that adding events of null probability to a sample space does not change the uncertainty and, finally, the fourth axiom

is related to the additivity of the entropy. However the latter can also be relaxed giving birth to a plethora of different definitions of entropy that can be used in different contexts.

From an information-theoretic point of view, the Shannon entropy can be seen as a quantification of the number of bits needed to encode a message [7]. On the other hand, from the point of view of the statistical mechanics, in what follows we will consider p_i as the probability of a given microstate to occur. This latter definition will be specified later on and it will appear to be crucial for the introduction of the notion of entropy production.

2.3 Entropy production for discrete-state systems

Consider a discrete-state system with a finite number N of accessible states, each with probability p_i, $i = 1, ...N$. In the spirit of an information-theoretic approach, we can define the entropy of such a system as in Eq. (1). Since p_i is the probability to be in a given microstate i, the latter expression is amenable to be interpreted as the entropy in statistical mechanics.

We have already seen that the dynamics of a discrete-state system can be described by Master Equation, Eq. (2). In this case, we can introduce the notion of entropy production, $\dot{S}$, in three different ways, each one leading to exactly the same expression, known in literature as Schnakenberg formula [61]:

$$\dot{S} = \frac{1}{2} \sum_{\langle i,j \rangle} (w_{i \to j} p_i - w_{j \to i} p_j) \log \frac{w_{i \to j} p_i}{w_{j \to i} p_j} \tag{31}$$

where the sum is performed over all pairs of states i, j with non-zero transition rates $w_{i \to j}$ and $w_{j \to i}$ and the factor $1/2$ avoids the double counting. Note that Eq. (31) is always positive and vanishes for systems for which detailed balance holds, i.e. systems at equilibrium, and therefore is a good candidate for the entropy production.

Here we describe these different methods of deriving Eq. (31), enlightening the difference between them and trying to shed some light on the physical interpretation of this expression under investigation.

2.3.1 Information theoretic approach

Let us start from Eq. (1), which represents the information entropy of a system. The simplest thing we could do is to define the entropy production,

$\dot{S}$, as the temporal derivative of this formula, using the fact that p_i is governed by a dynamics described by a Master Equation, as in Eq. (2). This leads to the following expression:

$$\dot{S}_{\text{Shannon}} = \frac{1}{2}\sum_{\langle i,j\rangle}(w_{i\to j}p_i - w_{j\to i}p_j)\log\frac{p_i}{p_j} \tag{32}$$

Unfortunately this term is not always positive, then we have to add an extra contribution to fix this problem. Although this could appear as a handmade trick, we will validate this expression a-posteriori in this chapter. Again, also in this case, let us choose the simplest possible solution:

$$\begin{aligned}\dot{S} = \frac{1}{2}\sum_{\langle i,j\rangle}(w_{i\to j}p_i - w_{j\to i}p_j)\log\frac{p_i}{p_j} + \frac{1}{2}\sum_{\langle i,j\rangle}(w_{i\to j}p_i - w_{j\to i}p_j)\log\frac{w_{i\to j}}{w_{j\to i}} = \\ = \frac{1}{2}\sum_{\langle i,j\rangle}(w_{i\to j}p_i - w_{j\to i}p_j)\log\frac{w_{i\to j}p_i}{w_{j\to i}p_j}\end{aligned} \tag{33}$$

From the fact that the first term corresponds to the time derivative of the system entropy under equilibrium conditions, i.e. the Shannon entropy, the second term can be interpreted as the contribution due to the coupling to an external set of thermodynamics forces which prevent the system from achieving an equilibrium state. It is worth noting that neither the latter or the first term are necessarily positive, but only the sum of the two, as shown in Eq. (33) [66, 61].

2.3.2 Chemical master equation approach

This approach retraces how the formula was derived by Schnakenberg in 1976 [61, 67]. Consider a fictitious chemical system that mimics the dynamics of a Master Equation, based on the following assumptions:

- the chemical species X_c, for $c = 1, ...N$ constitute an open homogeneous system;
- reactions are possible between species in the form $X_c \rightleftharpoons X_{c'}$, with the following reaction rate:

$$J'_{cc'} = (C_{c'}w_{c'\to c} - C_c w_{c\to c'}) \tag{34}$$

where C_c is the concentration of the specie X_c.

- other components involved in a reaction between two species not belonging to the set $X_1, ...X_N$ are assumed at a constant concentrations and these values are incorporated in the transition rates;

- the thermodynamics can be applied since we are dealing with slow rections.

It is obvious that these constraints do not define the system in a unique way. Every system which satisfy the above presciptions is accepted.

The change in concentration of the species X_c is then:

$$\frac{dC_c}{dt} = \sum_{c'} J'_{cc'} \tag{35}$$

By choosing $p_c = C_c / \sum_c C_c$ Eq. (35) becomes formally identical to a Master Equation, providing the substitution of $J'_{cc'}$ with $J_{cc'} = p_{c'} w_{c' \to c} - p_c w_{c \to c'}$, that is proportional to the first by a factor that is independent of c and c'.

Since the system is assumed to be homogeneous, the only irreversible processes which can take place are the reactions between any two species. In chemistry the "thermodynamic force" associated to a chemical reaction is the affinity $A_{cc'}$, defined as:

$$A_{cc'} = \mu_{c'} - \mu_c \tag{36}$$

where μ_c is the chemical potential of the species X_c. In the case of an ideal mixture, the chemical potential is given by:

$$\mu_c = \mu_c^{(0)} + T \log N_c \tag{37}$$

taking $k_B = 1$. $\mu_c^{(0)}$ is the chemical potential at equilibrium, when the thermodynamic forces and fluxes vanishes, so that:

$$A_{cc'} = \mu_{c'}^{(0)} - \mu_c^{(0)} + T \log \frac{N_{c'}^{\mathrm{eq}}}{N_c^{\mathrm{eq}}} \tag{38}$$

Substituting Eq. (38) in Eq. (36) and using the detailed balance condition (i.e. $N_{c'}^{\mathrm{eq}} w_{c' \to c} = N_c^{\mathrm{eq}} w_{c \to c'}$), we get the following expression for the chemical affinity:

$$A_{cc'} = T \log \frac{p_{c'} w_{c' \to c}}{p_c w_{c \to c'}} \tag{39}$$

Reminding how the entropy production is related to the thermodynamics of irreversible processes, Eq. (28), we obtain the following expression:

$$\dot{S} = \frac{1}{2} \sum_{cc'} J_{cc'} A_{cc'} = \alpha T \frac{1}{2} \sum_{\langle i,j \rangle} (w_{i \to j} p_i - w_{j \to i} p_j) \log \frac{w_{i \to j} p_i}{w_{j \to i} p_j} \tag{40}$$

where α is the constant of proportionality between $J'_{cc'}$ and $J_{cc'}$. Since the system we are considering is fictitious and homogeneous, the choice of the temperature will be completely irrelevent, then, again, we end up with the Schankenberg's formula for the entropy production, starting from the thermodynamics of a chemical system.

2.3.3 Path-dependent entropy approach

This derivation follows the work of Seifert [23] and the philosophy can be used also to derive an expression for the entropy production for a Langevin dynamics, as we will see later in this thesis.

Consider a system with N accessible states in which a transition from the state m to the state n occurs with a transition rate $w_{m \to n}(\lambda)$, which depends on an external time-dependent control parameter $\lambda(\tau)$. The system is driven from λ_0 to λ_1 according to a given protocol. A stochastic trajectory begins in the state n_0 and ends up in state n_t. We want to quantify the entropy associated to this single trajectory.

The form of Eq. (1) suggests to propose a trajectory-dependent entropy as:

$$s(\tau) \equiv - \log p_{n(\tau)}(\tau) \tag{41}$$

where $p_{n(\tau)}(\tau)$ is the solution of the Master Equation describing the system. Then, in order to estimate $s(\tau)$ from Eq. (41), we need to evaluate the probability to be at time τ in the state $n(\tau)$ for each trajectory.

We evaluate the time evolution of Eq. (41), obtaining:

$$\dot{s}(\tau) = - \frac{\partial_\tau p_n(\tau)}{p_n(\tau)} |_{n(\tau)} - \sum_j \delta(\tau - \tau_j) \log \frac{p_{n_j^+}(\tau_j)}{p_{n_j^-}(\tau_j)} \tag{42}$$

where the first term accounts for the time interval in which the system stays in the same state, while the second term stems from the jump at time τ_j from n_j^- to n_j^+. We split up this expression as follows:

$$\dot{s}_{\text{total}}(\tau) = -\frac{\partial_\tau p_n(\tau)}{p_n(\tau)}|_{n(\tau)} - \sum_j \delta(\tau - \tau_j) \log \frac{w_{n_j^+ \to n_j^-} p_{n_j^+}(\tau_j)}{w_{n_j^- \to n_j^+} p_{n_j^-}(\tau_j)} \tag{43}$$

$$\dot{s}_{\text{med}}(\tau) = -\sum_j \delta(\tau - \tau_j) \log \frac{w_{n_j^+ \to n_j^-}}{w_{n_j^- \to n_j^+}} \tag{44}$$

such that $\dot{s}_{\text{total}} = \dot{s} + \dot{s}_{\text{med}}$. This identification has been done in the same spirit of the derivation in Section 2.3.1 and can be understood after averaging over many trajectories. To do this we need the probability to perform a jump at time τ_j from n_j^- to n_j^+, that is $w_{n_j^- \to n_j^+} p_{n_j^-}(\tau_j)$. Finally, we obtain:

$$\begin{aligned}
\dot{S}_{\text{med}}(\tau) &= \langle \dot{s}_{\text{med}}(\tau) \rangle = \sum_{n,k} p_n w_{n,k} \log \frac{w_{nk}}{w_{kn}} \\
\dot{S}_s(\tau) &= \langle \dot{s}_s \rangle = \sum_{n,k} p_n w_{n,k} \log \frac{p_n}{p_k} \\
\dot{S}_{\text{total}}(\tau) &= \langle \dot{s}_{\text{total}}(\tau) \rangle = \sum_{n,k} p_n w_{n,k} \log \frac{p_n w_{nk}}{p_k w_{kn}}
\end{aligned} \tag{45}$$

Eq. (45) represents the Schnakenerg formula for the total entropy production, interpreted as the average value over many trajectories.

2.4 Technical remark: network theory

Since networks play a fundamental role in modeling a plethora of different systems [68, 69, 70, 71], we here present a brief review on some concepts of network theory that will be useful in the rest of the chapter to describe Master Equation systems as a network of accessible states.

Networks are around us. We can be considered netwoks as well, as an element of a grid of social interactons, or as a biological system, that is the outcome of a network of biochemical reactions. Networks can be both physical objects, as electrical circuits or neural networks, and mathematical objects, as, for example, the citation networks [72].

Let us start with the some definitions. A graph, or network, $G(N, L)$ consists of two ensambles N and L, such that $N \in \mathcal{N}$, $N \neq 0$, and L contains all the connected pairs of elements in N. Each component of N is called node of a graph, while each pair in L denotes a link between two nodes [73].

A network is called directed (or oriented) when it consists of ordered pairs of elements of N. This means that some connections have an orientation, i.e. one node is connected to the other, but not necessarily viceversa. In Fig. 1a an example of a directed network is shown.

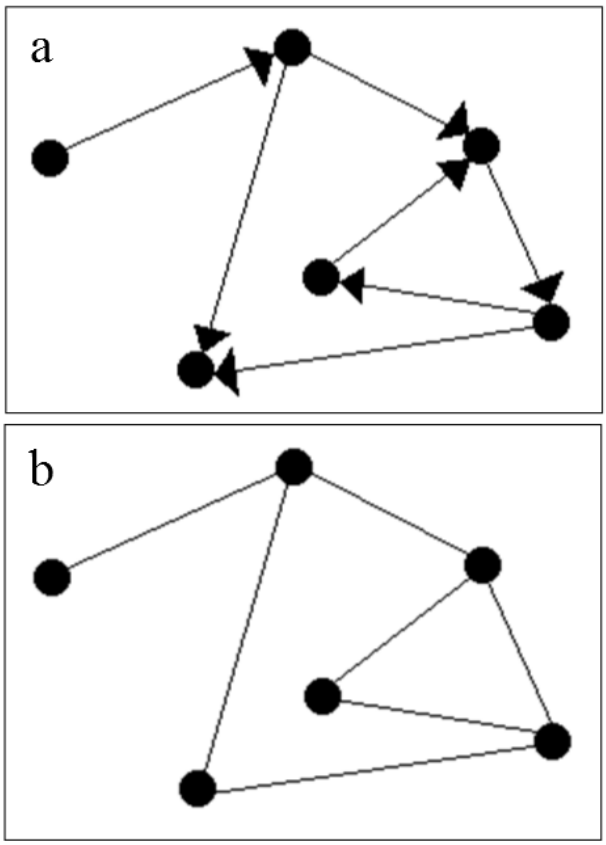

Figure 1: a) Example of a directed graph composed by 6 nodes and 7 links. b) Example of an undirected graph with 6 nodes and 7 links.

A graph is called undirected (or non-oriented) when L consists of unordered pair of elements. As a consequence, all the connections have no

orientation and if node i is connected to node j, also j has to be connected to i. In Fig. 1b we have presented an example of an undirected network.

Two nodes connected by a link are called adjacent nodes. A graph can be completely described by its adjacency matrix A_{ij}, that is a $N \times N$ matrix with the following structure:

$$\begin{aligned} A_{ij} &= 1 \quad \textit{if } i \textit{ and } j \textit{ are adjacent} \\ A_{ij} &= 0 \quad \textit{if } i \textit{ and } j \textit{ are not adjacent} \end{aligned}$$

In the case of an undirected graph, the adjacency matrix is symmetric, while it is asymmetric when the graph is directed.

Another important property of a graph is the connectivity C. It is defined as the percentage of active interactions among all the possible ones. Mathematically, $C = N_L/N^2$, where $N_L = \sum_{ij} A_{ij}$ is the number of the links in the network. In this case we are counting also the self-interactions, since we are considering that the number of all the possible interaction is N^2.

So far we have considered unweighted graph, i.e. graph where every link has the same weight. In general, each connection can be associated to a real coefficient which quantifies its magnitude. In order to characterize such a weighted graph we can introduce the weight matrix W, defined as follows:

$$\begin{aligned} W_{ij} &= w_{ij} \quad \textit{if } i \textit{ and } j \textit{ are connected by a link of weight } w_{ij} \\ W_{ij} &= 0 \quad \textit{if } i \textit{ and } j \textit{ are not adjacent} \end{aligned}$$

This matrix completely characterize the structure of a network.

2.4.1 Random networks - Erdos-Renyi algorithm

In this work we are going to deal with random networks, i.e. topologies that are randomly generated owing to specific contraints (e.g. number of nodes, connectivity). Random networks are used in literature, for example, to model interactions in biological systems [74, 75, 76, 77]; in this present context the idea is to provide a null model to elucidate the interplay between the system dynamics (described by a Master Equation and encoded in a network structure, as we will see in the next section) and the entropy production. Such a null model can also be used as a starting point for the analysis of more realistic biological models for which the same framework can be employed.

In particular, we focus on Erdos-Renyi random topologies, which are good proxies for networks with limited connectivity for which the property of small world holds [72]. Notice that, in the (rather general) case of a system composed by n elementary units, each of them taking m possible values, the total number of states is $N = n^m$. If the dynamics allows that each unit can change its value once at a time, the system can pass from one state to another through, roughly, n individual steps. This leads to a typical path distance of the order of $n = \log_m(N)$, which is actually the small world condition.

Here we present the algorithm that we used to build this kind of random topology in the case in which the nodes are distinguishable. A single graph is constructed by connecting nodes at random. Each element of the weight matrix W_{ij} (that represents a weighted link between nodes i and j) is different from zero with probability p. In other words, all graphs with N nodes and L links have the same probability to be built:

$$p^M(1-p)^{\binom{n}{2}-M} \tag{46}$$

The parameter p in this model can be seen as a weight function; as p increases from 0 to 1, networks with an increasing number of links are more likely to be built by this generating algorithm.

This section had just the role to introduce some basic concepts about network theory and to motivate the use of random Erdos-Renyi networks, in order to make the help the reader to understand the rest of this chapter.

2.5 Network representation

Now we aim at linking the discrete-state dynamics described by a Master-Equation to the network theory. It is possible, in fact, to encode all the dynamical information of a Master Equation system into a network representation [61].

Consider again our system with N accessible states, whose dynamics is characterized by the transition rates $w_{i\to j}$ of passing from the state i to the state j. First we associate a node to each state, building a network of N nodes. Then, we add a link between the node i and the node j if $w_{i\to j} \neq 0$, that, in our case, means that a link exist also between the nodes j and i. As a consequence, we will deal with symmetric adjacency matrix, i.e. undirected network. Moreover, each link has a weight, determined by the value of the transition rate between the involved states. Mathematically

speaking a weight matrix W_{ij} is associated to the transition network and it contains all the information about the dynamics. It is worth noting that the transition network must be connected, in the sense that for any pairs of states, there will be at least one transition connecting them, in order to avoid the presence of non-interacting subsystems.

Before moving to our analysis within this framework, let us see some advantages of describing a Master Equation system as a graph. First of all, the stationary solution can be determined by a graphical method. We shall briefly review this method without proof; anyway a detailed description was given by Hill (1966) [78]. Let us start by defining a maximal tree $T(G)$, where G is our transition network. $T(G)$ is uniquely characterized by the following properties:

- all links of $T(G)$ are links of G and $T(G)$ contains all nodes of G;
- $T(G)$ is connected;
- $T(G)$ contains no cyclic sequences of edges.

In Fig. 2a an example of how to build all possible maximal tree is shown.

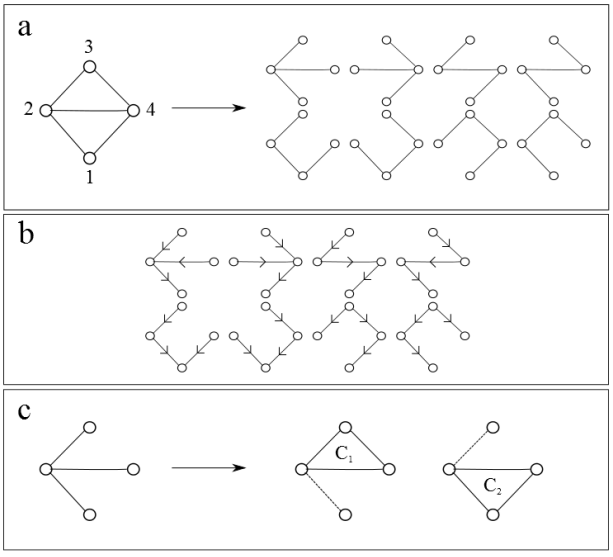

Figure 2: a) Example for constructing maximal trees from the graph on the right with 4 nodes and 5 links. b) 1-directed version of the maximal trees in the Panel a. c) Fundamental sets of circuits of the first maximal tree in Panel a.

Let us denote the set of all possible maximal trees by $T^{(k)}(G)$, with $k = 1, 2, ...M$. From each of the maximal trees $T^{(k)}(G)$ we obtain its i-directed version $T_i^{(k)}(G)$ by directing all links toward the node i. Since $T^{(k)}(G)$ is a maximal tree, this is a unique procedure to build the set of $T_i^{(k)}(G)$, for each node i. Fig. 2b shows the i-directed version of all the maximal tree for $i = 1$.

We can assing an algebraic value $A(T_i^{(k)}(G))$ to each $T_i^{(k)}(G)$ by multiplying all the transition rates of the network. Then the steady state solution is given by:

$$p_i^* = \frac{\sum_{k=1}^{M} A(T_i^{(k)}(G))}{\sum_{i=1}^{N}\sum_{k=1}^{M} A(T_i^{(k)}(G))} \tag{47}$$

It is easy to see that all the p_i^* are normalized and $p_i^* \in]0, 1[$.

Another important advantage of using this framework is that we can express the steady state value of the entropy production as a bilinear form as follows [61]:

$$\dot{S} = \sum_{\alpha=1}^{\nu} A(\vec{C}_\alpha) F(\vec{C}_\alpha) \tag{48}$$

where $\vec{C}_\alpha$ are the fundamental cycles. Each of these is obtained by adding to $T^{(k)}(G)$ one of the excluded link and giving an orientation to the cycle generated in this way. In Fig. 2c an illustrative example is provided. Eq. (48) here is given without proof, but we evidence its main features:

- $A(\vec{C}_\alpha)$ and $F(\vec{C}_\alpha)$ are uniquely determined by the fundamental cycle $\vec{C}_\alpha$;
- $A(\vec{C}_\alpha)$ is independent of the steady state probability p_i^*;
- $A(\vec{C}_\alpha) = 0$ for all α is equivalent to $F(\vec{C}_\alpha) = 0$ for all α which in turn is equivalent to the detailed balance condition, i.e. to the thermodynamic equilibrium;
- if the steady state is a thermodynamic equilibrium, there is a linear relation between $A(\vec{C}_\alpha)$ and $F(\vec{C}_\alpha)$ near equilibrium:

$$A(\vec{C}_\alpha) = \sum_{\beta} L_{\alpha\beta} F(\vec{C}_\beta) \tag{49}$$

with $L_{\alpha\beta} = L_{\beta\alpha}$.

This findings link the microscopic description in terms of a Master Equation to the macroscopic thermodynamic description in terms of forces $A(\vec{C}_\alpha)$ and fluxes $F(\vec{C}_\alpha)$, enforced by the parallelism between $L_{\alpha\beta}$ and the Onsager's coefficients. In the next sections we will focus on this mapping between microscopic and macroscopic thermodynamics from a different perspective aiming at providing a physical validation of the Schnakenberg's formula for the entropy production.

2.6 Introduction to the model

Now we introduce the question we will try to answer in this chapter. We want to study the statistical property of the entropy production at stationarity of a discrete-state system described by a Master Equation, using a model that is independent of the specific details of the dynamics. We focus on system close to equilibrium, nevertheless finding very interesting results.

The dynamical model under investigation is the following [79]:

$$\dot{p}_i = \sum_{j=1}^{N} (w_{j\to i} p_j - w_{i\to j} p_i) + J(t)(\delta_{i,1} - \delta_{i,N}) \tag{50}$$

where N is the number of accessible states. This represents a generic Master Equation with the injection of a current $J(t)$ in one of the states. Stationarity in ensured by the ejection of $J(t)$ by another arbitrary state of the system and imposing that $J(t \to \infty) = J$, i.e. constant at stationarity.

In our case the current enters in node 1 and exits through nodes N without loss of generality. The external current $J(t)$ can also be mimicked by two asymmetric transtion rates between nodes 1 and N,

$$J(t) = p_N(t)\omega_{N\to 1}(t) - p_1(t)\omega_{1\to N}(t) \tag{51}$$

where

$$\omega_{N\to 1}(t) = \frac{(J(t) + \omega_{1\to N} p_1(t))}{p_N(t)} \tag{52}$$

becomes constant at stationarity.

First of all we will study networks with symmetric transition rates, i.e. where $w_{i\to j} = w_{j\to i}$, deriving a fascinating mapping with a classical electrical

circuit, composed only by resistors. The latter allows us to derive also a thermodynamic validation of the Schnakenberg's formula and provides an estimation of the entropy production which depends on a unique topological parameter.

Then we will focus on system with asymmetric transition rates, deriving that the stationary entropy production has a distribution which depends on just two parameters, the first one accounting for the topology of the system, and the second one keeping track of the asymmetry of the transition rates.

In the next section we will analyze in details these two points.

2.7 Symmetric transition rates

Consider first the case in which $w_{i\to j} = w_{j\to i}$. Writing $\Delta p = p_1 - p_N$, we define the *equivalent transition rate* as

$$w_{\text{eq}} = J/\Delta p > 0 \tag{53}$$

which can be understood as a generalized Ohm's law for ME systems.

Indeed, w_{eq} is the strength of a symmetric transition rate in a network composed exclusively by nodes 1 and N that leads to the same Δp for a given current J, and depends on the topology of the underlying network (see Fig. 3). It is also useful to introduce the parameter $\alpha = p_1 + p_N$, so that $p_1 = (\alpha + \Delta p)/2$ and $p_N = (\alpha - \Delta p)/2$. At equilibrium (i.e. when $J = 0$), $p_i^* = 1/N$, and therefore $\alpha = 2/N$. In terms of the new variables,

$$\omega_{N\to 1} = \omega_{1\to N} + \frac{2J\,(w_{\text{eq}} + \omega_{1\to N})}{\alpha w_{\text{eq}} - J}. \tag{54}$$

It is worth noting that at stationarity the Schnakenberg entropy production reduces to [80]:

$$\dot{S} = \frac{1}{2}\sum_{\langle i,j\rangle}(w_{i\to j}p_i - w_{j\to i}p_j)\log\frac{w_{i\to j}p_i}{w_{j\to i}p_j} \tag{55}$$

From eq. (55), it can be seen that internal links do not contribute to the entropy production, and that the only contribution comes from the transition rates between nodes 1 and N:

$$\dot{S}^* = J\log\left(\frac{\omega_{N\to 1}}{\omega_{1\to N}}\right) \equiv \dot{S}_\omega. \tag{56}$$

We compute the entropy production at stationarity for the system close to equilibrium, i.e. for small values of J. Introducing the explicit form of $\omega_{N\to 1}$ in terms of J, eq. (54), and expanding for small values of the current, $J \ll N^{-1}$, we obtain that up to the leading order the entropy production is:

$$\dot{S}^* = N\left(\frac{1}{w_{\rm eq}} + \frac{1}{\omega_{1\to N}}\right) J^2 \equiv \dot{S}_{\mathcal{J}}, \tag{57}$$

an expected result since $\dot{S}^* \geq 0$ and so the linear contribution in J has to be absent.

Eq. (57) consists of two contributions: the first depends on the characteristics of the system itself, encoded in the value of $w_{\rm eq}$, while the second term keeps track explicitly of the dissipation phenomena in the environment, represented by the transition rates responsible for the external current $J(t)$.

A physical interpretation of the form of $\dot{S}_{\mathcal{J}}$ (eq. (57)) can be provided using a parallelism with classical electrical circuit. In fact, any electrical circuit composed exclusively by multiple resistors can be mapped into a ME system, and its corresponding entropy production turns out to be proportional to the heat dissipation rate, hence resembling by the so-called Joule's law. Here the parameter $w_{\rm eq}$ turns out to be proportional to the equivalent conductance, and then can be directly estimated by the structure of the transition network. Eq. (57) takes into account also the heat dissipated by the battery which induce a current into the system, where the ideal battery case corresponds to the limit $\omega_{1\to N} = \infty$.

Such a parallelism also works in the opposite way, as the stationary state p_i^* can be retrieved from a variational principle as the one that minimizes the entropy production, with the constraint imposed by the external flux.

2.7.1 Mapping: from an electrical circuit to a ME

Let us explain how the mapping can be constructed. Consider a circuit $\mathcal{C}$ composed of N nodes connected by multiple resistors, with conductances equal to c_{ij}. When a difference of potential $\Delta V = V_1 - V_N$ is applied between nodes 1 and N, the potential at each node i, V_i, is given by Kirchoff's law, which ensures the minimization of the heat dissipation [81]:

$$\dot{Q} = \sum_{\langle i,j\rangle} c_{ij}(V_i - V_j)^2 \tag{58}$$

where the sum is performed over all pairs of nodes i, j.

One can then build a fictitious dynamics for the potentials, whose stationary state corresponds to the physical state of $\mathcal{C}$. To proceed, we fix V_1 and V_N (with $V_1 - V_N = \Delta V$), and consider the following dynamics for nodes $i = 2, ..., N-1$:

$$\tau \dot{V}_i(t) = -\frac{\partial \dot{Q}}{\partial V_i} = \sum_{j=1}^{N} c_{ij} \left(V_j - V_i\right). \tag{59}$$

An arbitrary time scale τ can be introduced without changing the stationary state. Notice that eq. (59) leads to the state which minimizes $\dot{Q}$, as $\ddot{Q}(t) = \sum_i \frac{\partial \dot{Q}}{\partial V_i} \dot{V}_i = -2\tau \sum_i \dot{V}_i^2 < 0$.

Let us notice that, despite its analogy, eq. (59) is not a master equation, since $\sum_{i=1}^{N} \dot{V}_i(t) \neq 0$ for arbitrary t, and therefore normalization is not conserved. However, one can relax the constraint on nodes 1 and N to be obeyed only at stationarity. Defining the normalized potentials, $v_i = V_i / \sum_i V_i = V_i/V_T$ and introducing the new parameters $c_{1\to N}$ and $c_{N\to 1}$ ($c_{1\to N} \neq c_{N\to 1}$ in general), we study the following ME dynamics:

$$\tau \dot{v}_i(t) = \sum_j c_{ij}(v_j - v_i) + \left(c_{N\to 1} v_N - c_{1\to N} v_1\right)\left(\delta_{i,1} - \delta_{i,N}\right) \tag{60}$$

for $i = 1, ..., N$, where $c_{N\to 1}$ and $c_{1\to N}$ have to be chosen to ensure $v_1 - v_N = \Delta V/V_T$ at stationarity.

Notice that $\sum_{i=1}^{N} \dot{v}_i = 0$ for arbitrary t in eq. (60), which has an equivalent form to eq. (2). In addition, it leads to the state minimizing the heat dissipated by the circuit.

Note that this mapping has a meaning only in the stationary state, where the fictitious dynamics of the circuit leads to a physical solution that resembles the same characteristics of the steady state of a given Master Equation.

Without loss of generality we can fix $\tau = 1$.

The normalized current, $J = c_{N\to 1} v_N - c_{1\to N} v_1 = c_{\rm eq} \Delta V/V_T = I/V_T$, where $c_{\rm eq}$ is the conductance of the equivalent circuit formed by one single resistor and I is the supplied electrical current. For small values of the external current, Schnakenberg's entropy production at stationarity is given by eq. (57):

$$\dot{S}^* = N \left(\frac{1}{c_{\rm eq}} + \frac{1}{c_{1\to N}}\right) J^2, \tag{61}$$

which corresponds to Eq. (57) with $c_{\rm eq} = w_{\rm eq}$ and $c_{1\to N} = \omega_{1\to N}$. Written in terms of the heat dissipated by the circuit, $\dot{Q} = I^2/c_{\rm eq}$, the entropy production of the associated ME dynamics is:

$$\dot{S}^* = \frac{N}{V_T^2}\left(1 + \frac{c_{\rm eq}}{c_{1\to N}}\right)\dot{Q}. \tag{62}$$

Its important to note that the relation given by eq. (62) is determined up to the specific choice of parameters V_T and $c_{1\to N}$, as this is an intrinsic ambiguity of the mapping. Furthermore, there is a dissipation contribution coming from the battery, which vanishes in the the limit of a "perfect" battery, $c_{1\to N} \to \infty$.

Eq. (62) enlighten a thermodynamic meaning for the Schnakenberg entropy production, being this related, as expected, to the heat dissipated by a circuit in the same state (at stationarity) and, in turn, resembling the Joule's law in terms of probability current and transition rates [81].

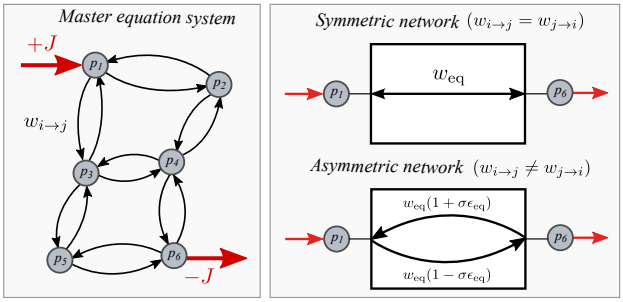

Figure 3: (Left) A master equation (ME) system as a graph in which nodes correspond to states and links to transition rates between them (sketched here as a 6-nodes network). An external probability current J enters into the system by one of the states and exits from another one to ensure stationarity. (Right) In symmetric ME systems ($w_{i\to j} = w_{j\to i}$), the entropy production can be computed from an equivalent network composed by the external nodes linked by a symmetric transition rate of strength $w_{\rm eq}$. Equivalently, the entropy production of slightly asymmetric networks can be found from an equivalent system composed by the external nodes and two asymmetric links $w_{\rm eq}(1\pm\sigma\epsilon_{\rm eq})$. Both $w_{\rm eq}$ and $\epsilon_{\rm eq}$ encode the topological structure of the underlying network.

Before moving to the more general case of non-symmetric transition rates and also for later comparison reasons we have checked numerically the validity of eq. (57) on randomly generated ME systems of size N and connectivity K (defined as the fraction of non-directed connections respect to the $N(N-1)/2$ links in the fully-connected case). In the symmetric case, each non-null entry of $w_{i\to j}$ is taken from a Gaussian distribution with average w and standard deviation $w\sigma$, with the constraint that $w_{i\to j} = w_{j\to i}$ for each pair of links. We

numerically integrate the corresponding ME by a finite-difference integration method and compute the entropy production at stationarity. The result is compared with eq. (57), where all the dependency on the network topology in eq. (57) is encapsulated in the parameter $w_{\rm eq}$. Results are shown in Top panel of Fig. 4 (in log-log scale), evidencing that eq. (57) perfectly works for a wide range of values of J.

2.8 Asymmetric transition networks

Now we want to generalize the simple result given by eq. (57) to networks generated as in the symmetric case but taking $w_{i\to j}$ and $w_{j\to i}$ as independent random variables. For each topology, $w_{\rm eq}$ is simply estimated taking $w_{i\to j} = w$. Then, we compute the entropy production of each network in the presence of a probability current J, and compare its value with the one given by $\dot{S}_{\mathcal{J}}$. Results are presented in the Bottom panel of Fig. 16 for different values of the heterogeneity σ; the prediction given by eq. (57) fails in the limit of small flux, as detailed balance does not holds for a general asymmetric network, and therefore $\dot{S} \neq 0$ when $J \to 0$.

Deviations from eq. (57) due to asymmetries in the network can be described within a perturbative framework when the system is close to equilibrium.

We focus on ensembles of random Erdos-Renyi topologies of connectivity K for which the non-null elements of $w_{i\to j}$ are independent Gaussian random variables of mean w and standard deviation $w\sigma$.

Introducing the adjacency matrix $A_{ij} = \Theta[w_{i\to j}]$ (Θ is the Heaviside step function with $\Theta(0) = 0$), we can write $w_{i\to j} = wA_{ij}(1 + \sigma\epsilon_{ij})$ in terms of independent Gaussian variables ϵ_{ij} of zero mean and unit variance.

The entropy production given by eq. (55) can be split into two contributions,

$$\dot{S}^* = \dot{S}_{\rm int} + \dot{S}_{\omega}, \tag{63}$$

where $\dot{S}_{\rm int}$ is the one given by internal links in the network and $\dot{S}_{\omega}$ the one given by the external links connecting nodes 1 and N, eq. (56). Formally, such a separation can be done if we do not allow the presence of internal links $w_{1\to N}$ and $w_{N\to 1}$, although whether considering them or not does not significantly change the value of the entropy production in large networks.

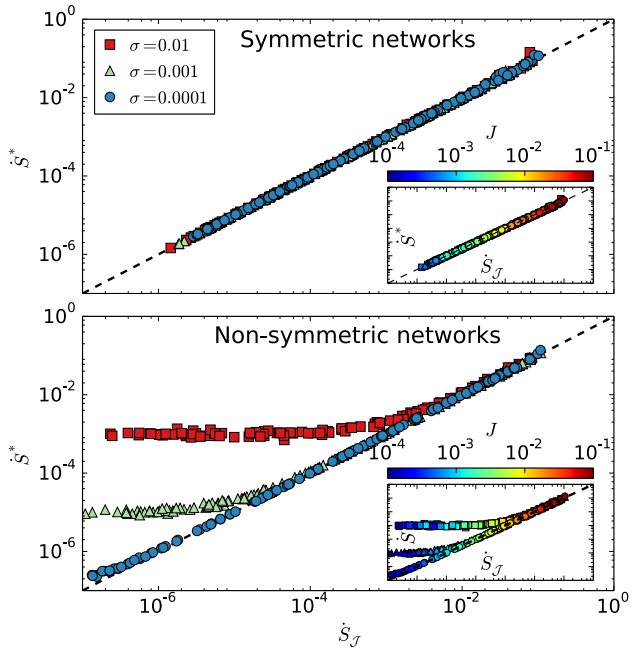

Figure 4: **Entropy production of ME systems represented by random (Erdos-Renyi) networks, compared to the theoretical prediction given by Eq.** (57). Transition rates $w_{i\to j}$ are randomly generated from a Gaussian distribution with mean $w = 1$ and standard deviation $w\sigma$. Each dataset is composed by 100 realizations of networks of size $N = 25$, fixing the parameter $\omega_{1\to N} = 10$. The external flux J is a random variable, being $\log_{10} J$ uniformly distributed in $[-4, -1]$ (so that $J \in [10^{-4}, 10^{-1}]$). All plots are in log-log scale. **(Top panel)** Symmetric networks, for which $w_{i\to j} = w_{j\to i}$ for each pair of links. The connectivity K is a uniform random variable in $K \in [0.25, 1]$. **(Bottom Panel)** - Non-symmetric networks: we remove the symmetric constraint, and therefore $w_{i\to j} \neq w_{j\to i}$ in general. In this case, we have fixed the connectivity $K = 0.5$. In both panels, insets represent the same corresponding points but using a color scale for the external probability flux J. Similar results can be obtained for other network topologies different from the Erdos-Renyi (Eq. (57) is valid in general).

We want to show that close to equilibrium, $J, \sigma \ll N^{-1}$, the entropy production, $\dot{S}^*$, differs from the corresponding one in absence of asymmetry, $\dot{S}_{\mathcal{J}}$, as given by eq.(57), by a gaussian random variable of mean $(KN - 2 - K + \mathcal{O}(1/N))w\sigma^2$ and variance $4Kw^2\sigma^4 + \mathcal{O}(1/N)$.

To show that we write the stationary state as $p_i^* \simeq (1 + \sigma q_i + Jr_i)/N$; the normalization constraint implies that $\sum_i q_i = \sum_i r_i = 0$. Then, we expand the entropy production in terms of σ and J, neglecting contributions of order higher than σJN^2, $\sigma^2 N^2$ and $J^2 N^2$. Defining the antisymmetric matrix $D_{ij} = \epsilon_{ij} - \epsilon_{ji}$ (whose entries are Gaussian variables with zero mean and standard deviation $\sqrt{2}$), the first order contributions to $\dot{S}_{\rm int}$ are:

$$\frac{\dot{S}_{\rm int}}{w\sigma^2} = \frac{1}{N}\sum_{\langle i,j\rangle} A_{ij}\left(D_{ij}^2 + D_{ij}\left(q_i + \frac{J}{\sigma}r_i\right)\right). \tag{64}$$

For large N, the first term of the r.h.s. of eq. (64), becomes a Gaussian random variable of mean $K(N-1)$ and standard deviation $2\sqrt{K}$ by means of the central limit theorem [60, 59]. Remarkably, this term is positive and scales linearly with the system size N.

The second and third terms in eq. (64) require to solve the ME close to equilibrium to obtain the values of q_i and r_i. Up to first order in N, we find that $q_i \simeq -\frac{1}{KN}\sum_j A_{ij}D_{ij}$. Such a dependency is meaningful: if in a node i, most of $D_{ij} = (w_{i\to j} - w_{j\to i})/w > 0$ (resp. < 0), an outgoing (incoming) flux is expected between node i and its neighbors, and therefore $p_i^* < 1/N$ ($> 1/N$).

Introduced in eq. (64), the second term gives a Gaussian random contribution to $\dot{S}_{\rm int}$ with mean -2 and standard deviation $\sqrt{8/N}$.

Equivalently, solving the ME we find that, up to first order in N, $r_i \simeq (\delta_{i1} - \delta_{iN})/(wK)$, evidencing the major role of the external nodes. This term gives another Gaussian contribution to $\dot{S}_{\rm int}$ which has zero mean and standard deviation $(2/\sqrt{KN})J/\sigma$. Assembling all the terms together, the leading contributions give that $\dot{S}_{\rm int}$ is normally distributed with mean and variance given by:

$$\langle \dot{S}_{\rm int}\rangle = (KN - (2+K))\, w\sigma^2 + \mathcal{O}(1/N) \tag{65}$$

$$\langle (\dot{S}_{\rm int})^2\rangle - \langle \dot{S}_{\rm int}\rangle^2 = 4Kw^2\sigma^4 + \mathcal{O}(1/N) \tag{66}$$

On the other hand, the term $\dot{S}_\omega$ can be computed in terms of a generalized Ohm's law for non-symmetric networks close to equilibrium, $\Delta p = J/w_{\rm eq} + \sigma\epsilon_{\rm eq}$, where $1/w_{\rm eq} = (r_1 - r_N)/N$ and $\epsilon_{\rm eq} = (q_1 - q_N)/N$ is a network parameter accounting for the asymmetry-induced unbalance between nodes 1 and N. More precisely, $\epsilon_{\rm eq}$ represents the asymmetry of an equivalent network composed exclusively by nodes 1 and N with the same Δp and $(w_{N\to 1} - w_{1\to N})/(w_{N\to 1} + w_{1\to N}) = \sigma\epsilon_{\rm eq}$ (see Fig. 3b). Notice that $w_{\rm eq}$ and $\epsilon_{\rm eq}$ exclusively depends on the network structure. In terms of these parameters, the leading contributions to $\dot{S}_\omega$ are:

$$\dot{S}_\omega(\sigma) = \dot{S}_{\mathcal{J}} + N\epsilon_{\rm eq}\sigma J, \tag{67}$$

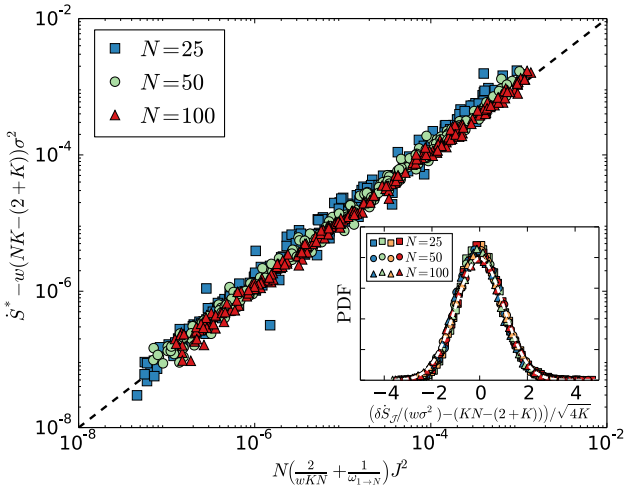

Figure 5: **Deviations from eq.** (57) **follow generic scaling relations**. The relation between $\dot{S}^*$ and J for networks generated with different N, K, J and σ can be enlightened plotting $\dot{S}^* - \langle \delta \dot{S}_{\mathcal{J}} \rangle$ against $\langle \dot{S}_{\mathcal{J}} \rangle$. All datasets collapse into the straight line $y = x$ (with deviations around). We have generated 250 networks for each system size with a random connectivity uniformly distributed in $K \in [0.25, 1]$ and a external flux J such that $\log_{10} J$ is a uniform random variable in $[-4, -1]$ ($J \in [10^{-4}, 10^{-1}]$); the heterogeneity has been taken $\sigma = J$ for each realization (this ensures that the current and heterogeneity contributions to the entropy production are of the same order and therefore both have to be considered). (Inset) We collapse the PDFs of $\delta \dot{S}_{\mathcal{J}}$ by subtracting the contribution given by Joule's law, eq. (57), and the mean $w(KN - (2+K))\sigma^2$, and dividing by the standard deviation $w\sqrt{4K}\sigma^2$ (blue, green, yellow and red points correspond to $K = 0.25, 0.5, 0.75$ and 1, respectively). The corresponding $w_{\rm eq}$ is computed setting $w_{i\to j} = w$ for each network topology. All histograms collapse into a Gaussian distribution of zero mean and unit variance (dashed line). We have generated 10^4 independent realizations for each set of parameters, setting $J = \sigma = 10^{-3}$. We have set $\omega_{1\to N} = 10$ in both panels.

where $\dot{S}_{\mathcal{J}}$ is defined in eq. (57). Deviations from eq. (57), $\delta \dot{S}_{\mathcal{J}} = \dot{S}^* - \dot{S}_{\mathcal{J}}$ are given by $\delta \dot{S}_{\mathcal{J}} = \dot{S}_{\rm int} + N \epsilon_{\rm eq} \sigma J$. For large networks we found that $\epsilon_{\rm eq}$ is normally distributed, $\epsilon_{\rm eq} \sim \mathcal{N}\left(0, 2/\sqrt{KN^3}\right)$. Consequently, deviations from eq. (57) are essentially given by $\delta \dot{S}_{\mathcal{J}} \approx \dot{S}_{\rm int}$, which is our main result.

The relation between S^* and J can be enlightened representing $\dot{S}^* - \langle \delta \dot{S}_{\mathcal{J}} \rangle = \dot{S}^* - (NK - (2+K)) w \sigma^2$ against $\langle \dot{S}_{\mathcal{J}} \rangle = N \left(\langle w_{\rm eq}^{-1} \rangle + \omega_{1\to N}^{-1} \right) J^2$. We can compute the distribution of $w_{\rm eq}$ for an ensemble of random networks of size N and connectivity K; interestingly, this problem is equivalent to computing the equivalent conductance of an electrical circuit in which resistors are randomly connected. $P(w_{\rm eq})$ becomes a Gaussian distribution with mean $NKw/2$ and standard deviation $w\sqrt{NK(1-K)/8}$ for large networks, becoming narrower when N increases (relatively to its mean). Therefore, we can use the approximation $\langle w_{\rm eq}^{-1} \rangle \simeq 2/(NKw)$ (in the next subsection we

will present a more formal derivation of this approximation). Pairs of (S^*, J) are represented with this procedure in the main panel of Fig. 5, evidencing that the entropy production of non-symmetric Master Equation systems of different sizes N, connectivity K, heterogeneity σ and external current J, all collapse around the straight line $y = x$, with deviations around decreasing for larger systems.

Finally, we check numerically that deviations from eq. (57) follow the scaling relations given by equations (65) and (66). Subtracting the mean and dividing by the standard deviation, all the histograms collapse into the Gaussian distribution with zero mean and unit variance, as depicted in the inset of Fig. 5.

At the end of this derivation we have identified two topological paramters ($w_{\rm eq}$ and $\epsilon_{\rm eq}$) that play the most important role in characterizing the value of the entropy production close to equilibrium. In this sense, Fig. 3 is emblematic, since it schematize how a Master Equation system can be seen in terms of this two variables only.

2.9 Derivation of the distribution of $\dot{S}^*$

This subsection is entirely dedicated to the formal derivation of the distribution of the entropy production.

2.9.1 Calculation of $\dot{S}_{\rm int}$

Writing the transition rates $w_{i\to j}$ in terms of independent Gaussian variables ϵ_{ij} of zero mean and unit variance, $w_{i\to j} = A_{ij} w(1 + \sigma\epsilon_{ij})$ (with $A_{ij} = \Theta[w_{i\to j}]$) and introducing $p_i^* = (1 + \sigma q_i + J r_i)/N$ in eq. (55), we obtain:

$$\dot{S}_{\rm int} = \sum_{\langle i,j\rangle} A_{ij} w \left((1+\sigma\epsilon_{ij}) \left(\frac{1}{N}(1 + \sigma q_i + J r_i) \right) \right.$$
$$\left. - (1+\sigma\epsilon_{ji}) \left(\frac{1}{N}(1 + \sigma q_j + J r_j) \right) \right) \log\left(\frac{1+\sigma\epsilon_{ij}}{1+\sigma\epsilon_{ji}} \right) \tag{68}$$

Close to equilibrium ($\sigma \ll N^{-1}, J \ll N^{-1}$), the leading contributions are:

$$\dot{S}^1_{\rm int} = \frac{w\sigma^2}{N}\sum_{\langle i,j\rangle} A_{ij}D^2_{ij} \tag{69}$$

$$\dot{S}^2_{\rm int} = \frac{w\sigma^2}{N}\sum_{\langle i,j\rangle} A_{ij}D_{ij}(q_i-q_j) = \frac{w\sigma^2}{N}\sum_{i,j} A_{ij}D_{ij}q_i \tag{70}$$

$$\dot{S}^3_{\rm int} = \frac{w\sigma J}{N}\sum_{\langle i,j\rangle} A_{ij}D_{ij}(r_i-r_j) = \frac{w\sigma J}{N}\sum_{i,j} A_{ij}D_{ij}r_i, \tag{71}$$

where $D_{ij}=\epsilon_{ij}-\epsilon_{ji}$. In the next section we compute each term separately, and we show that the major contribution is given by $\dot{S}^1_{\rm int}$, whereas the second and the third term can be neglected for large network sizes. For convenience, we will call $\mathcal{N}(a,b)$ the Gaussian distribution with mean a and standard deviation b.

It is worth mentioning that, in our calculations, we do not distinguish the cases in which the external nodes are or not connected also by internal nodes ($A_{1N}=0$ and 1 respectively), as this constitutes a minor contribution for the total entropy production.

Calculation of $\dot{S}^1_{\rm int}$

For each pair of links i and j, D_{ij} is an independent random variable of zero mean and standard deviation $\sqrt{2}$. Therefore, D^2_{ij} is distributed as a chi-square distribution whose mean and variance can be easily calculated:

$$\langle D^2_{ij}\rangle = 2 \tag{72}$$

$$\langle (D^2_{ij}-\langle D^2_{ij}\rangle)^2\rangle = \langle D^4_{ij}\rangle - \langle D^2_{ij}\rangle^2 = 2\langle D^2_{ij}\rangle^2 = 8. \tag{73}$$

Eq. (69) involves the sum of $KN(N-1)/2$ independent variables of this type. When N is large, by means of the Central Limit Theorem, we obtain that $\dot{S}^1_{\rm int}$ follows a normal distribution:

$$P\left(\frac{\dot{S}^1_{\rm int}}{w\sigma^2}\right) = \mathcal{N}\left(K(N-1), 2\sqrt{K\left(1-\frac{1}{N}\right)}\right) \simeq \mathcal{N}(K(N-1), 2\sqrt{K}). \tag{74}$$

Calculation of $\dot{S}^2_{\rm int}$

In the absence of external flux ($J = 0$) and for small asymmetry σ, the stationary state can be written as $p_i^* = \frac{1}{N}(1 + \sigma q_i)$. The values of q_i can be retrieved solving the master equation at stationarity:

$$0 = \sum_j A_{ij} w \left((1 + \sigma\epsilon_{ji}) \left(\frac{1}{N} (1 + \sigma q_j) \right) - (1 + \sigma\epsilon_{ij}) \left(\frac{1}{N} (1 + \sigma q_i) \right) \right), \tag{75}$$

that, up to first order in σ, leads to the implicit solution:

$$q_i = \frac{1}{k_i} \left(-\sum_j A_{ij} D_{ij} + \sum_j A_{ij} q_j \right), \tag{76}$$

where $k_i = \sum_j A_{ij}$ is the number of nodes connected to node i. For convenience, we introduce self-interactions ($A_{ii} = 1$), as this choice does not change the dynamics in the master equation and leads to simpler expressions in our notation. In the fully connected network ($A_{ij} = 1$), the second term on the r.h.s. of eq. (76) vanishes (as $\sum_j q_j = 0$), leading to the closed form $q_i = -\frac{1}{N} \sum_j D_{ij}$. This result is rather intuitive: if, for instance, the average rate of the outgoing links in a node i is greater than the ingoing one (the same argument applies in the opposite case) $\sum_j \epsilon_{ij} > \sum_j \epsilon_{ji} \Longrightarrow \sum_{ij} D_{ij} > 0$, there is a net outgoing flux to its neighbors and therefore $q_i < 0$, or equivalently, $p_i^* < 1/N$.

For a general connectivity K, we can neglect the implicit term in eq. (76), leading to:

$$q_i \simeq -\frac{1}{k_i} \sum_j A_{ij} D_{ij}, \tag{77}$$

which turns out to be a rather accurate approximation, especially for large N, as illustrated Fig. 6 (left panel). Corrections to this formula are of $\mathcal{O}(N^{-1})$ (see Fig 6, right panel), and therefore can be neglected for large system sizes. Indeed, notice that the approximate form of eq. (77) does not satisfy the constraint $\sum_i p_i^* = 1 + \sigma \sum_i q_i/N = 1$ in general, but the error vanishes when $N \to \infty$.

We can introduce eq. (77) into eq. (70), obtaining:

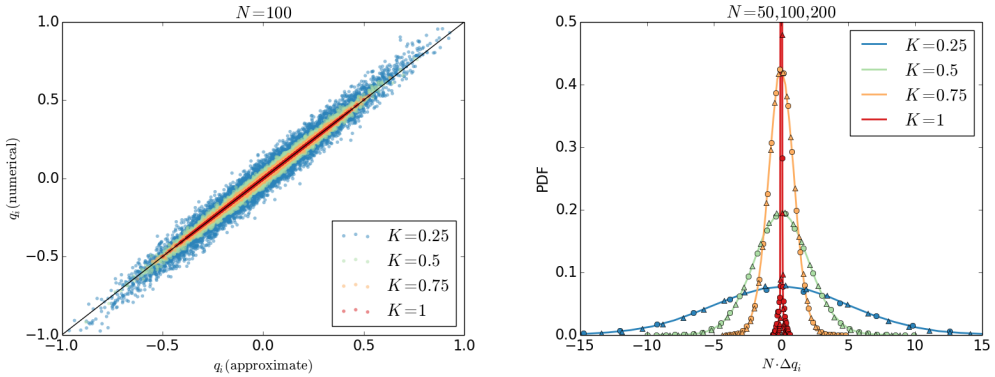

Figure 6: We generate random Erdos-Renyi topologies of mean connectivity K and size N, where each link $w_{i\to j}$ is an independent Gaussian variable of mean w and standard deviation σw. We set $w = 1$ and $\sigma = 10^{-2}$. In the absence of external flux ($J = 0$), we integrate numerically the associated master equation until stationarity, and calculate $q_i = (Np_i^* - 1)/\sigma$. **(Left panel)** We compare the numerical value of q_i with the one given by the approximation of eq. (77), for all the nodes in the network and for 10^3 randomly generated networks. Network size has been set to $N = 100$. **(Right panel)** PDF of the error made in eq. (77), rescaled with the system size N, for $N = 50$ (circles), $N = 100$ (solid line) and $N = 200$ (triangles), for different connectivities with the same colorcode as on the left panel. For each connectivity, the PDFs of the rescaled error $N\Delta q_i$ collapse into a single curve, illustrating that the error $\Delta q_i = \mathcal{O}(N^{-1})$.

$$\dot{S}^2_{\rm int} = -\frac{w\sigma^2}{N}\sum_i \frac{1}{k_i}\left(\sum_j A_{ij}D_{ij}\right)^2 . \tag{78}$$

For each i, $\sum_j A_{ij}D_{ij}$ is a Gaussian random variable with zero mean and variance $2(k_i - 1)$, and therefore $(\sum_j A_{ij}D_{ij})^2/k_i$ follows a chi-squared distribution of mean $2(1-k_i^{-1}) \simeq 2$ and variance $8(1-k_i^{-1})^2 \simeq 8$, as k_i^{-1} can be neglected for large network sizes.

Finally, we have to sum over nodes i; in principle, one cannot apply straightforwardly the Central Limit theorem, as the elements of the sum present correlations. Think, for instance, in the simple case of a triangle network, where one has to calculate $(D_{12} + D_{13})^2 + (D_{21} + D_{23})^2 + (D_{31} + D_{32})^2$, where $D_{ij} = -D_{ji}$. However, the number of correlated elements in the sum becomes negligible with the number of uncorrelated ones for large system sizes, so one can simply neglect such a correlation. After these approximations, we find:

$$P\left(\frac{\dot{S}^2_{\rm int}}{w\sigma^2}\right) \simeq \mathcal{N}\left(-2, \sqrt{\frac{8}{N}}\right) . \tag{79}$$

Notice that $\langle \dot{S}^2_{\rm int} \rangle$ is independent of N, whereas $\langle \dot{S}^1_{\rm int} \rangle$ grows linearly with N (eq. (74)). Therefore, the former can be neglected respect to the latter.

Calculation of $\dot{S}^3_{\rm int}$

We compute $\dot{S}^3_{\rm int}$ following a similar approach as for $\dot{S}^2_{\rm int}$. In the absence of asymmetry, $\sigma = 0$, and for small external flux J, the stationary state is written as $p^*_i = \frac{1}{N}(1 + Jr_i)$. To find r_i, we solve the master equation at stationarity:

$$0 = \sum_j A_{ij} \frac{w}{N} (r_j - r_i) J + J (\delta_{i1} - \delta_{iN}) \tag{80}$$

whose solution is:

$$r_i = \frac{N}{wk_i} \left(\delta_{i1} - \delta_{iN} + \frac{w}{N} \sum_j A_{ij} r_j \right). \tag{81}$$

In the fully connected network ($A_{ij} = 1$), the second term on the r.h.s. vanishes (since $\sum_j r_j = 0$), leading to $r_i = (\delta_{i1} - \delta_{iN})/w$. This means that all nodes have equal probabilities except for the 1st and Nth, that present a small unbalance $p_1 - p_N = 2J/(Nw)$. Consequently, $w_{eq} = Nw/2$ in the fully connected network). As we did for the calculation of $\dot{S}^2_{\rm int}$, we can use this solution as an approximation for a general connectivity K,

$$r_i \simeq \frac{N}{wk_i} (\delta_{i1} - \delta_{iN}). \tag{82}$$

As for the case of q_i, the approximate form above does not satisfy the constraint $\sum_i p^*_i = 1 + J \sum_i r_i/N = 1$ in general, but the error made vanishes when $N \to \infty$.

Plugging eq. (82) into eq. (71), we obtain:

$$\dot{S}^3_{\rm int} = \sigma J \left(\frac{1}{k_1} \sum_j A_{1j} D_{1j} - \frac{1}{k_N} \sum_j A_{Nj} D_{Nj} \right). \tag{83}$$

Let us remind that $\sum_j A_{ij} D_{ij}$ is a Gaussian variable with zero mean and variance $2k_i$. As we deal with Erdos-Renyi networks, we can assume that $k_1 \approx k_N \approx KN$; furthermore, if $A_{1N} = 0$, there is no correlation between the first and the second contribution in eq. (83); otherwise, a small correlation

may exist for large network sizes N, but this can be neglected. With these approximations, we finally obtain that

$$P\left(\frac{\dot{S}^3_{\rm int}}{\sigma J}\right) \simeq \mathcal{N}\left(0, \frac{2}{\sqrt{KN}}\right). \tag{84}$$

Observe that, $\langle \dot{S}^3_{\rm int} \rangle$ is independent of N, and therefore this contribution can be neglected respect to the one given by $\dot{S}^1_{\rm int}$.

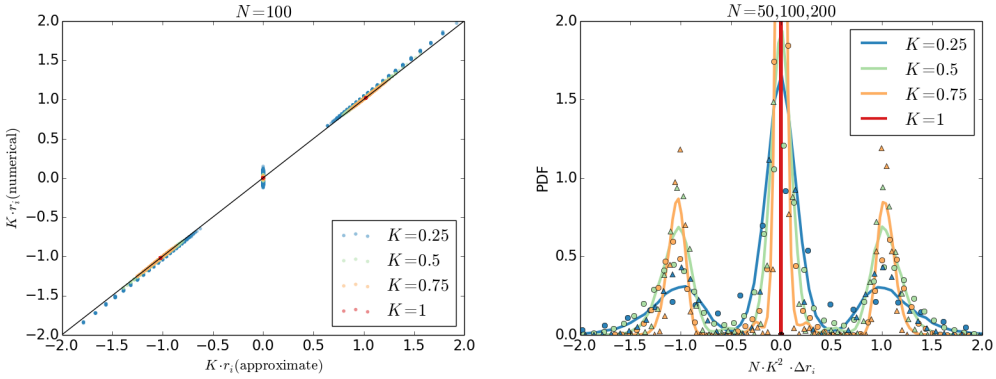

Figure 7: We generate random Erdos-Renyi topologies of mean connectivity K and size N, where each link $w_{i\to j} = w = 1$ (i.e. no asymmetry). The external flux is set to $J = 10^{-2}$. We integrate numerically the associated master equation until stationarity, and calculate $r_i = (Np_i^* - 1)/J$. **(Left panel)** We compare the numerical value of r_i with the one given by the approximation of eq. (82), for all the nodes in the network and for 10^3 randomly generated networks. Network size has been set to $N = 100$. **(Right panel)** PDF of the error made in eq. (82), rescaled with the system size, for $N = 50$ (circles), $N = 100$ (solid line) and $N = 200$ (triangles), for different connectivities with the same colorcode as on the left panel. In this case, we were able to capture also the scaling with the connectivity K. When rescaled properly, the location of the peaks approximately collapse, illustrating that the error made is $\Delta r_i = \mathcal{O}(K^{-2}N^{-1})$.

Distribution of $\dot{S}_{\rm int}$

We can obtain the PDF of $\dot{S}_{\rm int}$ assuming that, approximately, $\dot{S}_1$, $\dot{S}_2$ and $\dot{S}_3$ are independent random variables, so from Eqs. (74), (79) and (84) we find:

$$P\left(\dot{S}_{\rm int} = \dot{S}_1 + \dot{S}_2 + \dot{S}_3\right) \simeq$$
$$\mathcal{N}\left((K(N-1)-2)w\sigma^2, \sqrt{\left(4K\left(1-\frac{1}{N}\right)+\frac{8}{N}\right)(w\sigma^2)^2 + \frac{4}{KN}(\sigma J)^2}\right)$$
$$\xrightarrow{N\gg 1} \mathcal{N}\left((KN-(2+K))w\sigma^2, 2\sqrt{K}w\sigma^2\right), \tag{85}$$

where in the last expression we have considered the leading contribution for large system size N.

2.9.2 Distribution of $w_{\rm eq}$

The equivalent transition rate is defined close to equilibrium as $w_{\rm eq} = \frac{J}{p_1^* - p_N^*}$ when $\sigma = 0$. Introducing the explicit form of $p_i^* \simeq (1 + Jr_i)/N$, where r_i has the form of eq. (82) in large networks, we obtain:

$$w_{\rm eq} \simeq w \frac{k_1 k_N}{k_1 + k_N}. \tag{86}$$

Consequently, variability in $w_{\rm eq}$ comes, essentially, from the variability in the degrees of k_1 and k_N. We check numerically the validity of eq. (86). To this end, we generate master-equation systems described by random networks of size N and connectivity K, and for each one we compare the corresponding value of w_{eq} (obtained integrating numerically the master equation) with the one given by eq. (86). The result is plotted in Fig. 8 in log-log scale, showing a good agreement, especially for large network sizes and higher connectivities.

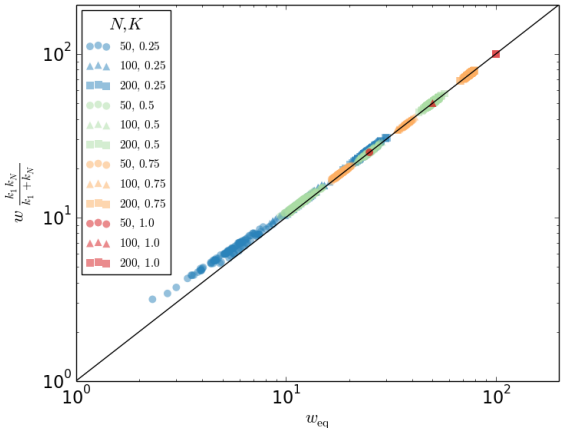

Figure 8: Comparison between $w_{\rm eq}$ with the approximation given by eq. (86) in symmetric master-equation systems with networks of size $N = 50, 100, 200$ and connectivity $K = 0.25, 0.5, 0.75, 1$. All existing links in the network has a rate value $w = 1$. For each network, $w_{\rm eq}$ has been obtained by integrating numerically the master equation with an additional external flux $J = 0.01$, and then calculating $w_{\rm eq} = (p_1^* - p_N^*)/J$.

The distribution of $w_{\rm eq}$ must be computed from the degree distribution of an Erdos-Renyi network of connectivity K, which is given by the binomial distribution $p(k) = \binom{N}{k} K^k (1-K)^{N-k}$. For large N, the binomial distribution

behaves as a Gaussian distribution with mean NK and variance $NK(1-K)$, and neglecting the correlation between k_1 and k_N we can write:

$$P(w_{\rm eq}) \simeq \int_{-\infty}^{\infty}\int_{-\infty}^{\infty} \delta\left(w_{\rm eq} - w\frac{k_1 k_N}{k_1+k_N}\right) P(k_1)P(k_N)dk_1 dk_N, \qquad (87)$$

where the limits of the integral have been extended the whole real axis and $P(k)$ represents a Gaussian distribution $\mathcal{N}(NK, \sqrt{NK(1-K)})$.

The non-linear dependency of w_{eq} on k_1 and k_N hinders the calculation of $P(w_{eq})$. However, as the Gaussian distributions becomes narrower (in relation to their mean) when N increases, we can calculate the PDF in the limit of large N using a saddle-point approximation. First, we write the delta function in terms of its Fourier representation:

$$P(w_{\rm eq}) = \int_{-\infty}^{\infty}\int_{-\infty}^{\infty}\int_{-\infty}^{\infty} \frac{1}{2\pi}\exp\left[-i\alpha\left(w_{\rm eq} - w\frac{k_1 k_N}{k_1+k_N}\right)\right] P(k_1)P(k_N)dk_1 dk_N d\alpha. \qquad (88)$$

Inserting the explicit form of $P(k)$, using the change of variables: $x_1 = \frac{k_1}{KN} - 1$, $x_N = \frac{k_N}{KN} - 1$, and introducing the intensive variable $\hat{w}_{\rm eq} = \frac{w_{\rm eq}}{N}$, we obtain:

$$\begin{aligned} P(w_{\rm eq}) &= \frac{NK}{(2\pi)^2(1-K)}\int_{-\infty}^{\infty}\int_{-\infty}^{\infty}\int_{-\infty}^{\infty} \exp\left[N\left(-i\alpha\left(\hat{w}_{\rm eq}\right.\right.\right. \\ &\left.\left.\left. -wK\frac{(1+x_1)(1+x_N)}{2+x_1+x_N}\right) - \frac{K}{2(1-K)}(x_1^2+x_N^2)\right)\right] dx_1 dx_N d\alpha \\ &\equiv \frac{NK}{(2\pi)^2(1-K)}\int_{-\infty}^{\infty}\int_{-\infty}^{\infty}\int_{-\infty}^{\infty} \exp\left[NF(x_1,x_N,\alpha)\right] dx_1 dx_N d\alpha. \end{aligned} \qquad (89)$$

The saddle-node approximation states that the integral $\int d^d z \exp[NF(\vec{z})] \simeq (2\pi/N)^{d/2}(-\det H(F)|_{\vec{z}^*})^{-1/2}\exp[Nf(\vec{z}^*)]$ in the limit of large N, where $\vec{z}^*$ is the stationary point of F, d its dimension and H the Hessian matrix of F. Imposing $\partial_{x_1}F = \partial_{x_N}F = \partial_\alpha F = 0$, we can find that in our case the stationary point is located at $x_1^* = x_N^* = 2\frac{\hat{w}_{\rm eq}}{KN} - 1$, $\alpha^* = 4i\frac{kw-2\hat{w}_{\rm eq}}{k(1-k)w^2}$. After some calculations, and written in terms of the original variable $w_{\rm eq}$, we find:

$$P(w_{\rm eq}) \simeq \frac{1}{\sqrt{2\pi\frac{NK(1-K)}{8}w^2\left(3-2\frac{wKN}{2w_{\rm eq}}\right)}}\exp\left[-\frac{\left(w_{\rm eq}-\frac{wKN}{2}\right)^2}{2\frac{NK(1-K)}{8}w^2}\right]. \qquad (90)$$

As the PDF concentrates around $w_{\rm eq} \simeq \frac{wKN}{2}$ when N increases, $\left(3-2\frac{wKN}{2w_{\rm eq}}\right) \simeq 1$. Therefore, we finally obtain that

$$P\left(\frac{w_{\rm eq}}{w}\right) \simeq \mathcal{N}\left(\frac{NK}{2}, \sqrt{\frac{1}{8}NK(1-K)}\right). \qquad (91)$$

We can collapse data of $w_{\rm eq}$ for different ensembles into a single PDF by substracting the mean and rescaling by the standard deviation as obtainable from eq. (91). Results are shown in Fig. 9. Deviations from a perfect collapse (that are higher for smaller networks) must stem from finite size corrections to the scaling formulas (see Section 2.9.2).

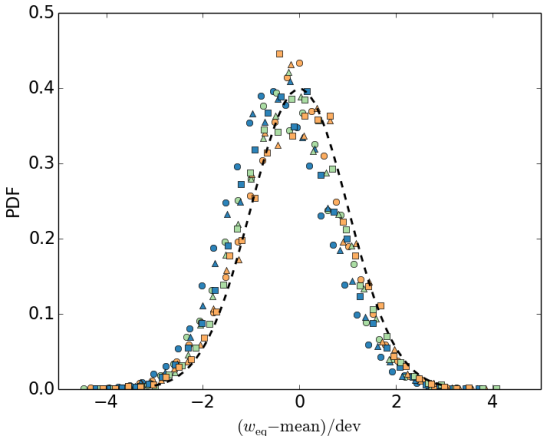

Figure 9: Collapse of the PDF for 9 datasets of $w_{\rm eq}$, for $K = 0.25$ (blue), $K = 0.5$ (green) and $K = 0.75$ (yellow), and for each one, for $N = 50$ (circles), $N = 100$ (triangles) and $N = 200$ (squares) (same datasets of Fig. 8), obtained by subtracting the corresponding mean $NKw/2$ and dividing by the standard deviation $NK(1-K)w/8$ on each data (Eqs. (93) and (94) for the left panel and Eqs. (95) and (96) for the right one). Dashed lines represent a Gaussian distribution of zero mean and unit variance. Deviations stem from finite size corrections, and indeed PDFs for larger system sizes fit better the Gaussian distribution.

Calculation of $\langle f(w_{\rm eq})\rangle$

We can calculate the expected value of some general function $f(w_{\rm eq})$ using the asymptotic form of $P(w_{\rm eq})$, Eq. (91). However, it can be useful to calculate next-to-leading order terms as it follows. We first write the expected value as

$$\begin{aligned}\langle f(w_{\rm eq})\rangle &= \int_{-\infty}^{\infty}\int_{-\infty}^{\infty} f\left(w\frac{k_1k_N}{k_1+k_N}\right)P(k_1)P(k_N)dk_1dk_N \\ &= \sum_{n,m=0}^{\infty}\frac{\mu_{2n}\mu_{2m}}{(2n)!(2m)!}\left.\frac{\partial f}{\partial k_1^{2n}\partial k_N^{2m}}\right|_{k_1=k_N=KN}, \end{aligned} \tag{92}$$

where μ_i is the i-th central moment of a Gaussian distribution of mean KN and variance $NK(1-K)$, and them simply truncate the series at the desired order. Using this expression, it is straightforward to calculate $\langle w_{\rm eq}\rangle$ expanding $\frac{k_1k_N}{k_1+k_N}$ up to the the forth moment:

$$\langle w_{\rm eq}\rangle = w\left(\frac{KN}{2}-\frac{1-K}{4}\right)-\frac{(1-K)^2}{8KN}+\mathcal{O}(N^{-2}) \tag{93}$$

and its variance $\langle\langle w_{\rm eq}^2\rangle\rangle = \langle w_{\rm eq}^2\rangle - \langle w_{\rm eq}\rangle^2$ from the expansion of $\left(\frac{k_1k_N}{k_1+k_N}\right)^2$:

$$\langle\langle w_{\rm eq}^2\rangle\rangle = \frac{w^2}{8}\left(NK(1-K)+2(1-K)^2\right)+\mathcal{O}(N^{-1}). \tag{94}$$

As expected, the leading orders agree with the mean and variance of $P(w_{\rm eq})$, eq. (91). Similarly, it is also useful to compute the mean and variance of $w_{\rm eq}^{-1}$ using the similar procedure; the result is:

$$\langle w_{\rm eq}^{-1}\rangle = \frac{2}{wKN}\left(1+\frac{1-K}{KN}\right)+\mathcal{O}(N^{-3}) \tag{95}$$

$$\langle\langle (w_{\rm eq}^{-1})^2\rangle\rangle = \frac{2(1-K)}{w^2(KN)^3}\left(1+20\frac{1-K}{KN}\right)+\mathcal{O}(N^{-5}). \tag{96}$$

Let us notice that the leading term of $\langle w_{\rm eq}^{-1}\rangle$ is the one used in the bottom panel of Fig. 5.

2.9.3 Distribution of $\epsilon_{\rm eq}$

To compute the unbalance parameter $\epsilon_{\rm eq}$, we set the external current to $J = 0$. In this setting, and for small asymmetry values, $\sigma \ll 1$, the stationary probability can be written as $p_i^* = 1/N(1 + \sigma q_i)$, so $\epsilon_{\rm eq}$ can be computed as:

$$\epsilon_{\rm eq} = \frac{p_1^* - p_N^*}{\sigma} = \frac{q_1 - q_N}{N}. \tag{97}$$

Introducing the approximation given by eq. (77) into the equation above, one finds the explicit formula:

$$\epsilon_{\rm eq} = \frac{1}{N}\left(\frac{1}{k_N}\sum_j A_{Nj}D_{Nj} - \frac{1}{k_1}\sum_j A_{1j}D_{1j}\right). \tag{98}$$

At this step, we neglect the heterogeneity in the connectivity degree and set $k_1 \simeq k_N \simeq KN$. Reminding that $D_{ij} = -D_{ji}$ are independent Gaussian variables for each pair of links with zero mean and variance 2, for large networks the Central Limit Theorem gives:

$$P(\epsilon_{\rm eq}) \simeq \mathcal{N}\left(0, \frac{2}{N\sqrt{KN}}\right), \tag{99}$$

where we have neglected a small correction arising if nodes 1 and N are connected (i.e. when $A_{1N} = 1$); in such a case the first and second term in eq. (98) would not be completely uncorrelated, as $D_{1N} = -D_{N1}$. In any case, this correction is negligible for large N.

2.9.4 Deviations from Joule's law

Close to equilibrium, we can write the total entropy production for asymmetric systems at stationarity as $\dot{S}^* = \dot{S}_{\mathcal{J}} + N\epsilon_{\rm eq}\sigma J + \dot{S}_{\rm int}$ (see text). Therefore, deviations from Joule's law, $\delta\dot{S}_{\mathcal{J}} = \dot{S}^* - \dot{S}_{\mathcal{J}}$ can be obtained combining the Gaussian distributions of $\epsilon_{\rm eq}$ (eq. (99)) and $\dot{S}_{\rm int}$ (eq. (85)):

$$\begin{aligned} &P\left(\delta\dot{S}_{\mathcal{J}} = \dot{S}_{\rm int} + N\epsilon_{\rm eq}\sigma J\right) \simeq \\ &\mathcal{N}\left((NK - (2+K))w\sigma^2, \sqrt{4K\left(w\sigma^2\right)^2 + \frac{4}{KN}\left(\sigma J\right)^2}\right) \\ &\xrightarrow{NK\gg 1} \mathcal{N}\left(NKw\sigma^2, 2\sqrt{K}w\sigma^2\right). \end{aligned} \tag{100}$$

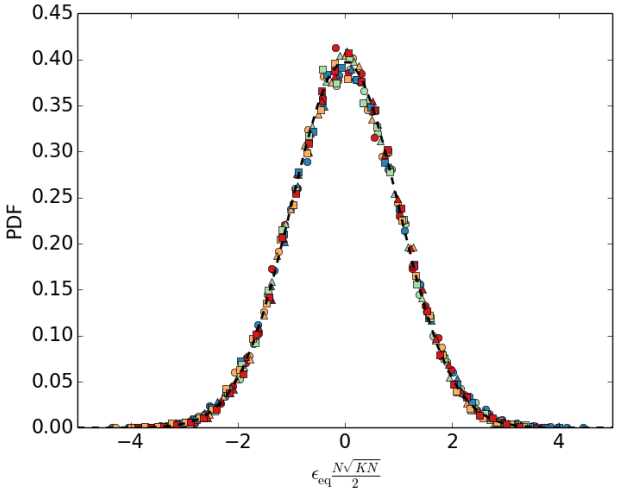

Figure 10: Collapse of different $P(\epsilon_{\rm eq})$ for asymmetric master-equation systems in ensembles of 10^4 networks of size $N = 50$ (circles), $N = 100$ (triangles) and $N = 200$ (squares), and for each one, for connectivities $K = 0.25$ (blue), $K = 0.5$ (green) and $K = 0.75$ (yellow). Link weights in the network are independent Gaussian variables of mean $w = 1$ and standard deviation $w\sigma = 0.01$. For each network, $\epsilon_{\rm eq}$ has been obtained by integrating numerically the master equation with the external flux $J = 0$, and then calculating $\epsilon_{\rm eq} = (p_1^* - p_N^*)/\sigma$. Dark dashed line represents the Gaussian distribution of zero mean and unit variance. The collapse has been obtained by dividing each value of $\epsilon_{\rm eq}$ by its corresponding standard deviation obtained analytically, $2/(N\sqrt{KN})$.

We can see that, for large systems, the contribution given by $\epsilon_{\rm eq}$ is negligible, obtaining the same result as in eq. (85).

2.10 Another thermodynamic validation

In literature there exist different justifications of the expression given by Schnakenberg for the entropy production [66, 23, 67, 61], but in this context we are interested in the ones lying on thermodynamic principles. Here we present a physical validation in terms of forces and fluxes, which acts also as an endorsement of the interpretation of Eq. (48) given in the original work and exposed in this chapter [80]. This constitutes a complete different approach from the one proposed before, but, again, it aims at understanding the thermodynamics behind the Schnakenberg's formula.

Consider a system amenable to be described by a Master Equation. Now we place this system in contact with two reservoirs with distinct sets of thermodynamic fields. This procedure keeps the system out of equilibrium.

In order to proceed further, we need to know the specific form of the

transition rates. Consider then a system for which the stationary state is an equilibrium state, i.e. the detailed balance holds. The transition rates are of the form:

$$w_{i\to j} = k_{ij}\left(\frac{p_i^*}{p_j^*}\right)^{1/2} \tag{101}$$

with $k_{ij} = k_{ji}$, such that $w_{i\to j}/w_{j\to i} = p_i^*/p_j^*$.

The equilibrium probability distribution is assumed to be the Gibbs distribution describing a system in contact with a reservoir exchanging heat and particles [82]:

$$p_i^* \propto exp^{-\beta(E_i-\mu N_i)} \tag{102}$$

where E_i and N_i are respectively the energy and the number of particles of the system, $\beta = 1/T$, where T is the temperature of the reservoir and k_B is taken equal to 1, and μ is the chemical potential of the reservoir.

Since in this model the system is in contact with two different reservoirs, we should have the following class of transition rates, each one belonging to a different reservoir:

$$w_{i\to j}^{(r)} = k_{ij}^{(r)} exp^{-\beta_r[(E_i-E_j)-\mu_r(N_i-N_j)]/2} \tag{103}$$

where the index $r = 1, 2$ indicates the reservoir.

Moreover, the system can also perform internal transitions that do not depend on the external reservoirs. Assume that these transitions can be described by:

$$\begin{aligned} w_{i\to j}^{(3)} = w_{j\to i}^{(3)} \quad & when\ E_i = E_j\ and\ N_i = N_j \\ w_{i\to j}^{(3)} = 0 \quad & otherwise \end{aligned} \tag{104}$$

Let us now evaluate the stationary entropy production, given by Eq. (55). It is easy to see that the only contribution is given by the two reservoirs, since the internal transitions produce no entropy at stationarity.

Since the flux of energy from the reservoir r into the system can be written as:

$$J_E = \sum_{ij} \gamma_{ij}^{(r)} w_{i\to j}^{(r)} p_j^* (E_i - E_j) \tag{105}$$

where $\gamma_{ij}^{(r)}$ is a projection operator that is equal to 1 if the transition between i and j is due to the class of transitions r ($r = 1, 2$ are the reservoirs, $r = 3$ is the internal class of transitions). Analogously, the flux of particles is:

$$J_N = \sum_{ij} \gamma_{ij}^{(r)} w_{i\to j}^{(r)} p_j^* (N_i - N_j) \tag{106}$$

Putting togheter all the formulas we obtain the following bilinear form for the stationary entropy production:

$$\dot{S}^* = X_E J_E + X_N J_N \tag{107}$$

where $X_E = 1/T_2 - 1/T_1$ and $X_N = \mu_1/T_1 - \mu_2/T_2$ are the thermodynamic forces conjugated to the energy and particle flux respectively. Summarizing, starting from the Schnakenberg's formula, we ended up with an expression of the stationary entropy production in terms of the thermodynamic fluxes and forces.

2.11 The meaning of an extremum principle

The framework proposed in our work provides a null-model on which compare the entropy production of specific systems and dynamics. In particular, some biological systems seem to have evolved in order to dissipate energy and produce entropy at the minimum or maximum possible rate [54, 57, 83]. It could be interesting to analyse the topological features of real dynamics (in particular the values of w_{eq} and ϵ_{eq}) with what we obtained for random networks, which have not been obtained through optimization/evolution processes.

The strong point is that we have to control just two parameters in order to understand the statistical properties of the entropy production of a system at stationarity. Nevertheless, a proper comparison with real-world systems could imply the application of this framework beyond the Erdos-Renyi random networks, and it could give us a deeper understanding on the meaning of an extremum principle of the entropy production.

This idea that living systems can adapt to cope with environmental changes can be analyzed also from a different perspective. In the Appendix A we present a work on this topic [77]. This collateral study is not related

to the analysis of the entropy production, but aim at justifying some empirical observations on the topology of the interaction network of living systems from the point of view of an optimization process.

In the next chapter we will try to go beyond the Master Equation dynamics and we will investigate the entropy production of system described by a Fokker-Planck equation.

3 Entropy production for coarse-grained dynamics

Countless works in the literature have investigated how coarse-graining influences our prediction of the physical properties of a system [51, 52, 50, 53]. In particular, we will focus on the coarse-graining of the dynamics. In fact, the Fokker-Planck equation can be obtained from a Master Equation, following a coarse-graining procedure [84, 60, 59, 85]. Here we aim at understanding how the entropy production changes passing from one description to the other by neglecting microscopic information.

3.1 Fokker-Planck equation

The Fokker-Planck equation is a second order partial differential equation describing how the probability to find a system in a certain position at a certain time evolves, starting from a given initial distribution [59, 60]. The general form is the following:

$$\frac{\partial p(z,t)}{\partial t} = -\sum_i \frac{\partial}{\partial z_i}\left[a_i(z,t)p(z,t)\right] + \frac{1}{2}\sum_{ij}\frac{\partial^2}{\partial z_i z_j}\left[b_{ij}(z,t)p(z,t)\right] \tag{108}$$

where $a_i(z,t)$ and $b_{ij}(z,t)$ are called, respectively, drift and diffusion coefficient. We have to add to this equation the initial condition on $p(z,t)$. Note that we are considering the general case of a n-dimensional state space.

The main difference between this description and the one provided by a Master Equation is constituted by the fact that here we are considering a probability distribution $p(z,t)$ which can change continuously, without performing jumps between states.

We note that Eq. (108) can also be written as a continuity equation:

$$\frac{\partial p(z,t)}{\partial t} + \sum_i \frac{\partial}{\partial z_i} J_i(z,t) = 0 \tag{109}$$

where $J_i(z,t)$ is a probability flux. Eq. (109) has the form of a conservation law. Supposing that $p(z,t)$ is defined over a volume Ω, the normalization condition, $\int_\Omega d^n z p(z,t) = 1$, can be interpreted as the absence of net flux across the boundaries of Ω:

$$0 = -\int_\Omega \sum_i \frac{\partial}{\partial z_i} J_i(z,t) d^n z = -\int_{\partial\Omega} \vec{J}\cdot\vec{n} dS \tag{110}$$

Also in this case, as for the Master Equation, we are interested only in the physical region, i.e. where $p(z,t)$ is non negative. Since Eq. (108) is linear in $p(z,t)$, a theorem on the second order partial derivatives ensures that there are no negative solutions to this equation [85].

In this section we will derive the Fokker-Planck equation following two different approaches, the first one consists in the derivation from the Chapman-Kolmogorov equation, while the second one lies on the so-called Kramers-Moyal expansion, which allows us to pass from a Master Equation dynamics to a Fokker-Planck equation, by making use of a coarse-graining procedure.

3.1.1 Derivation from Chapman-Kolmogorov equation

Consider the Chapman-Kolmogorov equation, Eq. (7), as introduced in the previous chapter. Let us remind that it is nothing but a rearrangement of the probability axiom in Eq. (8) for Markov processes. We have considered three working hypothesis, Eq.s (9) and (10). In the previous chapter we were interested in the derivation of the dynamical description of a jump process in term of probabilities, on the contrary here we want to describe a purely continous process. In other words, we want to avoid discrete jumps between states, let the probability $p(z,t)$ follow a continuous sample path [59, 60].

In order to do this, as already mentioned, we have to impose $W(z|x,t) = 0$, keeping $A_i(z,t)$ and $B_{ij}(z,t)$ in general different from zero.

Let us consider again an arbitrary function $f(z)$ that can be expanded as shown in Eq. (11). Following the same strategy as for the derivation of the Master Equation, and imposing the conditions that the process has a continous sample path, we obtain the following equation:

$$\begin{aligned} &\partial_t \int f(z) p(z,t|y,t') d^n z = \\ &= \int \left[-A_i(z,t)\partial_i f(z) + \frac{1}{2} B_{ij}(z,t)\partial_{ij} f(z) \right] p(z,t|y,t') d^n z \end{aligned} \tag{111}$$

where, for sake of simplicity, the sum is intended on repeated indices.

Then, we suppose that the process is confined in a region R. Integrating by parts and choosing $f(z)$ to be arbitrary but non-vanishing only in a subregion R' of R, Eq. (14) becomes:

$$\frac{\partial p(z,t)}{\partial t} = -\frac{\partial}{\partial z_i}\left[A_i(z,t)p(z,t)\right] + \frac{1}{2}\frac{\partial^2}{\partial z_i z_j}\left[B_{ij}(z,t)p(z,t)\right] \tag{112}$$

This equation has exactly the same form of Eq. (108), identifying $A_i(z,t)$ and $B_{ij}(z,t)$ with $a_i(z,t)$ and $b_{ij}(z,t)$, respectively.

3.1.2 Derivation from Master Equation: Kramers-Moyal expansion

Here we show another possible derivation of the Fokker-Planck equation. The latter, in fact, can be obtained as a limit of a Master Equation under proper conditions. The standard procedure to pass from one description to another is called Kramers-Moyal expansion [59, 60, 84, 85].

Consider a Master Equation system which performs jumps in a continuous state space. The dynamics describing this kind of process is shown in Eq. (15). Since in what follows we will deal with one-dimensional system, for sake of simplicity, let us write the following $1D$ continuous Master Equation:

$$\partial_t p(y,t) = \int dy' \left(W(y|y')p(y',t) - W(y'|y)p(y,t)\right) \tag{113}$$

where $W(y|y')$ is the rate related to the transition from the state y' to the state y. The latter can be rewritten in terms of the jump size $r = y - y'$ as follows:

$$\partial_t p(y,t) = \int dr \left(W(y-r,r)p(y-r,t) - W(y,-r)p(y,t)\right) \tag{114}$$

where $W(y,r)$ is the transition rate of a particle that starts from y and performs a jump of size r.

Suppose, now, that we can expand Eq. (114) around $r \approx 0$ up to the second order in r. This procedure lies on the assumption that the transition rates have to decay fast enough in space, such that this series expansion can capture all the dynamical information of the system. It is worth noting that we are passing from the description of a process with a discontinuous sample

path to the one of the same process as having a continuous sample path without losing, at least at this point, any information about the dynamics. The expansion around $r \approx 0$ leads to the following equation:

$$\partial_t p(y,t) = -\partial_y \left(\int dr r W(y,r) p(y,t) \right) + \frac{1}{2} \partial_{y^2} \left(\int dr r^2 W(y,r) p(y,t) \right) \tag{115}$$

that has the form of a Fokker Planck equation, making the following positions:

$$\begin{aligned} \int dr r W(y,r) &= a(y,t) \\ \int dr r^2 W(y,r) &= b(y,t) \end{aligned} \tag{116}$$

where the dependence of t in the transition rates has been omitted for sake of simplicity.

It is evident that we are keeping track just of the first two "pseudo-moments" of $W(y,r)$. We call them "pseudo-moments" because $W(y,r)$ does not represent a probability distribution. In other words, we have obtained a mapping between two different levels of description: the mesoscopic parameters (the drift $a(y,t)$ and the diffusion coefficient $b(y,t)$) can be estimated starting from the microscopic ones ($W(y,r)$) by getting rid of a certain amount of information, i.e. considering just the first two "pseudo-moments".

Here we have obtained a Fokker-Planck equivalent description for a Master Equation system, by neglecting some information about the shape of the transition rates $W(y,r)$. In this sense, the Kramers-Moyal expansion can be considered as a coarse-graining procedure of the dynamics, which can influence (and it does, as we will show later) our estimation of the physical features characterizing the system of interest, in particular the value of the entropy production.

3.2 Stochastic differential equations (SDE)

There is another equivalent way to obtain a Fokker-Planck equation, which is based on the theory of the stochastic differential equations. Since this is a fundamental topic that will be useful by itself throughout this chapter, we have dedicated this section to its analysis [59, 60].

Let us start by considering a particle on which act two different kinds of forces, a deterministic and a stochastic one. The physical meaning of a stochastic force has to be intended as the result of the effect of many degrees of freedom that cannot be controlled by a specific dynamics. Let us think to the simple example of a Brownian particle. The stochastic force represents nothing but the incessant impact of the "small" (respect to the particle) molecules of the surrounding liquid on the particle. The general equation describing a situation of this kind is called Langevin equation, it is classified as a stochastic differential equation (SDE) and it has the following general form:

$$\frac{dx}{dt} = \alpha(x,t) + \beta(x,t)\xi(t) \tag{117}$$

where $\alpha(x,t)$ identifies the deterministic motion, $\beta(x,t)$ is a known function related to the stochastic motion and $\xi(t)$ a rapidly fluctuating random term. Mathematically speaking, this means that, for $t \neq t'$, $\xi(t)$ is statistically independent from $\xi'(t)$. Adding also the requirement that $\langle \xi(t) \rangle = 0$, since any non-zero mean can be absorbed in $\alpha(x,t)$, we obtain:

$$\langle \xi(t)\xi(t') \rangle = \delta(t-t') \tag{118}$$

The formal solution of Eq. (117), as a SDE, is:

$$x(t) - x(0) = \int_0^t \alpha(x(t'),t')dt' + \int_0^t \beta(x(t'),t')dW(t') \tag{119}$$

where $dW(t)$ is defined as $\xi(t)dt$ and, formally speaking, it is the differential of a Wiener process.

Before moving on, let us summarize the main features of a Wiener process:

- a Wiener process is a stochastic process whose probability distribution satisfy the following Fokker-Planck equation:

$$\partial_t p(w,t) = \frac{1}{2}\partial_{w^2} p(x,t) \tag{120}$$

- The probability distribution of a Wiener process is then:

$$p(w,t_i|w',t_i') = \frac{1}{\sqrt{2\pi(t_i - t_i')}} exp^{-\frac{1}{2}\frac{(w-w')^2}{t_i - t_i'}} \tag{121}$$

In order to understand how $dW(t)$ has to be interpreted, let us start by discretizing Eq. (117):

$$x(t_i) = x(t_{i-1}) + \alpha(x(t_{i-1}), t_{i-1})\Delta t_i + \beta(x(t_{i-1}), t_{i-1}), t_{i-1})\Delta W(t_i). \quad (122)$$

Then we can write a discrete version of Eq. (119):

$$x(t_n) = x(t_0) + \sum_{i=1}^{n} \Delta t_i \alpha(x(t_{i-1}), t_{i-1}) + \sum_{i=1}^{n} \beta(x(\bar{t}_i), \bar{t}_i)\Delta W(t_i) \quad (123)$$

Note that the first summation represents the discretization of a standard integral, so we can arbitrarily choose to evaluate the function $\alpha(x,t)$ at the initial point of the dicrete interval $[t_{i-1}, t_i]$. On the contrary, the last summation involves a stochastic integral, so that, in principle, our choice of the point in which to evaluate $\beta(x,t)$ can influence its value. Indeed let us consider:

$$\bar{t}_i = \gamma t_i + (1-\gamma)t_{i-1} \quad (124)$$

$\bar{t}_i$ can take values in the whole discrete integral $[t_{i-1}, t_i]$, depending on the specific value of γ.

In order to understand if there exist a explicit dependence on γ in the value of the stochastic integral, let us take a specific example: $\beta(x,t) = W(t)$. Now we want to compute the mean value as follows:

$$\langle S_n \rangle = \sum_{i=1}^{n} \langle W(\bar{t}_i)\left(W(t_i) - W(t_{i-1})\right)\rangle \quad (125)$$

Note that it is easy to evaluate the correlation function of $W(t)$, obtaining, from Eq. (121), the following:

$$\langle W(t_i)W(s_i)\rangle = \int dw dw' w w' p(w, t_i; w', s_i | w_0 t_0)$$
$$= \int dw w^2 p(w, \min(t_i, s_i)|w_0 t_0) = w_0^2 + \min(t_i - t_0, s_i - t_0) \quad (126)$$

where we have used the fact that we are dealing with Markov processes. Resembling the mean of S_n, we get:

$$\langle S_n \rangle = \sum_i [\bar{t}_i - t_{i-1}] = \gamma(t_n - t_0) \tag{127}$$

From Eq. (127) it is evident that the mean value of the stochastic integral depends on γ, i.e. on the point in which we decide to evaluate the argument of the stochastic integral. To avoid this problem, we have to choose a specific presciption to perform this integral and, as a consequence, we have to find a way to consistently connect all the possible choices.

3.2.1 Ito prescription and Fokker-Planck equation

The first prescription we introduce is named by Ito, and it corresponds to the choice $\gamma = 0$. Mathematically speaking, we can define an Ito stochastic integral as follows:

$$\int dW(\tau)G(\tau) \xrightarrow{L^2} S_n = \sum_i G(t_{i-1}) \left(W(t_i) - W(t_{i-1})\right) \tag{128}$$

where L^2 is the notation for the L^2-convergence, i.e.

$$\lim_{n\to\infty} \langle \left(S_n - \int dW(\tau)G(\tau) \right)^2 \rangle = 0 \tag{129}$$

In this section we briefly review the properties of the Ito prescription:

- one can show that an Ito stochastic integral exists whenever the function $G(\tau)$ is continuous and non-anticipating, that is, for all s and t, with $t < s$, $G(t)$ is statistically independent of $W(s) - W(t)$;
- if $x(t)$ follows a Langevin dynamics as in Eq. (117), an arbitrary function $f(x(t))$ will obey to the following equation (the so-called Ito's formula):

$$\begin{aligned} df(x(t)) = &\left[\alpha(x(t),t)f'(x(t)) + \frac{1}{2}\beta(x(t),t)^2 f''(x(t),t)\right] dt \\ &+\beta(x(t),t)f'(x(t))dW(t) \end{aligned} \tag{130}$$

Note that the standard rules for the ordinary calculus do not hold in this case.

- It is possible to derive a Fokker-Planck equation from a Langevin dynamics as follows:

$$\langle df(x)\rangle = \langle \alpha(x,t)\partial_x f + \frac{1}{2}\beta(x,t)\partial_{x^2} f(x)\rangle dt = \int dx f(x)\partial_t p(x,t|x_0,t_0) \tag{131}$$

where $p(x,t|x_0,t_0)$ is the conditional probability density of $x(t)$. Now, as for the Chapman-Kolmogorov equation, we suppose that the process is confined in a region R. Choosing $f(x)$ to be arbitrary and non-vanishing only in a subregion R' of R, we can integrate by parts and neglect surface terms to obtain:

$$\int dx \left[-\partial_x \left(\alpha(x,t)p(x,t|x_0,t_0) + \frac{1}{2}\partial_{x^2}\left(\beta(x,t)^2 p(x,t|x_0,t_0)\right)\right)\right] f(x) = \int dx \partial_t p(x,t|x_0,t_0) f(x) \tag{132}$$

Noting that this equation has to hold for any $f(x)$, we recover the standard form of a Fokker-Planck equation, Eq. (108), identifying:

$$\begin{aligned} \alpha(x,t) &= a(x,t) \\ \beta^2(x,t) &= b(x,t) \end{aligned} \tag{133}$$

3.2.2 Stratonovich prescription and Fokker-Planck equation

The second prescription we introduce is relative to the choice $\gamma = 1/2$ and it is called Stratonovich prescription. As for the Ito's case, we define the Stratonovich stochastic integral by a L^2 convergence as follows:

$$\int dW(\tau)G(\tau) \xrightarrow{L^2} S_n = \sum_i G\left(\frac{t_i + t_{i-1}}{2}\right)(W(t_i) - W(t_{i-1})) \tag{134}$$

It is worth noting that in general there is no connection between Eq.s (134) and (128), since a stochastic integral has a meaning only after the specification of what kind of prescription we are using.

Here we summarize the main features of the Stratonovich stochastic integral:

- it can be show that a Langevin equation, Eq. (117), interpreted in the Stratonovich sense, is equivalent to the following Langevin equation, interpreted in the Ito sense, i.e. where the integrals have to be performed with the Ito prescription:

$$\dot{x} = \alpha(x,t) + \frac{1}{2}\beta(x,t)\beta'(x,t) + \beta(x,t)\xi(t) \tag{135}$$

- Using the mapping between Ito and Stratonovich prescription one can show that, in this case, the rules of ordinary differential calculus hold. In fact, if $x(t)$ follows a Langevin dynamics as in Eq. (117) interpreted in the Stratonovich sense, an arbitrary function $f(x(t))$ will obey to the following dynamics:

$$df(x(t)) = \left[\alpha(x(t),t)dt + \beta(x(t),t)dW(t)\right] f'(x(t)) \tag{136}$$

- From a Langevin equation it is easy to derive a Fokker-Planck equation of the system also in this case, obtaining the following equation:

$$\partial_t p(x,t) = -\partial_x \left(\alpha(x,t)p(x,t)\right) + \frac{1}{2}\partial_x \left(\beta(x,t)\partial_x \left(\beta(x,t)p(x,t)\right)\right) \tag{137}$$

The main physical difference between the choice $\gamma = 0$ or $\gamma = 1/2$ is that, in the latter case, we are supposing that our knowledge of the future can somehow influence the knowledge of the present, being also the end point of the discrete time interval t_i involved. This may sound to be not a physical reasonable approach, nevertheless it has a substantial mathematical advantage: the differential calculus can be performed in the ordinary way.

3.3 Entropy production for continuous systems

We have already shown the relevance of the entropy production and its role in different fields, from classical to stochastic thermodynamics. In this section we will define the entropy production for a continuous Master Equation and for a Fokker-Planck equation, since we aim at comparing these two different dynamical description.

3.3.1 For continuous Master Equation

Let us start from Eq. (15), that is the continuous version of the discrete-state Master Equation. We are interested in defining a measure of the entropy production in this continuous case.

The simplest form we can guess for the entropy production is a continuous version of the Schnakenberg formula:

$$\dot{S} = \int dzdx \left(W(z|x)P(x,t) \log \left(\frac{W(z|x)P(x,t)}{W(x|z)P(z,t)} \right) \right) \tag{138}$$

Eq. (138) has the form of a Kullback-Leibler divergence [86], then it is always positive and equal to zero if detailed balance holds, i.e. $W(z|x,t)p(x,t|y,t') = W(x|z,t)p(z,t|y,t')$. For these reasons, at first glance, Eq. (138) seems to be a good guess for the entropy production. We will justify further this formula a-posteriori, connecting our results to previous findings in literature.

In what follows, for sake of simplicity, we neglect the information about the initial conditions in the probability distribution.

3.3.2 For Fokker-Planck equation

The entropy production for a Fokker Planck equation has been found by Seifert [23] and here we aim at retracing the main steps of such a derivation.

The common definition of the Gibbs entropy in the continuous case [1]

$$S_s(t) = -\int dx p(x,t) \log p(x,t) \tag{139}$$

suggests the existence of a trajectory-dependent entropy, following the same procedure exposed for Master Equation systems:

$$s_s(t) = -\log p(x(t),t) \tag{140}$$

where the probability $p(x(t),t)$ obtained from the Fokker-Planck equation has to be evaluated along the stochastic trajectory $x(t)$ determined by the Langevin dynamics.

In this context we consider the following dynamics:

[1] in Eq. (139) the argument of the logarithm is not dimensionless. This problem has been widely discussed in literature [5, 6], and a possible solution is to use the relative entropy, defining a prior distribution to which compare $p(x,t)$ [86]. Here we use the definition, according to the derivation in [23].

$$\partial_t p(x,t) = -\partial_x j(x,t) = -\partial_x \left(\mu F(x,\lambda) - D\partial_x p(x,t)\right) \tag{141}$$

where $F(x,\lambda)$ is the external force, the diffusion coefficient is constant and λ is an external control parameter.

The rate of change of Eq. (140) is:

$$\begin{aligned} \dot{s}_s(t) &= -\frac{\partial_t p(x,t)}{p(x,t)}|_{x(t)} - \frac{\partial_x p(x,t)}{p(x,t)}|_{x(t)}\dot{x} \\ &= -\frac{\partial_t p(x,t)}{p(x,t)}|_{x(t)} + \frac{j(x,t)}{Dp(x,t)}|_{x(t)}\dot{x} - \frac{\mu F(x,\lambda)}{D}|_{x(t)}\dot{x} \end{aligned} \tag{142}$$

The last term can be related to the rate of the heat dissipated in the medium [18]:

$$\dot{q}(t) = F(x,\lambda)\dot{x} = T\dot{s}_{\mathrm{med}}(t) \tag{143}$$

where we are associating the heat dissipation into the medium to an increase in entropy at a certain temperature $T = D/\mu$. We can then write the following balance equation:

$$\dot{s}_{\mathrm{tot}}(t) = \dot{s}_s(t) + \dot{s}_{\mathrm{med}}(t) = -\frac{\partial_t p(x,t)}{p(x,t)}|_{x(t)} + \frac{j(x,t)}{Dp(x,t)}|_{x(t)}\dot{x} \tag{144}$$

in analogy to what we have shown in the previous section.

Upon averaging, the total entropy production has to become positive. Then, we first average over all the trajectories which at time time t are in the position $x(t)$, leading to:

$$\langle \dot{x}|x,t\rangle_{|x(t)} = \frac{j(x,t)}{p(x,t)} \tag{145}$$

After this, we average over the probability distribution $p(x,t)$, obtaining:

$$\dot{S}_{tot} = \langle s_s(t)\rangle = \int dx \frac{j(x,t)^2}{Dp(x,t)} \tag{146}$$

Eq. (146) represents the total entropy production for a system described by a Fokker-Planck equation in terms of only the drift and the diffusion coefficients, i.e. the mescoscopic variables.

3.4 Entropy production and coarse-graining in literature

Let us start now talking about the central problem of this chapter: the relation between coarse-graining and entropy production.

It is a well-known result that a coarse-graining procedure on a Master Equation leads to an underestimation of the entropy production. Since our work will present similar findings, even if from a completely different point of view, in this section we briefly review some previous results, aiming at helping the reader to understand the idea behind our analysis.

Consider a laboratory system whose dynamics can be described by a Master Equation, which is embedded in an environment [50]. Let us assume that the global system (laboratory plus environment) is amenable to be described, again, by a different Master Equation. If this global system is assumed to be isolated, the corresponding transition rates have to be symmetric, i.e.

$$w_{c\to c'} = w_{c'\to c} \tag{147}$$

where c is a possible configuration of the global system. This assumption lies on the fact that if the total system is finite and ergodic, the laboratory system can sustain a non-equilibrium state just for a transient period and it will eventually relax to an equilibrium state, in which detailed balance holds.

Since the laboratory is a part of the global system, there should be a map from its configurations i to the global configurations c:

$$\Pi : c \to i = \Pi(c) \tag{148}$$

that, in general, is not injective. This is intuitive, because for a given system configuration i there are many possible configurations c of the global system.

It is clear that the probabilities of a given system configuration can be obtained by coarse-graining over the possible global probabilities $\Pi(c)$ as follows:

$$p_i(t) = \sum_{c\in i} p_c(t) \tag{149}$$

where the sum is intended over all the configurations c with $\Pi(c) = i$.

If we define the probability current $J_{i\to j}(t) = p_i(t)w_{i\to j}$, the same rule holds also for these quantities:

$$J_{i\to j}(t) = \sum_{c\in i}\sum_{c'\in j} J_{i\to j}(t) \tag{150}$$

3.4.1 Instantaneous relaxation of the environment

We first consider the situation in which the environment equilibrates instantaneously, that is all the probability p_c belonging to the same laboratory state i are equal to $p_{c|i}$.

The entropy production of the global system can be written as:

$$\dot{S}_{\text{global}} = \sum_{c}\sum_{c'} J_{c\to c'} \log\frac{p_c}{p_{c'}} = \sum_{i}\sum_{j}\sum_{c\in i}\sum_{c'\in j} J_{c\to c'} \log\frac{p_c}{p_{c'}} \tag{151}$$

Using the equilibration condition we obtain:

$$\dot{S}_{\text{global}} = \sum_{ij} p_{c|i} \log\frac{p_{c|i}}{p_{c'|j}} \sum_{cc'} w_{c\to c'} \tag{152}$$

It is easy to see that, in this case, the Schnakenberg entropy production of this system can be reduced exactly to the same expression:

$$\begin{aligned}\dot{S} = \sum_{ij} J_{i\to j} \log\frac{J_{i\to j}}{J_{j\to i}} &= \sum_{ij}\left(p_{c|i}\sum_{cc'} w_{c\to c'}\right)\log\frac{p_{c|i}\sum_{cc'} w_{c\to c'}}{p_{c'|j} w_{c'\to c}} \\ &= \sum_{ij} p_{c|i}\log\frac{p_{c|i}}{p_{c'|j}}\sum_{cc'} w_{c\to c'} = \dot{S}_{\text{global}}\end{aligned} \tag{153}$$

3.4.2 Schankenberg's formula as a lower bound

In the more general case, we can derive an inequality between the Schnakenberg entropy production and the entropy production of the global system. To this aim let us define a function $h(x,y) = (x-y)\log(x/y)$. Then, we can write:

$$\dot{S} = \frac{1}{2}\sum_{ij}(J_{i\to j} - J_{j\to i})\log\frac{J_{i\to j}}{J_{j\to i}} = \frac{1}{2}\sum_{ij} h(J_{i\to j}, J_{j\to i}) \tag{154}$$

Analogously, we obtain:

$$\dot{S}_{\text{global}} = \frac{1}{2} \sum_{cc'} h(J_{c\to c'}, J_{c'\to c}) \tag{155}$$

Assuming that n_i is the number of global configuration c consistent with the laboratory state i and $n = n_i n_j$, it is possible to derive the following inequality:

$$\begin{aligned} h(J_{i\to j}, J_{j\to i}) &= h\left(\frac{1}{n}\sum_{c\in i}^{n_i}\sum_{c'\in j}^{n_j} J_{c\to c'}, \frac{1}{n}\sum_{c\in i}^{n_i}\sum_{c'\in j}^{n_j} J_{c'\to c}\right) \\ = \frac{1}{n} h\left(\sum_{c\in i}^{n_i}\sum_{c'\in j}^{n_j} J_{c\to c'}, \sum_{c\in i}^{n_i}\sum_{c'\in j}^{n_j} J_{c'\to c}\right) &\leq \frac{1}{n}\sum_{c\in i}^{n_i}\sum_{c'\in j}^{n_j} h(J_{c\to c'}, J_{c'\to c}) \end{aligned} \tag{156}$$

Summing over i and j on both sides, eliminating the factor $\frac{1}{n}$ and dividing by 2, we straightforwardly obtain the following inequality between the values of the entropy productions:

$$\dot{S} \leq \dot{S}_{\text{global}} \tag{157}$$

Here we have presented an estimation of the entropy production by embedding our system into a larger environment. We have shown that the formula found by Schnakenberg is exact only in the case of instantaneous equilibration, since Schnakenberg himself derived this formula by using methods of equilibrium thermodynamics.

Moreover, another possible interpretation of this results is that, by coarse-graining the system (neglecting the information about c and c', keeping only the ones on i and j), we can just underestimate the entropy production, at least in this setting where we are assuming that our system is amenable to be described as a discrete-state Markov process obeying a Master Equation.

The work here presented is not the only result on the relation between entropy production and coarse-graining. In particular, it is worth citing the work done by Esposito using a thermodynamic setting [51], then developed further in the context of hidden entropy production [87, 88, 89] and the work done by Bo and Celani where the coarse-graining is performed on the temporal scale [53].

3.5 Introduction to the problem

So far we have introduced two different definitions of the entropy production, each one referring to a different underlying dynamical model.

On one hand, for a Master Equation type of dynamics, we can estimate the entropy production by using the Schnakenberg formula, Eq. (31), which has been extensively analyzed in the previous chapter; on the other hand, if the system obeys a Langevin dynamics, which in turn can be mapped into a Fokker-Planck equation, the value of entropy production is predicted by the Seifert's formula, given in Eq. (146).

We have also seen that it is possible to describe the same system both using a Master Equation and a Fokker-Planck equation, passing from one to the other using the Kramers-Moyal expansion. To some extent, this procedure constitutes a coarse-graining procedure performed on the system, since we neglect all the details of the transition rates $W(y, r)$, keeping only its first two "pseudo-moments".

In this section we want to address the following basic question: how Eq. (31) and Eq. (146) are related?

Since both these formulas give an estimation of the entropy production for the same system, but described at a different level of coarse-graining, naively we could expect a relation between the two. Nevertheless, we know that the coarse-graining can play a non trivial role in the estimation of the entropy production, than we would like to quantify this effect in this case.

Note that the main difference of this approach is that we are dealing with a coarse-graining at the level of the dynamics, in the sense that we are comparing two different, but related, descriptions. We aim at finding a refinement of the Seifert's formula for the entropy production which can include the corrections given by all the neglected information.

3.6 An illustrative example: n-step random walk

Let us first consider the very simple model of a one-dimensional random walk on a ring that can make jumps of length $k = 1, 2, ..., n$ at any time in both directions, as sketched in Fig. 11 (for $n = 2$). Jump rates are:

$$w_{i\to j} = \begin{cases} W_{\pm k}\delta_{j,i+k}, & k = 1, ..., n \\ 0 & \text{otherwise.} \end{cases} \tag{158}$$

The associated master equation can be written in terms of the incoming and outgoing probability currents on each node,

$$\dot{p}_i(t) = \mathcal{J}_i^{\text{in}}(t) - \mathcal{J}_i^{\text{out}}(t) \tag{159}$$

where we have used the following definition for the ingoing and outgoing currents:

$$\mathcal{J}_i^{\text{in}}(t) = \sum_k \mathcal{J}_{i-k}^{(k)}(t), \tag{160}$$

$$\mathcal{J}_i^{\text{out}}(t) = \sum_k \mathcal{J}_i^{(k)}(t) \tag{161}$$

with $\mathcal{J}_i^{(k)}(t)$ is the microscopic probability current of the node i:

$$\mathcal{J}_i^{(k)}(t) = W_{+k}P_i(t) - W_{-k}P_{i+k}(t), \quad k = 1, ...n. \tag{162}$$

Note that this definition of the current is slightly different respect to the one used before in this chapter, but it is just a matter of convenience.

Schnackenberg's entropy production can be written in terms of these microscopic currents as:

$$\dot{S}_{\text{ME}} = -\sum_i \sum_k \mathcal{J}_i^{(k)}(t) \log\left(1 - \frac{\mathcal{J}_i^{(k)}(t)}{W_{+k}P_i(t)}\right). \tag{163}$$

We are interested in the continuous limit of the Master Equation and, as a consequence, of Eq. (175). To this aim, consider this random walk to be in a continuous space, so we have to understand how the currents and the transition rates scale with the space interaval Δx.

Moreover, performing a Kramers-Moyal expansion of the Eq. (159), we end up with a Fokker-Planck equation with a certain drift and diffusion coefficient. In order to obtain a macroscopic contribution for the latter two quantities, the terms $\mathcal{J}_i^{(k)}$ should scale with Δx^{-1} and $W_{\pm k}$ with Δx^{-2}. Therefore, the argument of the logarithm approaches to 1 in when $\Delta x \to 0$. Expanding in series of Δx and taking the continuous limit, the entropy production is:

$$\dot{S}_{\text{ME}}^{\Delta x \to 0} = \sum_k \int dx \frac{\mathcal{J}^{(k)}(x,t)^2}{D^{(k)}p(x,t)}, \tag{164}$$

where we have defined the following quantities in the continuous limit:

$$\mathcal{J}^{(k)}(x,t) = \lim_{\Delta x\to 0} k\mathcal{J}^{(k)}_{i(x)}\Delta x \tag{165}$$

$$D^{(k)} = \lim_{\Delta x\to 0} k^2 W_{+k}\Delta x^2. \tag{166}$$

with $\mathcal{J}^{(k)}(x,t)$ the probability current (crossing the point x at time t) that should appear in the Fokker-Planck equation if we consider just the particular process with steps of size k. Since the whole process contains jumps of size $k = 1, ...n$, the probability current of the Fokker-Planck equation is actually $\sum_{k=1}^{n}\mathcal{J}^{(k)}$.

Notice that, when $\Delta x \to 0$, $W_{+k} \approx \frac{1}{2}(W_{-k} + W_{+k})$, and therefore $D^{(k)}$ is the diffusion coefficient for the process with jump of size k. Also in this case the whole process, in a Fokker-Planck type of description, has a diffusion coefficient that is $\sum_{k=1}^{n} D^{(k)}$. In this example we are considering a constant diffusion coefficient as in the setting proposed by Seifert to derive his seminal expression for the entropy production.

Now we introduce an alternative way to write the master equation. Let us consider the current accounting for *all* the probability flux crossing a fictitious barrier located at node i (see Figure):

$$J_i(t) = \sum_k \mathcal{J}^{(k)}_{i-k}(t) + \sum_{k>1}\sum_{m=1}^{k-1}\mathcal{J}^{(k)}_{i-m}(t) = \sum_k\sum_{m=1}^{k}\mathcal{J}^{(k)}_{i-m}, \tag{167}$$

so that $\dot{p}_i(t) = -(J_{i+1}(t) - J_i(t))$. Remarkably, $J_i(t)\Delta x$ gives in the continuous limit the probability current $J(x,t)$ in the Fokker-Planck equation, Eq. (108).

As the first remarkable point in this work, notice that if $\mathcal{J}^{(k)}_i = 0$ at stationarity (microscopic detailed balance condition) then $J_i = 0$ (mesoscopic detailed balance), but not the other way round. Consequently, mesoscopic equilibrium does not necessarily indicate that the underlying microscopic dynamics is also at equilibrium.

Let us now write the entropy production for the same system, described in the framework of a Fokker-Planck equation, as derived by Seifert:

$$\dot{S}_{\rm FPE} = \int dx \frac{(\sum_k \mathcal{J}^{(k)})^2}{\sum_k D^{(k)} p(x,t)} = \int dx \frac{J(x,t)^2}{Dp(x,t)} \tag{168}$$

where D is the constant diffusion coefficient (here named D instead of $b(x,t)$ for sake of clarity).

Note that Eq. (164) has the same form as Eq. (168), but for each "sub"-process involving jumps of only size k, with the sum performed over the number of different "sub"-processes.

Between Eq.s (164) and (168) he following inequality holds:

$$\dot{S}_{\mathrm{ME}}^{\Delta x \to 0} \geq \dot{S}_{\mathrm{FPE}} \tag{169}$$

The prove of Eq. (169) is performed by considering the following integral:

$$\int \sum_k \left[\left(\frac{J^{(k)}(x,t)}{D^{(k)}} - \frac{J(x,t)}{D} \right)^2 \frac{D^{(k)}}{p(x,t)} \right] dx = \dot{S}_{\mathrm{ME}} - \dot{S}_{\mathrm{FPE}} \geq 0 \tag{170}$$

3.6.1 Deriving the correction

We have demonstrated in general (also far from the steady state) that an inequality holds between the Schankenberg entropy production and the Seifert entropy production relative to the same system. Here we try to derive an explicit expression for the discrepancy at the stationarity.

For convenience, we rewrite the transition rates $W_{\pm k}$ in terms of the new variables w_k and α_k ($k = 1, 2$). Considering also the right scaling with the space interval Δx, we obtain:

$$W_{-k} = \frac{w_k}{\Delta x^2} \tag{171}$$

$$W_{+k} = (1 + \alpha_k \Delta x) \frac{w_k}{\Delta x^2}. \tag{172}$$

With this choice, the Kramers-Moyal expansion leads to a Fokker-Planck equation with

$$\begin{aligned} a(x,t) &= \alpha_1 w_1 + 2\alpha_2 w_2 \\ b(x,t) \equiv D &= w_1 + 4w_2 \end{aligned} \tag{173}$$

Higher-order terms are proportional to Δx^{n+1} ($n > 0$), and therefore can be neglected in the expansion.

It is easy to check that the stationary solution to the master equation with Eq. (175) corresponds to the homogeneous state $p_i^* = 1/N$, and therefore the Schnakenberg entropy production at stationarity is:

$$\dot{S}^*_{\rm ME} = \frac{\alpha_1 w_1}{\Delta x}\log\left(1+\alpha_1\Delta x\right) + \frac{\alpha_2 w_2}{\Delta x}\log\left(1+\alpha_2\Delta x\right), \tag{174}$$

that, expanding in series of Δx and taking the continuous limit $\Delta x \to 0$, can be simply written as:

$$\dot{S}^*_{\rm ME} = \alpha_1^2 w_1 + \alpha_2^2 w_2. \tag{175}$$

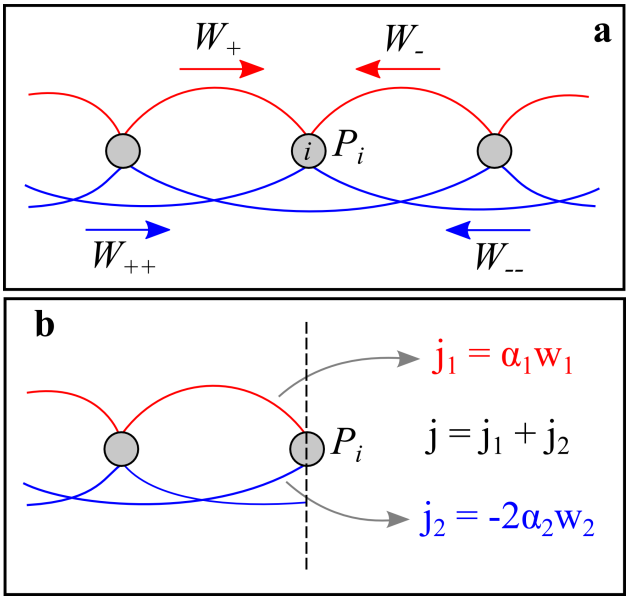

Figure 11: We use a two-step random walk as a simple example to derive the inequality between the entropy production evluated starting from the Master Equation and the one derived by a Fokker-Planck mesoscopic description. a) The microscopic model is sketched: the red lines indicate the one-step microscopic process, while the blue lines represent all the jumps of size 2. b) In coarse-graining the system we need to estimate the global current passing through a single state. The Kramers-Moyal expansion gives the exact expression of this quantity as the sum of one contribution due to the one-step process and two contribution from the two-step process, as depicted in the panel. The signs of the current depends on the particular choice for the transition rates, which is arbitrary and does not affect the results.

On the other hand, Seifert's formula for the entropy production in the mesoscopic dynamics (Eq. (146)) at stationarity leads to :

$$\dot{S}^*_{\rm FPE} = \frac{(\alpha_1 w_1 + 2\alpha_2 w_2)^2}{w_1 + 4w_2} = \dot{S}^*_{\rm ME} - \frac{w_1 w_2}{w_1 + 4w_2}(2\alpha_1 - \alpha_2)^2 \tag{176}$$

We can see that the two differs by a positive amount that keeps into account all the neglected information in passing from the microscopic description to the mesoscopic one. The extra term is zero, as expected, when there are no two-step jumps ($w_2 = 0$). Moreover, it is possible to explain this discrepancy as the contribution of the microscopic currents induced by the interplay between the one-step and the two-step process.

Interestingly, the previous result evidences that the definition of equilibrium depends on the level of description. Indeed, if $\alpha_1 w_1 = -2\alpha_2 w_2$ ($\alpha_{1,2}$ can be also negative), we obtain that $\dot{S}_{\mathrm{ME}} > 0$ whereas $\dot{S}_{\mathrm{FP}} = 0$. Consequently, the system may seem at equilibrium in a mesoscopic description, while detailed balance is violated at the microscopic level.

3.7 Refinement of the entropy production

In this section we aim at generalizing the conclusions stated in the simple example of a n-step random walk.

Let us start directly from the continuous expression of the Schankenberg entropy production, Eq. (138). We can rewrite this equation in terms of the jump size $r = y - y'$ as we did for the continuous Master Equation. Then we can perform the Kramers-Moyal expansion, taking the first and the second order around $r \approx 0$. Note that this procedure lies on the assumption previously stated that the transition rates should decay fast enough in space.

Since the derivation is quite cumbersome, let us consider for the moment the terms up to the first order:

$$\dot{S}^{(0)}_{\mathrm{KM}} + \dot{S}^{(1)}_{\mathrm{KM}} = \int dydr \left(W(y,r)P(y,t) \log\left(\frac{W(y,r)}{W(y,-r)}\right) - r\frac{\partial}{\partial y}\left[W(y,r)P(y,t)\right] \right.$$
$$\left. -r\frac{\partial}{\partial y}\left[W(y,r)P(y,t)\right] \log\left(\frac{W(y,r)}{W(y,-r)}\right)\right) \tag{177}$$

Now we introduce the following quantities:

$$J(y,t) = -a(y,t)P(y,t) + \frac{1}{2}\frac{\partial}{\partial y}[b(y,t)P(y,t)]$$
$$J_0(y,r,t) = \frac{1}{2}\left(W(y,r) - W(y,-r)\right)P(y,t)\log\left(\frac{W(y,r)}{W(y,-r)}\right)$$
$$J_1(y,r,t) = \frac{1}{2}\left(W(y,r) + W(y,-r)\right)P(y,t)\log\left(\frac{W(y,r)}{W(y,-r)}\right)$$
$$J_2(y,r,t) = \frac{1}{2}\frac{\partial}{\partial y}\left[\left(W(y,r) - W(y,-r)\right)P(y,t)\right]\log\left(\frac{W(y,r)}{W(y,-r)}\right) \qquad (178)$$

The first term is nothing but the probability flux of the Fokker-Planck equation, while the other terms keep track of the internal probability flux of the system due to the asymmetry between the transition rates.

The idea is to express the entropy production in terms of the known quantity of the FPE ($a(y,t)$ and $b(y,t)$). If this were possible, it will mean that no other iformation about the microscopic transition rates are needed and the coarse-graining will have no effect on this physical quantity. Since we know that this is not the case, we obtain:

$$\dot{S}^{(0)}_{\rm KM} + \dot{S}^{(1)}_{\rm KM} = \int dydrJ_0 - \int dy\frac{\partial}{\partial y}\left(\int drrW(y,r)P(y,t)\right)$$
$$-\int dydr\frac{1}{2}\frac{\partial}{\partial y}\left[r(W(y,r)+W(y,-r))P(y,t)\right]\log\left(\frac{W(y,r)}{W(y,-r)}\right) =$$
$$= \int dydrJ_0 - \int dy\frac{\partial}{\partial y}\left[a(y,t)P(y,t)\right] - \int drrJ_1|_{\rm ext}$$
$$+\frac{1}{2}\int dydrr(W(y,r)+W(y,-r))P(y,t)\frac{\partial_y W(y,r)W(y,-r) - W(y,r)\partial_y W(y,-r)}{W(y,r)W(y,-r)} =$$
$$= \int dydrJ_0 - \int dy\frac{\partial}{\partial y}\left(a(y,t)P(y,t)\right) - \int drrJ_1|_{\rm ext}$$
$$+\int dydrr\left(1+\frac{W(y,-r)}{W(y,r)}\right)P(y,t)\frac{\partial}{\partial y}[W(y,r)] \qquad (179)$$

where $|_{\rm ext}$ indicates that the quantity is evaluated at the extrema of the integration.

Now we want to add also the second order of the expansion, getting the following expression:

$$\dot{S}^{(2)}_{\rm KM} = \frac{1}{2}\left(\int dydr \frac{\partial^2[r^2 W(y,r)P(y,t)]}{\partial y^2} + \frac{\partial^2[r^2 W(y,r)P(y,t)]}{\partial y^2}\log\left(\frac{W(y,r)}{W(y,-r)}\right)\right.$$
$$\left. + \frac{\partial[r^2 W(y,r)P(y,t)]}{\partial y}\frac{\partial \log\left(W(y,r)P(y,t)\right)}{\partial y}\right) =$$
$$= \frac{1}{2}\int dy \frac{\partial^2}{\partial y^2}\left(\int dr r^2 W(y,r)P(y,t)\right) + \frac{1}{2}\int dr \frac{\partial[r^2 W(y,r)P(y,t)]}{\partial y}\log\left(\frac{W(y,r)}{W(y,-r)}\right)\Big|_{\rm ext}$$
$$-\frac{1}{2}\int dydr\left(\frac{\partial[r^2 W(y,r)P(y,t)]}{\partial y}\frac{\partial}{\partial y}\log\left(\frac{W(y,r)P(y,t)}{W(y,-r)P(y,t)}\right)\right.$$
$$\left. - \frac{\partial[r^2 W(y,r)P(y,t)]}{\partial y}\frac{\partial}{\partial y}\log\left(W(y,r)P(y,t)\right)\right) =$$
$$= \frac{1}{2}\int dy \frac{\partial^2}{\partial y^2}\left(b(y,t)P(y,t)\right) + \frac{1}{2}\int dr r^2 J_2|_{\rm ext} +$$
$$+\frac{1}{2}\int dydr r^2 \frac{\partial[W(y,r)P(y,t)]}{\partial y}\frac{\partial}{\partial y}\log\left(W(y,-r)P(y,t)\right) \qquad (180)$$

Then, joining Eq.s (179) and (180), we obtain:

$$\dot{S}_{\rm KM} = \int dr\left(\int dy J_0 - r J_1|_{\rm ext} + \frac{1}{2}r^2 J_2|_{\rm ext}\right)$$
$$-\int dy \frac{\partial}{\partial y}\left(a(y,t)P(y,t) - \frac{1}{2}\frac{\partial}{\partial y}\left(b(y,t)P(y,t)\right)\right)$$
$$+\int dydrr\left(1 + \frac{W(y,-r)}{W(y,r)}\right)P(y,t)\frac{\partial}{\partial y}[W(y,r)]$$
$$+\frac{1}{2}\int dydr r^2 \frac{\partial[W(y,r)P(y,t)]}{\partial y}\frac{\partial \log\left(W(y,-r)P(y,t)\right)}{\partial y} \qquad (181)$$

Notice that the argument of the second integral is nothing but the gradient of the flux in the Fokker-Planck, $J(y,t)$.

The expression in Eq. (181) is manifestly different from the one in Eq. (146) and this is the first central result of this chapter: since we are not neglecting a-priori some microscopic information (indeed starting from a Master Equation description), there are some different contributions that arise. This is a completely new definition of entropy production at an intermediate level of coarse-graining between Schnakenberg's and Seifert's formulas. If during

this coarse-graining procedure we are not losing any information about the system, then Eq. (181) and Eq. (146) should be exactly equal; we will then show than the latter is a very singular situation, while in general an inequality between the two expressions can be stated.

3.7.1 Gaussian transition rates

In order to evaluate Eq. (181) for a specific model, we need to propose a form of the transition rates $W(y, r)$. The simplest choice is to consider Gaussian transition rates:

$$W(y,r) = \frac{1}{\sqrt{2\pi D\epsilon}} \exp\left(-\frac{(r - a(y)\epsilon)^2}{2D\epsilon}\right) \tag{182}$$

With this choice for the transition rate the drift and diffusion coefficient of the corresponding Fokker-Planck equation are:

$$\begin{aligned} a(y,t) &= a(y)\epsilon \\ b(y,t) &= D\epsilon + \mathcal{O}(\epsilon^2) \end{aligned} \tag{183}$$

It is worth noting that ϵ is a new scale defined such that $\epsilon \to 0$ resembles the continous limit. Note also that the first and the second "pseudo-moments" of $W(y, r)$ are of the same order in ϵ, while all the higher ones are $\mathcal{O}(\epsilon^{\eta>1})$. This setting justifies a truncation of the Kramers-Moyal expansion up to the second order in r, which corresponds to the first order in ϵ.

Inserting Eq. (182) in Eq. (181) it is possible to see that:

$$\dot{S}_{\mathrm{KM}}(\tau) = \dot{S}_{\mathrm{FPE}}(\tau) = \int dy \frac{J(y,\tau)^2}{Dp(y,\tau)} \tag{184}$$

In writing this equation we have absorbed the expansion parameter ϵ in the time scale: $\tau = \epsilon t$.

Then there exist some particular forms of the transition rates for which our coarse-grained version of the entropy production is equal to the one obtained directly from a Fokker Planck equation. Physically speaking this means that, at least in the continuous limit, the value of the entropy production is not affected by any microscopic contribution. The form of $W(y, r)$ that leads to Eq. (184) is not unique, so the Gaussian shape is just a simple example.

3.8 Entropy production inequality

To extend this framework over the Gaussian case, we propose a more general form of $W(y,r)$ with the property that the first two "pseudo-moments" are of order ϵ and all the higher ones are of $\mathcal{O}(\epsilon^{\eta>1})$, as before. Our suggested expression is:

$$W(y,r) = \frac{1}{\sqrt{\epsilon D}} e^{-f\left(\frac{r-A(y)\epsilon}{\sqrt{\epsilon D}}\right)} \tag{185}$$

where f is an arbitrary function. Also in this case the first two "pseudo-moments" of $W(y,r)$ are the only ones of order ϵ, while the other are of order higher than ϵ. This justifies the truncation of the Kramers-Moyal expansion up to the first order in ϵ.

After some (quite general) conditions on the function f, we obtain the following inequality:

$$\lim_{\epsilon\to 0}\left(\dot{S}_{KM}(\tau) - \dot{S}_{FP}(\tau)\right) \geq 0 \tag{186}$$

where again $\tau = \epsilon t$ is a new time scale. In the next section we will provide the derivation of this inequality.

This equation constitutes the main result of this chapter, evidencing that, for a quite general choice of the transition rates, $W(y,r)$, neglecting a-priori the microscopic contributions leads to an underestimation of the entropy production. In other words, there exist some microscopic fluxes that make inroads in the system that cannot be ignored in a coarse-grained approximation of the dynamics.

As an example, we can choose $f(z) = |z|$. In this particular case it is possible to see that:

$$\dot{S}_{KM}(\tau) = \dot{S}_{FP}(\tau) + 2\int dy \frac{a(y)^2}{D} p(y,\tau) \tag{187}$$

where the correction term is a positive quantity.

The interpretation of Eq. (186) comes in the same spirit as in the simple example of the n-step random walk. As we can see in the next section, the only term that give this extra contribution is $\int dr \int dy J_0$. This has explicitly the form of an entropy production generated by a system in which $P(y-r,t) = P(y,t) + \mathcal{O}(\epsilon^2)$. We see that this is analogous to an infinite system where locally the probability is roughly the same, but the main contribution

to the entropy production stems from the unbalance between $W(y,r)$ and $W(y,-r)$; remarkably, in the previous example, the source of the discrepancy is given exactly by the same term.

3.8.1 Derivation of the inequality

In order to deal with the most general case, we can introduce a space dependence also in the diffusion coefficient:

$$W(y,r) = \frac{1}{\sqrt{\epsilon D(y)}} e^{-f\left(\frac{r-A(y)\epsilon}{\sqrt{\epsilon D(y)}}\right)} \tag{188}$$

First of all we calculate the coefficient of the Fokker-Planck equation that the transition rates in Eq. (188) will generate. Here, for sake of simplicity, $a^{(1)}(y) = a(y,t)$ and $a^{(2)}(y) = b(y,t)$, expliciting the fact that they represents the first two "pseudo-moments" of $W(y,r)$.

$$a^{(n)}(y) = \int r^n W(y,r) dr \to z = \frac{r - A(y)\epsilon}{\sqrt{D(y)\epsilon}} \to \int dz \sum_{k=0}^{n} \binom{n}{k} z^{n-k} e^{-f(z)} A(y)^k D(y)^{\frac{n-k}{2}} \epsilon^{\frac{n+k}{2}} =$$

$$= \sum_{k=0}^{n} \binom{n}{k} < z^{n-k} > A(y)^k D(y)^{\frac{n-k}{2}} \epsilon^{\frac{n+k}{2}} \tag{189}$$

where:

$$< z^n >= \int z^n e^{-f(z)} dz \quad \text{such that} < z >= 0 \tag{190}$$

We will see that we need the ansatz $< z >= 0$. Indeed, up to the first order in ϵ, we get:

$$\begin{aligned} a^{(1)} &=< z > \sqrt{D(y)\epsilon} + < z^0 > A(y)\epsilon =< z^0 > A(y)\epsilon \\ a^{(2)} &=< z^2 > D(y)\epsilon + < z^0 > A(y)^2\epsilon^2 =< z^2 > D(y)\epsilon \\ a^{(n>2)} &= \mathcal{O}\left(\epsilon^{\frac{n}{2}}\right) = 0 \end{aligned} \tag{191}$$

Now we want to introduce some other approximations that will be useful in what follows:

$$z = \frac{r}{\sqrt{\epsilon D(y)}} + \mathcal{O}(\sqrt{\epsilon}) \to \partial_y z(y) \approx -\frac{1}{2}\frac{1}{\sqrt{\epsilon D}}\frac{\partial_y D(y)}{D(y)} r \tag{192}$$

$$f\left(\frac{-r - A(y)\epsilon}{\sqrt{\epsilon D(y)}}\right) = f(-z) - \sqrt{\epsilon}\frac{2A(y)}{\sqrt{D(y)}}\partial_z f(-z) + \mathcal{O}(\epsilon) \tag{193}$$

Furthermore, because $< z >$ has to be null, the leading term in ϵ of $f(z)$ should be even, i.e. we guess that

$$f(z) = \sum_{n=0}^{2N} c_n z^n = \sum_{n=0}^{2N} c_n \frac{r^n}{\sqrt{\epsilon D(y)}^n} \approx c_{2N} \frac{r^{2N}}{\sqrt{\epsilon D(y)}^{2N}}$$
$$\partial_z f(-z) \approx c_{2N} 2N (-z)^{2N-1} \approx -\partial_z f(z) \tag{194}$$

Now we can consider term by term the entropy production in Eq. (181). To this aim we first split the entropy production in several terms, knowing, from the case of a Gaussian $W(y, r)$, which term is related to which one in the Seifert's formula. Then we ask ourselves whether the correction to each term due to this more general form of $W(y, r)$ is greater or equal to zero. If so, the Seifert's formula will be a lower bound for the entropy production of a stochastic system, neglecting the microscopic contributions which come from the detailed Master Equation dynamics. We proceed through the derivation of these terms, by splitting Eq. (181) as follows:

- Part 1 of $\dot{S}_{\rm KM} \to$ terms $a(y)$, $b(y)$ and $c(y)$;

$$\int \frac{r^2}{2}\partial_y(W(y,r)P(y,t))\partial_y(\log(W(y,-r)P(y,t)))dydr = \int a(y)\frac{(\partial_y P(y,t))^2}{P(y,t)}dy +$$
$$+ \int b(y)P(y,t)dy + 2\int c(y)\partial_y P(y,t)dy \tag{195}$$

where:

$$a(y) = \int \frac{r^2}{2} W(y,r) dr$$
$$b(y) = \int \frac{r^2}{2} \frac{(\partial_y W(y,-r))(\partial_y W(y,r))}{W(y,r)} dr$$
$$c(y) = \int \frac{r^2}{2} \left(\frac{W(y,-r)}{W(y,r)} + 1 \right) \partial_y W(y,r) dr \tag{196}$$

- Part 2 of $\dot{S}_{\mathrm{KM}} \rightarrow$ term $g(y)$;

$$-\int r \partial_y J_1(y,r,t) dy dr = \int g(y) \partial_y P(y,t) dy + \int \partial_y g(y) P(y,t) dy \tag{197}$$

where:

$$g(y) = -\int \frac{r}{2} \left(W(y,r) + W(y,-r) \right) \log \left(\frac{W(y,r)}{W(y,-r)} \right) dr \tag{198}$$

- Part 3 of $\dot{S}_{\mathrm{KM}} \rightarrow$ term $h(y)$;

$$\int r \left(1 + \frac{W(y,-r)}{W(y,r)} \right) \partial_y W(y,t) P(y,t) dy dr = \int \left(\partial_y a^{(1)}(y) + h(y) \right) dy \tag{199}$$

where:

$$h(y) = \int r \frac{W(y,-r)}{W(y,r)} \partial_y W(y,r) dr \tag{200}$$

- Part 4 of $\dot{S}_{\mathrm{KM}} \rightarrow$ terms $e(y)$ and $m(y)$;

$$\int \frac{r^2}{2} \partial_y J_2(y,r,t) dy dr = \int e(y) \partial_y^2 P(y,t) dy + \int \partial_y m(y) P(y,t) dy + \\ + \int \left(m(y) + \partial_y e(y) \right) \partial_y P(y,t) dy \tag{201}$$

where:

$$e(y) = \int \frac{r^2}{2}(W(y,r) - W(y,-r)) \log\left(\frac{W(y,r)}{W(y,-r)}\right) dr$$
$$m(y) = \int \frac{r^2}{2}\partial_y(W(y,r) - W(y,-r)) \log\left(\frac{W(y,r)}{W(y,-r)}\right) dr \qquad (202)$$

- Part 5 of $\dot{S}_{\mathrm{KM}} \rightarrow$ term $d(y)$;

$$\int J_0(y,r,t)dydr = \int d(y)P(y,t)dy \qquad (203)$$

where:

$$d(y) = \int (W(y,r) - W(y,-r)) \log\left(\frac{W(y,r)}{W(y,-r)}\right) dr \qquad (204)$$

Now we want to analyze each of these terms separately and compare them with the value that they will get if the Seifert expression were valid (evidenced by a S as apex). In order to do this, we have to return to the simple case in which the diffusion coefficient does not depend on space, i.e. $a^{(2)} = \langle z^2 \rangle D\epsilon$, as in the original work of Seifert [23].

- term $a(y) = a(y)^{(S)} + \mathcal{O}(\epsilon^2) = \frac{1}{2}a^{(2)} + \mathcal{O}(\epsilon^2)$

$$a(y) = \int \frac{r^2}{2} W(y,r)dr = \frac{1}{2}a^{(2)}(y) \qquad (205)$$

- term $b(y) \geq b(y)^{(S)} = 0$

$$b(y) = \int \frac{r^2}{2} \frac{(\partial_y W(y,-r))(\partial_y W(y,r))}{W(y,r)} dr =$$
$$= \int dr \frac{r^2}{2} \sqrt{\epsilon D} e^{f(z)} \partial_y \left(\frac{1}{\sqrt{\epsilon D}} e^{-f(z)} \right) \partial_y \left(\frac{1}{\sqrt{\epsilon D}} e^{-\left(f(-z) - \sqrt{\epsilon} \frac{2A(y)}{\sqrt{D}} \partial_z f(-z) \right)} \right) =$$
$$= \int dr \frac{r^2}{2} \frac{1}{\sqrt{\epsilon D}} e^{f(z)} \partial_y \left(e^{-f(z)} \right) \partial_y \left(e^{-f(z)} \right) =$$
$$= \int dr \frac{r^2}{2} \frac{1}{\sqrt{\epsilon D}} e^{-f(z)} \partial_z f(z) \partial_y z(y) =$$
$$= \int dr \frac{r^2}{2} \frac{1}{\sqrt{\epsilon D}} e^{-f(z)} \partial_z f(z) \left(-\frac{1}{2} \frac{1}{\sqrt{\epsilon D}} \frac{\partial_y D}{D} r \right) = 0 \qquad (206)$$

This term has no counterpart in the Seifert's formula, so it is enough to see that it is of order ϵ^2.

- term $c(y) \geq c(y)^{(S)} = 0$

$$c(y) = \int \frac{r^2}{2} \left(\frac{W(y,-r)}{W(y,r)} + 1 \right) \partial_y W(y,r) dr =$$
$$= \partial_y a^{(2)} + \int dr \frac{r^2}{2} \frac{e^{-\left(f(-z) - \sqrt{\epsilon} \frac{2A(y)}{\sqrt{D}} \partial_z f(-z) \right)}}{e^{-f(z)}} \partial_y \left(\frac{1}{\sqrt{\epsilon D}} e^{-f(z)} \right) =$$
$$= 0 + \int dr \frac{r^2}{2} \frac{1}{\sqrt{\epsilon D}} \frac{e^{-\left(f(z) + \sqrt{\epsilon} \frac{2A(y)}{\sqrt{D}} \partial_z f(z) \right)}}{e^{-f(z)}} e^{-f(z)} \partial_z f(z) \partial_y z(y) = 0 \quad (207)$$

- term $g(y) = g(y)^{(S)} + \mathcal{O}(\epsilon^2) = -2\epsilon A(y) \int W(y,r) dr + \mathcal{O}(\epsilon^2)$

$$g(y) = -\int \frac{r}{2} \left(W(y,r) + W(y,-r) \right) \log \left(\frac{W(y,r)}{W(y,-r)} \right) dr =$$
$$= -\int dr \frac{1}{\sqrt{\epsilon D}} \left(e^{-f(z)} + e^{-\left(f(z) + \sqrt{\epsilon} \frac{2A(y)}{\sqrt{D}} \partial_z f(z) \right)} \right) \log \left(\frac{e^{-f(z)}}{e^{-\left(f(z) + \sqrt{\epsilon} \frac{2A(y)}{\sqrt{D}} \partial_z f(z) \right)}} \right) =$$
$$= -\int dr \frac{r}{2} \frac{2}{\sqrt{\epsilon D}} e^{-f(z)} \sqrt{\epsilon} \frac{2A(y)}{\sqrt{D}} \partial_z f(z) =$$
$$= -2A(y)\epsilon \int dz e^{-f(z)} z \partial_z f(z) = -2A(y)\epsilon \langle 1 \rangle = -2a^{(1)} \qquad (208)$$

- term $h(y) = h(y)^{(S)} + \mathcal{O}(\epsilon^2) = \partial_y a^{(1)}(y) + \mathcal{O}(\epsilon^2)$

$$
\begin{aligned}
h(y) = \int r \frac{W(y,-r)}{W(y,r)} \partial_y W(y,r) dr = \\
= \int dr r \frac{e^{-\left(f(-z) - \sqrt{\epsilon}\frac{2A(y)}{\sqrt{D}}\partial_z f(-z)\right)}}{e^{-f(z)}} \partial_y \left(\frac{1}{\sqrt{\epsilon D}} e^{-f(z)} \right) = \\
= \partial_y a^{(1)} + \int dr r \frac{1}{\sqrt{\epsilon D}} \frac{e^{-\left(f(z) + \sqrt{\epsilon}\frac{2A(y)}{\sqrt{D}}\partial_z f(z)\right)}}{e^{-f(z)}} e^{-f(z)} \partial_z f(z) \partial_y z(y) = \partial_y a^{(1)}
\end{aligned}
\tag{209}
$$

- term $e(y) \geq e(y)^{(S)} = 0$

$$
\begin{aligned}
e(y) = \int \frac{r^2}{2} (W(y,r) - W(y,-r)) \log \left(\frac{W(y,r)}{W(y,-r)} \right) dr = \\
= - \int dr \frac{r^2}{2} \frac{1}{\sqrt{\epsilon D}} \left(e^{-f(z)} - e^{-\left(f(z) + \sqrt{\epsilon}\frac{2A(y)}{\sqrt{D}}\partial_z f(z)\right)} \right) \log \left(e^{-\sqrt{\epsilon}\frac{2A(y)}{\sqrt{D}}\partial_z f(z)} \right) = \\
= \int dr \frac{r^2}{2} \frac{1}{\sqrt{\epsilon D}} e^{-f(z)} \sqrt{\epsilon} \frac{2A(y)}{\sqrt{D}} \partial_z f(z) \sqrt{\epsilon} \frac{2A(y)}{\sqrt{D}} \partial_z f(z) = \\
= 2A(y)^2 \epsilon^2 \int dz e^{-f(z)} z^2 \left(\partial_z f(z) \right)^2 = 0 + \mathcal{O}(\epsilon^2)
\end{aligned}
\tag{210}
$$

- term $m(y) \geq m(y)^{(S)} = 0$

$$
\begin{aligned}
m(y) = \int \frac{r^2}{2} \partial_y (W(y,r) - W(y,-r)) \log \left(\frac{W(y,r)}{W(y,-r)} \right) dr = \\
= \int dr \frac{r^2}{2} \frac{1}{D} e^{-f(z)} \partial_y \left(2A(y) \partial_z f(z) \right) \sqrt{\epsilon} \frac{2A(y)}{\sqrt{D}} \partial_z f(z) = \\
= 2A(y) \epsilon^2 \int dz z^2 e^{-f(z)} \partial_y \left(A(y) \partial_z f(z) \right) \partial_z f(z) = 0 + \mathcal{O}(\epsilon^2)
\end{aligned}
\tag{211}
$$

- term $d(y) \geq d(y)^{(S)} = \left(a^{(1)}\right)^2 / a^{(2)}$

$$d(y) = \int \frac{1}{2}(W(y,r) - W(y,-r)) \log\left(\frac{W(y,r)}{W(y,-r)}\right) dr =$$
$$= -\int dr \frac{1}{2}\frac{1}{\sqrt{\epsilon D}}\left(e^{-f(z)} - e^{-\left(f(z)+\sqrt{\epsilon}\frac{2A(y)}{\sqrt{D}}\partial_z f(z)\right)}\right) \log\left(e^{-\sqrt{\epsilon}\frac{2A(y)}{\sqrt{D}}\partial_z f(z)}\right) =$$
$$= 2\frac{A(y)^2}{D}\epsilon \int e^{-f(z)} \left(\partial_z f(z)\right)^2 dz =$$
$$= 2\frac{\left(a^{(1)}\right)^2}{a^{(2)}}\frac{< z^2 >}{< 1 >^2} \int \left(\partial_z f(z)\right)^2 e^{-f(z)} dz =$$
$$= 2\frac{\left(a^{(1)}\right)^2}{a^{(2)}} \langle z^2 \rangle_0 \langle (\partial_z f(z))^2 \rangle_0 \tag{212}$$

where:

$$\langle \cdot \rangle_0 = \frac{\langle \cdot \rangle}{\langle 1 \rangle} \tag{213}$$

Putting all these terms togheter in the entropy production and using the Holder inequality, we obtain:

$$\dot{S} = 2\int dy \frac{(a^{(1)}P(y) - \frac{a^{(2)}}{2}\partial_y P(y))^2}{a^{(2)}P(y)} + 2\int dy \frac{\left(a^{(1)}\right)^2}{a^{(2)}} \left(\langle z^2 \rangle_0 \langle (\partial_z f(z))^2 \rangle_0 - 1\right) \geq$$
$$\geq \dot{S}_{Seifert} + 2\int dy \frac{\left(a^{(1)}\right)^2}{a^{(2)}} \left(|\langle z\partial_z f \rangle_0|^2 - 1\right) \geq \dot{S}_{Seifert} \tag{214}$$

where we have written the Seifert's formula in terms of the drift and diffusion coefficient. In particular,

$$\dot{S} = \dot{S}_{Seifert} \quad \textit{iff } \partial_z f(z) \propto z \rightarrow \textit{Gaussian transition rates} \tag{215}$$

This result confirms the finding of the previous section about the Gaussian transition rates and clearly shows that our entropy production is in general greater than the Seifert's entropy production. Our intuition about this finding is that the microscopic contributions play a fundamental role in determining the entropy production of a system and any coarse-graining process will necessarily generate an underestimation of this quantity, as previously stated in other works in literature.

3.9 Entropy production with a space-dependent diffusion coefficient

Our formula for the entropy production is valid in general, also when the diffusion coefficient depends on space. Although in this particular case we cannot compare directly our entropy production with the one derived by Seifert, it is interesting to note that, guessing the simple Gaussian form for the transition rate $W(y, r)$ as follows:

$$W(y,r) = \frac{1}{\sqrt{2\pi D(y)\epsilon}} \exp\left(-\frac{(r - a(y)\epsilon)^2}{2D(y)\epsilon}\right) \tag{216}$$

we end up with an expression for the entropy production that is composed by two terms: the first one is formally equivalent to the one derived by Seifert, while the second one is a correction which depends on the space dependence of $D(y)$:

$$\dot{S} = 2\int dy \frac{\left(a^{(1)}P(y) - \partial_y\left(\frac{a^{(2)}}{2}P(y)\right)\right)^2}{a^{(2)}P(y)} + \frac{3}{4}\int dy \frac{(\partial_y D(y))^2}{D(y)} P(y) \tag{217}$$

3.10 Conclusions

In this chapter we have derived a refinement of the formula for the estimation of the entropy production of a system whose dynamics can be described by a Fokker-Planck equation. It is clear that this new expression is useful only when some details on the microscopic underlying process are known, otherwise it will be impossible to keep track of the neglected information during the Kramers-Moyal expansion.

From a more general point of view, this result states that the process of coarse-graining leads to an underestimation of the entropy production, as pointed out by other works in literature [50, 53, 51, 52]. The main difference, as we said before, is that we have performed the coarse-graining at the level of the dynamics. In other words, one can pass from one dynamics to the other by ignoring details on the transition rates, leading to different formulations of the entropy production. The two different formulas that we obtain can nevertheless become equal for particular choices of the transition rates (e.g. Gaussian case).

Another important result which it is worth noting is that our framework enlighten the fact that the definition of equilibrium strongly depends on the level of description we are adopting, especially when we compare a Master Equation and a Fokker-Planck equation type of dynamics.

It will be very interesting, in the future, to see wheter this new formulation could lead to novel insights in all the cases in which additional microscopic information can be added in the physical modeling.

4 Mimicking non-equilibrium steady states with time-periodic driving

In this chapter we aim at connecting two different frameworks used to describe systems that operate out of equilibrium: the time-periodic driving and the non-equilibrium steady states. We will see that these two share a lot of common features that stimulate a possible mapping between them. In particular we briefly review some results derived for discrete-state Master Equation systems and then we formulate analogous results for continuous systems described by a Fokker-Planck equation.

4.1 Time-periodic driving

We already know that any ergodic system coupled to a thermal environment will spontaneously relax into an equilibrium state, which is well characterized by statistical mechanics and thermodynamics [38]. However, since many interesting phenomena, both in the microscopic and mesoscopic world, involve system constantly maintaned out of equilibrium [15, 16, 57, 54], we need a framework to characterize them.

A way to maintain a system out of equilibrium is to drive it by time-periodic changing some external parameters in the presence of a thermal reservoir. Typically, it is assumed that the dynamics satisfy detailed balance at every instant in time. In other words, if the parameters were suddenly frozen at their instantaneous values, the system would relax to an equilibrium state, satisfying detailed balance with the forces corresponding to the frozen parameters. We call this kind of procedure stochastic pumping (SP) or, in general, time-periodic driving.

A periodically driven system reaches a time-periodic state with a non-vanishing value of the current averaged over a period. These currents stems from the periodic variation of the parameters, and the cost associated to their generation is represented by the work invested in driving the parameters. Eventually, the energy provided by this work is dissipated into the thermal reservoir, resulting in a positive production of entropy.

The study of time-periodic driving has been stimulated by experiments on artificial molecular machines, which are controlled by the variation of external parameters (e.g. temperature, pressure, pH) to achieve some desired behavior [48, 49]. For instance, in experiments on mechanically interlocked ring-like

molecules the aim was to produce unidirectional rotation of one ring around the other [90]. Theoretical investigations have focused on weakly or slowly driven pumps [91, 92, 93], no-pumping theorems [94, 95, 96, 97, 98], the role of interactions and fluctuations [99, 100], and the ability to extract work from stochastic pumps [101]. The underlying aim is to produce controlled motion at the molecular level, where the fluctuations are large. The focus on time-dependent driving is mainly motivated by the difficulty of building artificial molecular systems driven by chemical potential differences, i.e. by a non detailed balance condition. It is often simpler to manipulate the system by varying external parameters.

4.1.1 Discrete-state description

Consider a system with N accessible states which obeys to a Master Equation with time-periodic transition rates:

$$\partial_t p_i(t) = \sum_{j=1}^{N} \left(w_{j\to i}(t) p_j(t) - w_{i\to j}(t) p_i(t) \right) \tag{218}$$

Eq. (218) can be rewritten as follows:

$$\partial_t \vec{p}(t) = \mathcal{W}(t)\vec{p}(t) \tag{219}$$

where $\mathcal{W}(t)$ is a $N \times N$ matrix such that $\mathcal{W}(t) = \mathcal{W}(t+T)$, with T the period of the external driving, encoded in the time dependence of the rate matrix $\mathcal{W}$.

We also know that, for a fixed value of the time t, $\mathcal{W}(t)$ has to admit a unique stationary solution $\vec{\pi}$, such that:

$$\mathcal{W}_{ij}(t)\pi_j - \mathcal{W}_{ji}(t)\pi_i = 0 \tag{220}$$

This is just a restatement of the detailed balance condition, implying that $\vec{\pi}$ is an equilibrium state for a particular time t.

Under Eq. (219) the system evolves asymptotically to a unique time periodic state $\vec{p}^{ps}(t) = \vec{p}^{ps}(t+T)$. For any solution of this kind, we can define the following time periodic quantities:

$$J_{ij}^{ps}(t) = \mathcal{W}_{ij} p_j^{ps} - \mathcal{W}_{ji} p_i^{ps}$$
$$\sigma_{ij}^{ps}(t) = J_{ij} \log \frac{\mathcal{W}_{ij} p_j^{ps}}{\mathcal{W}_{ji} p_i^{ps}} \tag{221}$$

representing, respectively, the instantaneous probability flux and the instantaneous entropy production for each pair of connected states i and j. Note that the entropy production has been evaluated using the Schnakenberg's formula.

Since we will be interested in comparing this scenario of time-periodic driving with the one provided using the framework of non-equilibrium steady states (that we will discuss in the next section), we introduce the following time-averaged quantities that will be useful in what follows [33]:

$$\overline{p_i^{ps}} = \frac{1}{T} \int dt p_i^{ps}(t)$$
$$\overline{J_{ij}^{ps}} = \frac{1}{T} \int dt J_{ij}^{ps}(t)$$
$$\overline{\sigma_{ij}^{ps}} = \frac{1}{T} \int dt \sigma_{ij}^{ps}(t) \tag{222}$$

A stochastic pumping protocol can be identified in terms of these three quantities only.

4.1.2 Fokker-Planck description

In the same vein as for discrete-state systems, we can extend the description to continuous systems.

Consider a system described as a diffusion process on a ring $x \in [-L, L]$ with the end points identified (periodic boundary conditions). First of all, we need a Fokker-Planck equation which is time-dependent and such that, for any fixed time t, it admits an equilibrium solution, i.e. a Boltzmann distribution [82]:

$$\pi(x) = \mathcal{N} \exp^{-\beta U(x,t)} \tag{223}$$

where β is the inverse temperature (with $k_B = 1$), $\mathcal{N}$ is the normalization factor and $U(x,t)$ is the value of the potential at time t.

It is easy to see that the following Fokker-Planck equation has all the required properties:

$$\partial_t p(x,t) = \gamma \partial_x \left((\partial_x U(x,t)) p(x,t) \right) + D \partial_{x^2} p(x,t) \tag{224}$$

where $U(x,t) = U(x,t+T)$ and $U(-L,t) = U(L,t)$. In this model the temporal variation of the parameters is encoded in the time dependent potential, while the diffusion coefficient D is kept constant.

By Floquet theory [102], the probability distribution $p(x,t)$ of such a system converges into a unique periodic state, both in x and t. We denote this unique periodic solution by $P^{ps}(x,t)$.

A probability distribution $p(x,t)$ evolving under Eq.(224) can be associated with a probability current, $J(x,t)$ defined by:

$$J(x,t) = -D \left[\partial_x p(x,t) + \beta p(x,t) \partial_x U(x,t) \right], \tag{225}$$

such that the probability obeys a continuity equation,

$$\partial_t p(x,t) + \partial_x J(x,t) = 0. \tag{226}$$

Of special interest (in analogy to the discrete-state case) will be the current associate with the periodic solution, which we denote by $J^{ps}(x,t)$ and which is given by:

$$J^{ps}(x,t) = -D \left[\partial_x p^{ps}(x,t) + \beta p^{ps}(x,t) \partial_x U(x,t) \right]. \tag{227}$$

It is worth noting that, by construction, the time-averaged value of $J^{ps}(x,t)$ must be constant in x: indeed, if we integrate the continuity equation Eq.(226) we get:

$$\begin{aligned} &\int_0^T \Big(\partial_t p^{ps}(x,t) + \partial_x J^{ps}(x,t) \Big) dt = \\ &= p^{ps}(x,T) - p^{ps}(x,0) + \partial_x \overline{J^{ps}(x,t)} = 0. \end{aligned} \tag{228}$$

The first two terms cancels due to the temporal periodicity of p^{ps}, hence $\overline{J^{ps}(x,t)}$ must be x independent. This implies that the same total probability flux must flow through all positions in a cycle.

In addition to probability densities and currents, we will be interested in the environment's entropy production given by

$$\dot{S}^{ps}(t) = \int dx \frac{J^{ps}(x,t)^2}{Dp^{ps}(x,t)} \tag{229}$$

In this case the entropy production has been evaluated using the Seifert's formula [23], since we have no information about the microscopic details of the process (see the previous chapter). Moreover, note that in this case we have defined the entropy production by integrating over the probability distribution $p(x,t)$, while, for a discrete-state system, we have considered the entropy production for each possible transition between states.

Again, also in this case, we define the following time-averaged quantities (over a period), which fully characterize, in our setting, a stochastic pumping protocol for a diffusive system:

$$\begin{aligned} \overline{p^{ps}(x)} &= \frac{1}{T}\int dt p^{ps}(x,t) \\ \overline{J^{ps}} &= \frac{1}{T}\int dt J^{ps}(x,t) \\ \overline{\dot{S}^{ps}} &= \frac{1}{T}\int dt \dot{S}^{ps}(t) \end{aligned} \tag{230}$$

4.2 Non-equilibrium steady states (NESS)

Although we have already introduced the concept of non-equilibrium steady states in the previous sections, here we will try to understand the main features which characterize them.

Consider a system coupled with more than one environment, e.g. several baths with different equilibrium properties as temperature or chemical potential. The constant fluxes between the baths can drive the system into a steady state which is not an equilibrium state, since it can be maintaned only at the cost of some thermodynamic resources (e.g. heat, fuel, photons) consumed by the baths. These steady states exhibit non-vanishing currents, reflecting the violation of detailed balance, and they are referred as non-equilibrium steady states (NESS). They can by used to model a variety of systems, from photo-syntesis in which photons are consumed in the carbon fixation process, through the syntheses of ATP by an ATP-synthase where

the chemical potential difference of H^+ ions between the two sides of the membrane is used to convert ADP+P_i into an ATP molecule, to molecular motors as kynesin, which consumes ATP molecules to generate directed motion, responsible for much of the transport in the cell [15, 16].

4.2.1 Discrete-state description

Suppose that the evolution of the system is governed by the following Master Equation:

$$\partial_t p_i(t) = \sum_{j=1}^{N} \left(w_{j\to i} p_j(t) - w_{i\to j} p_i(t) \right) \tag{231}$$

where N is the number of accessible states. This can be rewritten in a more compact form:

$$\partial_t \vec{p}(t) = \mathcal{R} p(t) \tag{232}$$

where $\mathcal{R}$ is a time independent $N \times N$ transition matrix, in analogy to Eq. (219).

Eq. (232) has a unique steady state solution, that we denote by $\vec{p}^{ss}$. In this case we must have that this solution does not satisfy detailed balance, in order to let the system exhibit a stationary probability current for each possible transition (for each link of the interaction network), defined as:

$$J_{ij}^{ss} = w_{j\to i} p_j^{ss} - w_{i\to j} p_i^{ss} \tag{233}$$

We are also interested in the entropy production associated with these currents:

$$\sigma_{ij}^{ss} = J_{ij}^{ss} \log \frac{w_{j\to i} p_j^{ss}}{w_{i\to j} p_i^{ss}} \tag{234}$$

Again we have a characterization of the NESS of the system in terms of the same quantities considered for a system with time-periodic driving [33].

4.2.2 Fokker-Planck description

Consider now a diffusive system acting on a ring $x \in [-L, L]$, with periodic boundary conditions. In order to describe a NESS in this context, we have

to inroduce a dynamics which violates detailed balance, therefore admitting a non-equilibrium steady state as unique solution.

Consider the following Fokker-Planck equation:

$$\partial_t p(x,t) = \gamma \partial_x \Big(\left(\partial_x U(x,t)\right) p(x,t) \Big) + D\partial_{xx} p(x,t) + v\partial_x p(x,t) \tag{235}$$

where $U(x)$ is a spatially periodic potential, $U(-L) = U(L)$, which, in this case, does not depend on time, since we have no temporal variation of external parameters. In this case v can be interpreted as a characteristic velocity of the probability flow. The term $v\partial_x P(x,t)$ violates the detailed balance condition for any $v \neq 0$. In other words v is an additional linear potential which breaks the periodic boundary condition of the potential $U(x)$.

For a finite v and bounded $U(x)$, Eq.(235) has a unique steady state solution, denoted by $p^{ss}(x)$. In analogy with the probability current J defined in Eq. (225), we can define, for any probability $p(x,t)$ evolving under Eq.(235), a probability current as:

$$J = -D\left[\partial_x p(x) + \beta p(x)\partial_x \left(U(x) + \frac{v}{\beta D}x\right)\right] \tag{236}$$

such that J and $p(x)$ satisfy the continuity equation Eq.(226). Note that this definition reduces to Eq.(225) when $v = 0$. Of special interest is the probability current associate with the steady state:

$$J^{ss} = -D\left[\partial_x p^{ss}(x) + \beta p^{ss}(x)\partial_x \left(U(x) + \frac{v}{\beta D}x\right)\right] \tag{237}$$

Note that J^{ss} is x independent since $\partial_x J^{ss}(x) = -\partial_t p^{ss}(x) = 0$.

The constant entropy production rate for NESS is estimated according to the Seifert's formula [23], as for the case of time-periodic driving. In this case it can be simplified into:

$$\dot{S}^{ss} = (J^{ss})^2 \int \frac{dx}{D p^{ss}(x)} \tag{238}$$

It is worth noting that also in the NESS scenario, the entropy production of a diffusive system has no spatial dependence, since we are integrating over the probability $p^{ss}(x)$.

4.3 Mapping for Master Equation systems

Let us start our analysis on the comparison between NESS and time-periodic driving with the case of a discrete-state system, whose evolution can be described by a Master Equation [33].

Then we want to study the following problem: given a time-independent rate matrix $\mathcal{R}$, corresponding to the steady state quantities $\vec{p}^{ss}$, J_{ij}^{ss} and σ_{ij}^{ss}, we want to build a time-periodic detailed balance rate matrix $\mathcal{W}(t)$, whose periodic state is characterized by the same quantities, after averaging over time. Mathematically speaking we have to require that:

$$\begin{aligned} p_i^{ss} &= \overline{p_i^{ps}} = \frac{1}{T}\int_0^T dt p_i^{ps}(t) \\ J_{ij}^{ss} &= \overline{J_{ij}^{ps}} = \frac{1}{T}\int_0^T dt J_{ij}^{ps}(t) \\ \sigma_{ij}^{ss} &= \overline{\sigma_{ij}^{ps}} = \frac{1}{T}\int_0^T dt \sigma_{ij}^{ps}(t) \end{aligned} \tag{239}$$

We are also interested in solving the reverse problem: given a time-dependent detailed balance rate matrix $\mathcal{W}(t)$, we want to construct a time-independent rate matrix $\mathcal{R}$ such that Eq. (239) holds.

Once $\mathcal{R}$ and $\mathcal{W}(t)$ were found such that they give rise to dynamics that satisfy Eq. (239), we will say that the time-periodic driving mimics the NESS, and viceversa.

4.3.1 From time-periodic driving to NESS

In this section we consider the reverse problem first. Let us suppose to have a given time-dependent rate matrix $\mathcal{W}(t)$, so that $\overline{p_i^{ps}}$, $\overline{J_{ij}^{ps}}$ and $\overline{\sigma_{ij}^{ps}}$ are known.

To build a $\mathcal{R}$ with the required properties, we introduce the following rate matrix decomposition [63]:

$$\mathcal{R} = \left(\mathcal{S} + \frac{1}{2}\boldsymbol{J}^{ss}\right) \cdot P^{-1} \tag{240}$$

where $\mathcal{S}$ is a symmetric matrix whose elements in each column sum up to zero, with negative entries only in the diagonal, $\boldsymbol{J}^{ss}$ is the antysimmetric matrix of the currents, where each element is equal to J_{ij}^{ss}, and $P = \mathrm{diag}(\vec{p}^{ss})$, i.e. a diagonal matrix with elements $P_{ii} = p_i^{ss}$.

Note that when $\boldsymbol{J}^{ss} = 0$ there are no currents flowing in the system and $\mathcal{R}$ satisfy the detailed balance condition.

From Eq. (240), it is easy to see that if all the currents in the graph are non-zero, then p_i^{ss}, J_{ij}^{ss} and σ_{ij}^{ss} uniquely determine $\mathcal{R}$. In order to see this, let us write the entropy production using the rate matrix decomposition [33]:

$$\sigma_{ij}^{ss} = J_{ij}^{ss} \log \frac{\mathcal{S}_{ij} + \frac{1}{2}\mathcal{J}_{ij}}{\mathcal{S}_{ij} - \frac{1}{2}\mathcal{J}_{ij}} \tag{241}$$

J_{ij}^{ss} and σ_{ij}^{ss} uniquely determine $\mathcal{S}$ if all the currents are non-zero. Otherwise some elements of $\mathcal{S}$ can be arbitrarily chosen, since they are not determined by the currents and the entropy production only.

Then we can combine $\mathcal{S}$ with the probability matrix P to get $\mathcal{R}$.

We can conclude that, one we have fixed currents, entropy production and probabilities to match the condition in Eq. (239), the time-independent rate matrix $\mathcal{R}$ can be readily found using the strategy shown above.

4.3.2 From NESS to time-periodic driving

Now, let us suppose that a time-independent rate matrix $\mathcal{R}$ is given.

Current loops

In order to construct a time-periodic driving that mimics a given NESS, we need to understand first the main difference between these two frameworks for what concerns the currents. In fact, the steady state currents of a NESS must form at least one current loop. To see this let us consider a current going out from the node i, say to the node j. Now, from the site j, for the conservation of the probability, there should be at least one current going out, let us say, to the node k and so on. Since the number of states is finite and equal to N, after no more than N steps the current has to come back to the initial node i, then forming a current loop.

On the contrary, a current loop is inconsistent with detailed balance for any instantaneous solution of the time-periodic driving. To show this, let us decompose the rate matrix $\mathcal{W} = \mathcal{S}\Pi^{-1}$, where Π is the diagonal matrix associated to the equilibrium solution $\vec{\pi}$. The current generated by an instantaneous distribution $\vec{q}$ on the link forming the loop $i, j, k, ...m, i$ satisfy:

$$\frac{J_{ij}}{\mathcal{S}_{ij}} = \pi_j^{-1} q_j - \pi_i^{-1} q_i$$
$$\frac{J_{jk}}{\mathcal{S}_{jk}} = \pi_k^{-1} q_k - \pi_j^{-1} q_j$$
$$\dots$$
$$\frac{J_{mi}}{\mathcal{S}_{mi}} = \pi_i^{-1} q_i - \pi_m^{-1} q_m \tag{242}$$

Summing up these equations we get zero on the r.h.s. This means that, since $\mathcal{S}_{ij} > 0$, not all the current can have the same sign around the loop, being consistent with the no current loop condition.

The main consequence of this finding is that we cannot match all the currents with a "single driving", since it is impossible to build current loops using a stochastic pumping. We then split the whole period T in two halves, building the currents in a way that just the average over T will form the required current loops, not the current along each single half [33].

Constructing the currents

Let us start by choosing an equilibrium state for the first half of the period, $\vec{\pi}^a$, and a symmetric rate matrix $\tilde{\mathcal{S}}$ from which we can construct the rate matrix $\tilde{\mathcal{W}}^a = \tilde{\mathcal{S}}(\Pi^a)^{-1}$. Then we choose another distribution $\vec{q}^a$ such that:

$$\left| \log \frac{\pi_i^a q_j^a}{\pi_j^a q_i^a} \right| < \left| \log \frac{\mathcal{R}_{ij} p_j^{ss}}{\mathcal{R}_{ij} p_i^{ss}} \right| \tag{243}$$

We will see that this condition is crucial further on.

For the second half of the period let us choose an equilibrium distribution such that $\pi_i^b = 1/\pi_i^a$ and a distribution $q^b = 1/q_i^a$, such that the rate matrix is $\tilde{\mathcal{W}}^b = \tilde{\mathcal{S}}(\Pi^b)^{-1}$.

It is easy to see that the current generated by $\tilde{\mathcal{W}}^{a,b}$ and $\vec{q}^{a,b}$, $\tilde{J}_{ij}^a$ and $\tilde{J}_{ij}^b$ respectively, have opposite sign.

Along all the edges that involve no loop, we can compare the required current J_{ij}^{ss} with $\tilde{J}_{ij}^{a,b}$ and set the value of the currents for each half of the period as follows [33]:

- if the direction of J_{ij}^{ss} is the same as $\tilde{J}_{ij}^a$, in the first half of the period we set $J_{ij}^a = (2 + \alpha_{ij}) J_{ij}^{ss}$, while in the second half $J_{ij}^b = -\alpha_{ij} J_{ij}^{ss}$;

- if the direction of the NESS current J_{ij}^{ss} is not the same as $\tilde{J}_{ij}^{a}$, in the first half of the period we set $J_{ij}^{a} = -\alpha_{ij} J_{ij}^{ss}$ and $J_{ij}^{b} = (2 + \alpha_{ij}) J_{ij}^{ss}$.

In this way, $J_{ij}^{a,b}$ has the same direction as $\tilde{J}_{ij}^{a,b}$ for each half of the period and, moreover, they have the correct average over T, since:

$$\frac{1}{2}\left(J_{ij}^{a} + J_{ij}^{b}\right) = J_{ij}^{ss} \tag{244}$$

Assuming for now that the probability distribution in the first and second half of the period are given by $\vec{q}^{a}$ and $\vec{q}^{b}$ respectively, and that the equilibrium distribution are $\vec{\pi}^{a,b}$, the entropy production generated by the currents $J_{ij}^{a,b}$ are:

$$\sigma_{ij}^{a,b} = J_{ij}^{a,b} \log \frac{\pi_i^{a,b} q_j^{a,b}}{\pi_j^{a,b} q_i^{a,b}} \tag{245}$$

Imposing that the entropy production has the required average over the whole period, $\sigma_{ij}^{a} + \sigma_{ij}^{b} = 2\sigma_{ij}^{ss}$, we get an equation for determining α_{ij}:

$$\alpha_{ij} = \left| \left(\log \frac{\pi_i^a q_j^a}{\pi_j^a q_i^a} \right)^{-1} \log \frac{\mathcal{R}_{ij} p_j^{ss}}{\mathcal{R}_{ij} p_i^{ss}} \right| - 1 \tag{246}$$

Eq. (243) ensures the positivity of α_{ij}.

Choosing the symmetric part of $\tilde{\mathcal{W}}$

So far we have constructed the currents for both half cycles with the same directions as the currents of $\tilde{\mathcal{W}}^{a,b}$ with $\vec{q}^{a,b}$. We now want to transform the symmetric part $\tilde{\mathcal{S}}$ into a new matrix $\mathcal{S}$, such that the currents generated by $\hat{\mathcal{W}}^{a,b} = \mathcal{S}(\Pi^{a,b})^{-1}$ with $\vec{q}^{a,b}$ have the constructed value $J_{ij}^{a,b}$, not only the same directions.

To this aim, we have to make the following choice [33]:

$$\mathcal{S}_{ij}^{a,b} = \frac{J_{ij}^{a,b}}{(\pi_j^{a,b})^{-1} q_j^{a,b} - (\pi_i^{a,b})^{-1} q_i^{a,b}} \tag{247}$$

Finding a periodic solution

Up to now we have a rate matrix $\hat{\mathcal{W}}^{a,b}$ which produces the desired currents and entropy production with the distribution $\vec{q}^{a,b}$. However the time average of the latter is different from $\vec{p}^{ss}$, also because $\vec{q}^{a,b}$ are not solutions of the master equation: $\partial_t \vec{q}^{a,b} \neq \hat{\mathcal{W}}^{a,b}\vec{q}^{a,b}$.

First of all we have to build the probability distributions $\vec{p}^{a,b}$ with the right temporal average. It can be shown that the following is a good choice:

$$\begin{aligned} p_i^a(t) &= p_i^{ss} - \frac{T}{4} m_i^a + m_i^a t \\ p_i^b(t) &= p_i^{ss} - \frac{3T}{4} m_i^b + m_i^b t \end{aligned} \tag{248}$$

where $\vec{m}^{a,b} = \hat{\mathcal{W}}^{a,b}\vec{q}^{a,b}$ are the temporal slopes during each half of the period. Moreover, we have to choose T such that $0 < p_i^{ss} \pm (T/4)m_i^{a,b} < 1$, $\forall i$, in order to have a probability between 0 and 1 [33].

Since we want $\vec{p}^{a,b}$ to be a solution of the Master Equation, $\partial_t \vec{p}^{a,b} = \mathcal{W}^{a,b}\vec{p}^{a,b}$, we have introduce a rate matrix $\mathcal{W}^{a,b}$ such that

- $\hat{\mathcal{W}}^{a,b}\vec{q}^{a,b} = \mathcal{W}^{a,b}\vec{p}^{a,b}$ in order to match the right temporal slopes;
- if $\hat{\mathcal{W}}$ is detailed balance, then so does $\mathcal{W}$;
- the instantaneous current generated by $\hat{\mathcal{W}}^{a,b}$ with $\vec{q}^{a,b}$ are the same as the ones generated by $\mathcal{W}^{a,b}$ with $\vec{p}^{a,b}$, and the same holds for the instantaneous entropy production along each link.

It is possible to see that the following definition has all the required properties:

$$\mathcal{W}(t) = \begin{cases} \mathcal{S}^a(\Pi^a)^{-1}\mathcal{Q}^a(\mathcal{P}^a)^{-1}(t), & t < T/2 \\ \mathcal{S}^b(\Pi^b)^{-1}\mathcal{Q}^b(\mathcal{P}^b)^{-1}(t), & t > T/2 \end{cases} \tag{249}$$

where $\mathcal{Q}^{a,b}$ and $\mathcal{P}^{a,b}$ are the diagonal matrices associated to $\vec{q}^{a,b}$ and $p^{a,b}$ respectively.

This completes the mapping between NESS and time-periodic driving, since we have found a protocol to build a time-dependent rate matrix which satisfies all the conditions in Eq. (239). In [33] this mapping is presented for an illustrative, although quite general, example.

4.4 Mapping for Fokker-Planck equation systems

In this section we want to address the problem of the mapping between NESS and time-periodic driving when the system obeys a diffusive Fokker-Planck equation.

The problem can be stated as follows: given a NESS and a SP characterized by the quantities defined above, we will consider them equivalent if the following conditions hold:

$$\begin{aligned} \overline{p^{ps}(x)} &= \frac{1}{T}\int_0^T dt p^{ps}(x,t) = P^{ss}(x) \\ \overline{J^{ps}} &= \frac{1}{T}\int_0^T dt J^{ps}(x,t) = J^{ss} \end{aligned} \tag{250}$$

In principle, an exact equivalence between NESS and time-periodic driving should also include an equation for the time averaged entropy production, since we normally can interpret the probability density and the currents as the desired output and the entropy production as the cost to keep the system out of equilibrium. However, as we will discuss below, a similar equality for the entropy production cannot hold simultaneously with the two conditions in Eq.s (250). Mathematically speaking:

$$\overline{\dot{S}^{ps}} = \frac{1}{T}\int_0^T dt \dot{S}^{ps}(x,t) \neq \dot{S}^{ss} \tag{251}$$

In the next section we will see that an inequality can be stated for the entropy production.

4.4.1 Entropy production inequality

Let us start by understanding why the entropy production cannot be matched between as in the discrete-state case.

Given $J^{ss}(x)$, $P^{ss}(x)$, $J^{ps}(x,t)$ and $P^{ps}(x,t)$, by Eqs. (229) and (238), the values of the entropy production $\dot{S}^{ss}$ and $\dot{S}^{ps}(t)$ are automatically set. Therefore, in diffusive systems with a uniform diffusion constant D we can no longer impose an independent condition on the entropy production, as before for system described by a Master Equation. This constitutes a fundamental difference between continuous and discrete-state systems. Let us see if we can nevertheless say something about this quantity in this case.

Let us suppose, for the moment, the existence of a mapping between NESS and time-periodic driving in the sense of Eqs.(250). Under this assumption, we can compare the entropy production of the two different scenarios. To this aim, consider the following integral:

$$\mathcal{I} = \frac{1}{DT}\int dt \int dx \left(\frac{J^{ps}(x,t)}{p^{ps}(x,t)} - \frac{J^{ss}}{p^{ss}(x)}\right)^2 p^{ps}(x,t) \geq 0 \tag{252}$$

$\mathcal{I}$ is non-negative as it is the integral of a non-negative function. Expanding the square root in the integral and rewriting each term, using Eqs. (229) and (238), after some simple manipulations, it is possible to derive the following inequality:

$$\mathcal{I} = \frac{1}{T}\int dt \dot{S}^{ps}(x,t) - \dot{S}^{ss} = \overline{\dot{S}^{ps}} - \dot{S}^{ss} \geq 0 \tag{253}$$

As a first result of this chapter, we can thus state that a NESS always has a lower entropy production with respect to a time-periodic driving with the same time-averaged probability densities and the same time-averaged probability current.

4.4.2 From time-periodic driving to NESS

So far we have seen that maintaining a given (time averaged) current and probability density with time-periodic driving generates at least the same amount of entropy as maintaining the same current and probability using a NESS. In this section, we show that mimicking a time-periodic state of a system with a NESS is possible, namely that a NESS can generate the same currents and probability distributions as using stochastic pumping.

Let us suppose that we have a given time-periodic driving, i.e. $\overline{p^{ps}(x)}$ and $\overline{J^{ps}}$. We remind that the Fokker-Planck equation allowing a NESS is determined by a potential $U(x)$ and a velocity parameter v which breaks detailed balance. To build a mapping, we aim at finding $U(x)$ and v such that Eqs. (250) holds.

The explicit solution of Eq. (235) can be written as:

$$p^{ss}(x) = \mathcal{N}\left(e^{-\beta U(x)-\frac{v}{D}x} + \frac{J^{ss}}{D}e^{-\beta U(x)-\frac{v}{D}x}\int^x e^{\beta U(y)+\frac{v}{D}y}dy\right) \tag{254}$$

where $\mathcal{N}$ is a normalization factor, which can be interpreted as a shift in the potential. We can always choose $U(x)$ such that $\mathcal{N} = 1$, and hence we will ignore it from here on.

Imposing $J^{ss} = \overline{J^{ps}}$ as required, Eq. (254) gives the following expression for $\overline{P^{ps}(x)}$:

$$\overline{P^{ps}(x,t)} = \frac{\overline{J^{ps}(x,t)}}{D} e^{-\beta U(x) - \frac{v}{D}x} \int^x e^{\beta U(y) + \frac{v}{D}y} dy e^{-\beta U(x) - \frac{v}{D}x} \tag{255}$$

This equation, which should be solved for v and a periodic $U(x)$, can be easily inverted by writing it in terms of a new variable $\Phi(x) = \beta U(x) + \frac{v}{D}x$:

$$\Phi(x) = \frac{\overline{J^{ps}(x,t)}}{D} \int^x \frac{1}{\overline{p^{ps}(y,t)}} dy - \log \overline{p^{ps}(x,t)} \tag{256}$$

Imposing periodicity on $U(x)$, we derive the following expression for $U(x)$ and v:

$$\begin{aligned} \beta U(x) &= \frac{\overline{J^{ps}(x,t)}}{D} \int^x \frac{1}{\overline{p^{ps}(y,t)}} dy - \log \overline{p^{ps}(x,t)} - \frac{v}{D}x \\ v &= \frac{\overline{J^{ps}(x,t)}}{2L} \int_{-L}^{L} \frac{1}{\overline{p^{ps}(y,t)}} dy \end{aligned} \tag{257}$$

These equations determine how to build a system such that its NESS corresponds to the desired time-periodic state of a system with time-periodic driving, in the sense of Eqs. (250).

4.4.3 From NESS to time-periodic driving

In the previous section we have shown how to construct a NESS that mimics a given time-periodic driving. This direction was relatively easy since we could use the explicit solution of the NESS, Eq. (254). In this section we consider the opposite problem of mimicking a given NESS using a system driven by a time-periodic potential, in which detailed balance holds instantaneously. Unfortunately, there is no simple explicit solution for the time periodic system, hence the construction is more complicated. An implicit solution has been analytically derived in [103], in the context of no-pumping theorem, but it provides no particular advantages in building a map for diffusive systems.

Current Loop

In discrete systems, a useful constraint on periodic driving is set by the condition of no current loop, which implies that if a system satisfies the detailed balance condition at any instant, then it has no current loops regardless of the instantaneous probability distribution.

A similar condition holds also for $1D$ diffusive systems. In fact, given the instantaneous values of $p(x,t)$ and $J(x,t)$, we can consider the following integral:

$$\mathcal{L} = \int_{-L}^{L} \frac{J(x,t)}{P(x,t)} dx \tag{258}$$

This integral vanishes if and only if the system satisfy the detailed balance condition. To show this, we start considering the general relation between the current and the probability given by Eq.(236):

$$\mathcal{L} = -D \int_{-L}^{L} \partial_x \left(\log p(x,t) + \beta U(x,t) + \frac{v}{D} x \right) dx = -2vL \tag{259}$$

where we have used the spatial periodicity of $p(x,t)$ and $U(x,t)$. Thus, an instantaneous current pattern $J(x,t)$ can be driven by a detailed balance diffusion operator and probability distribution $p(x,t)$ only if the corresponding $\mathcal{L}$ is zero.

In periodic driving, $v = 0$ hence $\mathcal{L}_{ps} = 0$. As $p^{ps}(x,t)$ is always positive, the only way $\mathcal{L}_{ps}$ can vanish is that $J^{ps}(x,t)$ changes its sign as a function of x. This implies that we cannot hope to achieve the equality $J^{ps}(x,t) = J^{ss}$ at each time. Rather, the periodic current must be non-trivially time dependent.

Importantly, given arbitrary instantaneous normalized probability density $p(x,t)$ and current pattern $J(x,t)$, there exist a periodic potential $U(x,t)$ that will drive the current $J(x,t)$ for the probability $p(x,t)$ if and only if $\mathcal{L} = 0$. This can be seen by solving for $U(x,t)$ in Eq. (225):

$$\begin{aligned} U(x) &= U(-L) + \int_{-L}^{x} \left(\partial_x \log P(x) - \frac{J(x)}{D\beta P(x)} \right) dx \\ &= U(-L) + \log P(x) \Big|_{-L}^{x} - \int_{-L}^{x} \frac{J(x)}{D\beta P(x)} dx \end{aligned} \tag{260}$$

For $x = L$, this implies

$$U(L) \;=\; U(-L) - \frac{\mathcal{L}}{D\beta} \tag{261}$$

Thus, $U(x)$ is periodic if and only if $\mathcal{L} = 0$.

Compatibility of $P(x,t)$ with detailed balance

As we have seen, any $p^{ss}(x)$ and v can be maintained by a NESS. It is thus natural to ask: can any smooth, periodic and normalized $p(x,t)$ be driven by periodically varying the potential $U(x,t)$? As we next show, this indeed can be done for arbitrary (normalized, smooth and periodic) $p(x,t)$. First, given $p(x,t)$ we construct the corresponding current, $J(x,t)$. For $p(x,t)$ and $J(x,t)$ to solve the continuity equation (Eq. (226)) we must have:

$$J(x,t) \;=\; J(-L,t) - \int_{-L}^{x} \partial_t p(x',t) dx' \tag{262}$$

As $p(x,t)$ is normalized at each t, any $J(-L,t)$ is compatible with $p(x,t)$ and the continuity: the only constraint on $J(x,t)$ is its spatial periodicity, $J(-L,t) = J(L,t)$, which always holds since $\partial_t \int_{-L}^{L} p(x',t)dx' = 0$ for normalized probabilities.

Next, we note that, although any $J(-L,t)$ is compatible with $p(x,t)$ and the continuity equation, not any $J(-L,t)$ and $p(x,t)$ are compatible with the constraint posed by detailed balance, namely that $\mathcal{L} = 0$. Substituting Eq. (262) in the definition of $\mathcal{L}$ gives:

$$\mathcal{L} = \int_{-L}^{L} \frac{J(-L,t) - \int_{-L}^{x} \partial_t p(x',t)dx'}{p(x,t)} dx \tag{263}$$

Choosing

$$J(-L,t) = \left(\int_{-L}^{L} \frac{1}{p(x,t)} dx \right)^{-1} \int_{-L}^{L} \frac{\int_{-L}^{x} \partial_t p(x',t)dx'}{p(x,t)} dx \tag{264}$$

assures that $\mathcal{L} = 0$, hence that $p(x,t)$ can be driven by a periodic potential $U(x,t)$ and this is always possible by choosing an appropriate value for the flux at the boundary $J(-L,t)$.

Building the map

Given a target NESS, we can construct a time-periodic driving such that the mapping conditions in Eqs. (250) holds.

As we have shown in the previous section, any normalized $p(x,t)$ can be driven by some periodic potential $U(x,t)$, namely by a detailed balance time dependent driving. Given $p(x,t)$, Eq. (264) expresses the corresponding value of $J(-L,t)$. Since, for the periodic solution $p^{ps}(x,t)$, the average current is position independent, all we have to do is to find a periodic (in x and t) $p(x,t)$ that will average, over a period, to $P^{ss}(x)$, and such that the time average of the corresponding current given in Eq. (264) will be equal to J^{ss}. This can be done by choosing

$$p^{ps}(x,t) = f\left(x - x_0\left(\frac{t}{T}\right)\right) \tag{265}$$

for any $f(x)$ which is positive and normalized. $f\left(x - x_0\left(\frac{t}{T}\right)\right)$ has a constant shape that translates with time, at a velocity dx_0/dt. We next find $x_0(t)$ such that:

$$x_0(0) = -L \tag{266}$$

$$x_0(1) = L \tag{267}$$

$$\frac{1}{T}\int_0^T f\left(x - x_0\left(\frac{t}{T}\right)\right) dt = p^{ss}(x) \tag{268}$$

The last demand can be written as an integral over x_0 rather than as a function of t:

$$\int_{-L}^{L} f(x - x_0)\frac{dt}{dx_0}dx_0 \;\; = \;\; P^{ss}(x) \tag{269}$$

The left hand side of the above equation is a convolution between $f(x)$ and $t(x)$, hence given a $p^{ss}(x)$ and a chosen $f(x)$ we can solve for $t(x_0)$ and invert into $x_0(t)$. Note, however, that not any $f(x)$ will work with every $p^{ss}(x)$: dt/dx_0 must be positive, and $f(x)$ must have all the Fourier modes that $P^{ss}(x)$ has for the convolution to be possible.

Lastly, from $p^{ps}(x,t)$ we solve for $J(-L,t)$ through Eq. (264). The time average of this current is the position independent current associated with

the driving. In general, it will not have the desired value, namely it will not be equal to J^{ss}. However, $J(-L,t)$ is inversely proportional to T because of the time derivative, whereas the solution for $x_0(t/T)$ is T independent. Hence, by changing T we can tune the average J to have any required value, and equate it with J^{ss}.

In this section we have derived a solution for our mapping that can be applied to any target NESS. However, although this procedure ensures that a mapping is always possible, finding it along this line could be quite demanding both numerically and analytically. In the next section we will show another way to build the mapping and we will provide a numerical proof.

Building the map using Fourier expansion

A simple way to approach the problem is to exploit the periodicity of $p^{ps}(x,t)$ and $J^{ps}(x,t)$ in both x and t, expanding them in Fourier modes [104]. Hence we write:

$$\begin{aligned} p^{ps}(x,t) &= \sum_{k,\omega} p_{k,\omega} e^{ik\frac{\pi}{L}x} e^{i\omega\frac{2\pi}{T}t} \\ J^{ps}(x,t) &= \sum_{k,\omega} j_{k,\omega} e^{ik\frac{\pi}{L}x} e^{i\omega\frac{2\pi}{T}t} \end{aligned} \tag{270}$$

Let us write all the conditions for the probability distribution and the currents, as well as the relations between them, in terms of the Fourier coefficients. First, the definition of the flux can be recasted as:

$$j_{k,\omega} = -\frac{\omega}{k} p_{k,\omega} \quad ; \quad j_{k,0} = 0 \tag{271}$$

Additional requirement is that the normalization of $p^{ps}(x,t)$ does not change in time. In Fourier coefficients, this implies $p_{0,\omega\neq 0} = 0$.

Next, we rephrase the mapping, Eq.s (250), in the Fourier coefficients. First we expand the target steady state distribution in Fourier modes:

$$p^{ss}(x) = \sum_k \overline{p}_k e^{ik\frac{\pi}{L}x}. \tag{272}$$

With these coefficients we can write:

$$p_{k,0} = \overline{p}_k \quad ; \quad j_{0,0} = J^{ss} \tag{273}$$

Finally, to complete the mapping, we have to impose that the integral $\mathcal{L}$ vanishes. To do this we propose a Fourier series expansion also for $U(x,t)$, with the coefficients $u_{k,\omega}$. Since, by construction, if the potential is periodic in space and time, also $\mathcal{L} = 0$, we formally rewrite Eq. (225) in terms of the Fourier coefficients, obtaining the following linear equation:

$$-D\left(\beta(iku * p)_{k,\omega} + ikp_{k,\omega}\right) = j_{k,\omega} \tag{274}$$

where the notation "$*$" indicates the convolution. This equation has to be solved for the variables $u_{k,\omega}$ that fully describe the unknown time-periodic potential.

Note that all the variables in Eq. (274) but $\overline{p}_k$ and J^{ss} have to be specified, so we can solve the equation iteratively by numerical integration. Although in principle an infinite number of unknowns has to be taken into account, we guess that a limited number of them is sufficient to find an approximate solution to the mapping. In the next section a simple numerical example is carried out to evalidate our theoretical approach.

Numerical example

Let us consider a NESS characterized by the following probability density and current:

$$p^{ss} = \frac{1}{2\pi} + \frac{1}{4\pi}\cos(x) \qquad J^{ss} = -0.011 \tag{275}$$

We aim at solving Eq. (274) to find a time-periodic potential $U(x,t)$ which allows a time-periodic state with the same time-averaged quantities. To do this we use the following approach: first we limit the number of parameters, i.e. we suppose that only some of the k and ω have a non-zero corresponding coefficient. In particular, we guess that:

$$\begin{aligned} p_{k,\omega} &= 0 \qquad if \quad |k| > 2\,, \quad |\omega| > 2 \\ u_{k,\omega} &= 0 \qquad if \quad |k| > 4\,, \quad |\omega| > 4 \end{aligned} \tag{276}$$

Then we solve the equation for $u_{k,\omega}$, fixing all the arbitrary component of $p_{k,\omega}$ (the ones that are not fixed by Eq. (273)). Finally we plug this solution in the same equation and we solve for $p_{k,\omega}$, and so forth using a least square algorithm. In this case this simple method provides a good approximate solution (see Fig. 12) and it is easy to understand that increasing the number of fitted parameters, i.e. the number of k and ω for which the Fourier coefficient are non-zero, will increase the accuracy of the solution.

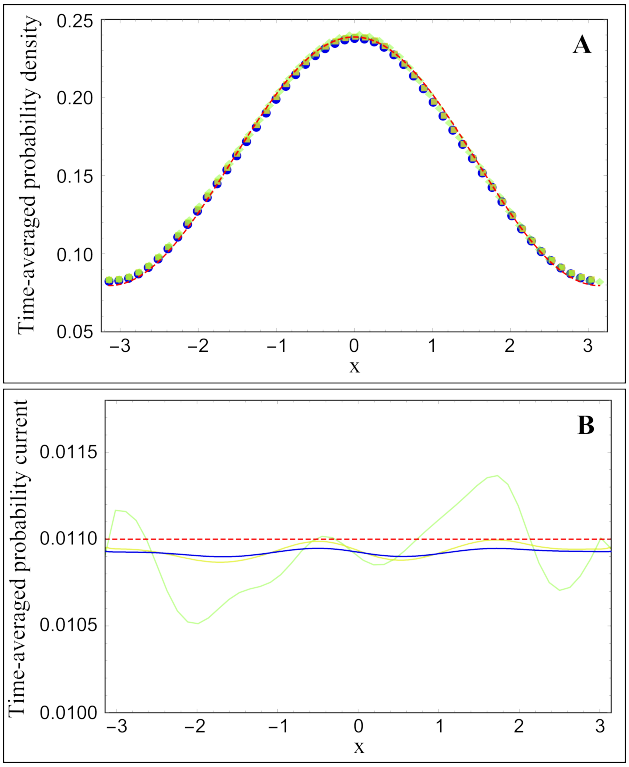

Figure 12: Numerical validation of the mapping, using an approximate solution for the potential $U(x,t)$. *Panel A* - A comparison between the time-averaged probability density, $\overline{p^{ps}(x,t)}$, obtained by numerical integration and the analytical expected one of the given NESS, $p^{ss}(x)$ (dashed red curve) for different choice of the discretization in the numerical simulation. The green diamonds represents the time-averaged probability current obtained by numerical simulation with a discretization of 50 points for x between $[-\pi,\pi]$ and 500 for t with $T=2\pi$, the yellow squares refers to 250 points for x and 2500 points for t, and the blue circles is related to the simulation carried out with 650 points for x and 6500 for t. *Panel B* - Value of the time-averaged probability current, $\overline{J^{ps}(x,t)}$, for the same choices of points for the discretization of x and t (the same colorcode as in Panel A has been adopted). It is easy to see that a more fine discretization leads to a better estimation of $\overline{J^{ps}(x,t)}$, which, by definition, should be constant in x. The red dashed line represents the theoretical value of the current of the given NESS, J^{ss}.

4.5 Conclusions

In this chapter we have shown that a stochastic pump (SP) can mimic a nonequilibrium steady state, having the same time-averaged probability density function and the same time-averaged probability current also for diffusive systems. Although the exact form of the time-periodic potential $U(x,t)$ to build this mapping can be easily found only numerically (with a certain degree of approximation), the inverse mapping of a SP with a NESS is rather simple. In fact we have shown that an analytical solution exist for the potential $U(x)$ and the velocity v of a system without detailed balance, whose NESS mimicks a given time-periodic driving.

Moreover, we want to point out an interesting result on the entropy production which can be found only in the continuous case. Indeed, we have derived an inequality, finding that the entropy production rate of a system with time-periodic driving is always higher than the one of NESS with the same time-averaged probability densities and currents. This result constitutes an unavoidable limitation in building an artificial machine for diffusive systems to mimic a given NESS.

Many important aspects were not discussed here and they could be subjects of future investigations, mainly a map between NESS and time-periodic driving to match some other important features (e.g. heat or work) [33], and a more in-depth discussion on the entropy production inequality. On the latter, some further analysis could reveal wheter it is just a consequence of the coarse-grained approach of a Fokker-Planck equation or wheter it lies on different theoretical justifications.

It is worth noting that we assumed a constant diffusion coefficient D, in order to use the epression for the entropy production given by Seifert. Another interesting generalization could involve the analysis of a time-periodic driving with a time-dependent diffusion coefficient which, indeed, preserves detailed balance at any instant.

5 General conclusions

In this last chapter we will summarize the conclusions derived from the works presented in the thesis, evidencing the connection between them and their relevance in the general context of stochastic thermodynamics.

In Chapter 2 we have derived some statistical properties of the entropy production for a system whose dynamics can be described by a Master Equation. This kind of systems can be modeled as transition networks, encoding all the information about the dynamics. Interestingly, close to equilibrium, we are capable to evaluate the entropy production from two topological parameters of such a network, w_{eq} and ϵ_{eq}. The first one keeps track of the symmetric part of the transition rates, while the second one is related to asymmetry between each forward and backward transitions. From the point of view of the stochastic thermodynamics, this result is remarkable by itself, since it give birth to a novel universal behaviour of the entropy production for a large variety of systems. Another important application of this finding is related to the maximum (minimum) entropy production principle. In fact, it could be interesting to compare the dynamical adaptive evolution of different living systems with what we expect from an extremum principle of the entropy production, studying how the topology of the transition network changes to cope with external perturbations.

Another important result of this first part of the thesis is the thermodynamic validation of the Schnakenberg's formula for the entropy production, carried out using a mapping between transition networks and classical electrical circuits.

These findings stimulate the onset of an interesting question: what can we say about systems amenable to be described by different dynamics, for example a Fokker-Planck equation? In Chapter 3 we aim at answering this question, by starting from the entropy production of a Master Equation systems and studying how this expression changes when the dynamics is mapped into a Fokker-Planck equation. The latter can be seen as a coarse-grained version of a discrete-state Markov process: in the continuum limit we can get the same Fokker-Planck equation, with its entropy production, starting from different Master Equations, each one with a different value of $\dot{S}$. In this chapter we derive a fundamental inequality: neglecting some information about the dynamics, i.e. after a coarse-graining procedure, we can only underestimate the entropy production. The novel proposed formula for $\dot{S}$ keeps track not only of the coarse-grained parameters of the Fokker-Planck

(as the Seifert's formula does), but it depends on the microscopic transition rates. This is a theoretical result on the fundaments of the stochastic thermodynamics and it could be interesting to see how this new insight on the entropy production changes our understanding of phenomena in which some details of the microscopic dynamics are known, although usually neglected.

This inequality has a consequence also on the meaning of a maximum (minimum) entropy production principle. Since talking about an extremum principle in general becomes even more difficult when dealing with coarse-grained dynamics, it could be considered not a general law or we may need a refinement of its statement, depending, again, on the micrscopic details we are neglecting.

In the last Chapter we deal with the problem of mimicking a non equilibrium steady states (NESS) with time-periodic driving (e viceversa). This problem is of fundamental importance in building artificial molecular machines, in which the system is driven out of equilibrium by the variation of an external parameter, to simulate biological motors. This mapping has been studied for discrete-state systems and in this thesis we have derived an analogous mapping for diffusive systems. In the latter case the entropy production, usually associated to the cost of maintain a certain probability distribution and a certain flux, cannot be mapped. In other words, an artificial molecular machine, i.e. a system with time-periodic driving, always produce more entropy than its biological counterpart, i.e. a system in a NESS. Wheter this inequality is just a consequence of the coarse-graining, in the same spirit of the results discussed in Chapter 2, or has a more fundamental basis, related to the external parameters that we can control in this diffusive systems, is something that needs to be investigated in the future.

The most unlucky point is that any contribution that we add to our knowledge of the entropy production has the inescapable consequence of producing entropy in the world of non-equilibrium physics, then we can just aim at evaluating the cost of our understanding, trying to reduce it at its minimum. Unfortunately we are far from this point, but maybe this thesis can help along this line... and I feel that this could be the main contribution of my work!

A Appendix: the origin of sparsity in living systems

In this section we aim at understanding the self-adaptation of living systems from a different perspective respect to the stochastic thermodynamics. Here, in particular, we will try to build a theoretical framework to justify an empirical evidence on the topology of many living system: the sparsity, i.e. the percentage of active interactions scales inversely proportional to the system size.

A.1 Introduction to the problem

In inanimate matter, elementary units, such as spins or particles, always have their mutual interactions turned on (with the intensity decaying with their relative distance). Thus, the interaction network is dense, with all connections present, i.e. particles do not have the freedom to adjust or change their interactions unless they change their relative distances. In contrast, living systems are composed of interacting entities, such as genes [105, 106, 107, 108], metabolites [105, 109, 110], individuals [111, 112, 113] and species [114, 108, 115, 116, 117, 118], with the ability to rearrange and tune their own interactions in order to achieve a desired output [105]. Indeed, thanks to advances in experimental techniques, which are generating an increasing volume of publicly available ecologically and biologically relevant data, several studies indicate that interaction networks in living systems possess a non-random architecture characterised by the emergence of recurrent patterns and regularities [114, 115, 119, 68].

Analysing different data sets of ecological, gene-regulatory, metabolic and other biological interaction networks [115, 106, 105, 120, 116, 121, 122] (see Supplementary section for details), we find that one ubiquitous emergent pattern is sparsity, i.e. the percentage of the active interactions (connectivity) scales inversely proportional to the system size (illustrated in Fig. 13). For example, in the case of ecological systems, species interact selectively even when they coexist at short distances and most of the interactions are turned off. A generic system formed by S interacting units may have a maximum number of interactions equal to S^2 (including self-interactions), i.e. a connectivity C (defined as the fraction of active interactions) equal to 1. On the other hand, the minimum number of interactions that guar-

antees that the interaction network is connected is of the order of S, that is $C \sim 1/S$, corresponding to the percolation threshold of random networks [123]. Thus, in this range of possible connectivities, it is quite surprising that the observed ones in the analysed interaction networks all correspond to the lowest possible values. However, it is not known if this recurrent property gives any advantage or reward to the system and a theoretical framework to understand the origin of sparsity is still lacking.

Guided by such an intriguing observation, the main goal of our work is to shed some light on why this pattern emerges and to study, from a theoretical point of view, if the sparsity of interactions confers any advantage to the system. In this context, variational principles have been proven to be a useful tool to elucidate some of the recurrent patterns in Nature [124, 115]. In the same vein, in this work we propose an optimisation approach to describe the role of active interactions in living systems. We show that sparse networks offer, at the same time, a maximum capability of the system to visit as many stable attractors as possible by simply tuning the interaction strengths (explorability), as well as the largest robustness of the underlying dynamics, guaranteeing that such attractors remain stable (dynamical robustness).

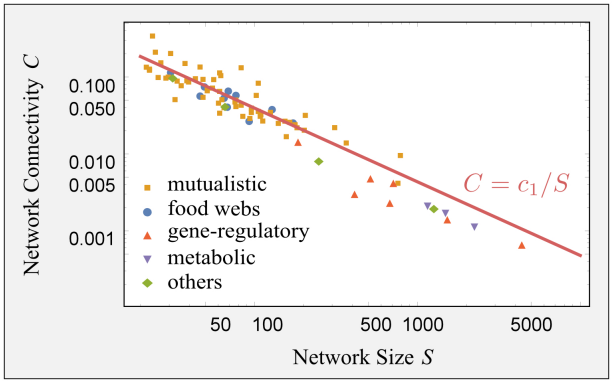

Figure 13: **Sparsity of interactions in living systems.** The connectivity, C, is defined as the fraction of active interactions among the S^2 possible links (including self-interactions), whereas the system size, S, refers to the number of nodes in the graph. We plotted C as a function of S in log-scale for 83 biological networks (ecological mutualistic communities and food webs, gene-regulatory networks, metabolic networks and others). The data show a clear emergent pattern of sparsity in empirical biological networks, as evidenced by the red line $C = c_1/S$ (with $c_1 = 3.8 \pm 0.2$). Details on the database are given in the Supplementary section.

A.2 Mathematical framework

We consider a system composed of S nodes (e.g. species, metabolites, genes) characterised by dynamical variables, $\mathbf{x} = (x_1, x_2, ..., x_S)$ (e.g. populations, concentrations, levels of expression), following a generalised Lotka-Volterra (GLV) dynamics:

$$\dot{x}_i = G_i(x_i) F_i \left(\sum_{j=1}^{S} w_{ij} x_j \right) \qquad \text{for } i = 1, \ldots, S. \tag{277}$$

In the simplest case $G_i(x) = x,\ F_i(x) = \alpha_i + x$, we recover the classic S species Lotka-Volterra equations and we refer to the parameter α_i as the growth rate. In this case the interaction of node i with node j is encoded in the matrix element w_{ij}, whose diagonal entries set the scale of the interaction strengths, which for the sake of simplicity [125] we set to -1. For convenience, we also introduce the adjacency matrix A_{ij}, whose entries are 1 if the corresponding $w_{ij} \neq 0$ and 0 otherwise. A non-trivial stationary point of the dynamics of Eq.(277), $\mathbf{x}^*$, is determined by the interactions within the system, i.e. when $F_i(\sum_{j=1}^{S} w_{ij} x_j^*) = 0$, $\mathbf{x}^* = -\mathbf{w}^{-1}\boldsymbol{\alpha}$, and its stability is guaranteed if all the eigenvalues of the Jacobian matrix evaluated at this point, $J_{ij} = x_i^* w_{ij}$, have a negative real part. GLV dynamics have been used to model the time evolution of ecological systems [125, 126], human microbiota dynamics [127], gene expression[128] and other biological systems [129], where x_i represents the density of the i-th species, and therefore we focus on the stable and feasible stationary solutions of the dynamics [125, 122] ($x_i^* > 0$). For simplicity, here we focus on the simpler case with $G_i(x) = x,\ F_i(x) = \alpha_i + x$, but in the Supplemetary section we recast all the results for the more general non-linear dynamics, Eq. (277).

A.3 Explorability

Depending on the model parameters, the dynamics of (277) exhibits different fixed points, $\dot{x}_i^* = 0$, that may correspond to feasible/non-feasible and either stable/unstable solutions. We do not study more complicated possibilities such as limit cycles or chaotic strange attractors, as this would require to go beyond linear stability analysis. Focusing on the interaction strengths as our tuning parameters, by varying them we can pass from one fixed point to another, and change its feasibility and stability. In brief, we take the

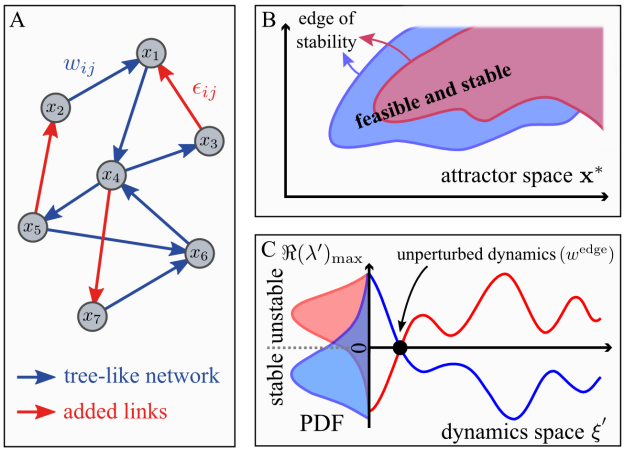

Figure 14: **Measuring explorability and dynamical robustness.** We considered a system of S nodes representing species, genes, metabolites, ... ($S = 7$ in the picture), whose state $\mathbf{x} = (x_1, ..., x_S)$ obeys a non-linear dynamics of the type $\dot{x}_i = G_i(x_i)F_i(\sum_{j=1}^{S} w_{ij}x_j)$, with w_{ij} encoding the network structure and the strength of the interactions. **(Panel A)** We started from a tree-like network with S links, represented by the blue-colored links, and, for such a topology, we searched for the feasible and stable fixed points as we varied the interaction strengths. **(Panel B)** The spanned volume sketched by the blue-shaded region (a 2D projection of the S-dimensional space) corresponds to the network explorability. **(Panel C)** The dynamical stability quantifies the robustness of the system to perturbations of the dynamics itself, $(\mathbf{G} + \delta\mathbf{G})(\mathbf{F} + \delta\mathbf{F})$, and should not be confused with the standard stability or resilience that measures the response to perturbations on the fixed point (which is already implicit in the measure of explorability). Starting from an interaction matrix whose fixed point of the underlying dynamics is at the edge of stability, denoted by w_{ij}^{edge} (for which $\Re(\lambda)_{\max} = 0$, black dot in the picture), the dynamics was perturbed, and the stability of the new fixed point was evaluated in order to test the dynamical robustness of the system. As demonstrated in the Supplementary section, this can be simply encompassed by computing the principal eigenvalue $\Re(\lambda')_{\max}$ of the perturbed Jacobian matrix, $J'_{ij} = \xi'_i w_{ij}$, where $\boldsymbol{\xi}'$ depends on the details of the perturbation, that we take to be a random vector. The histogram of $\Re(\lambda')_{\max}$ is sketched in panel C as the dynamics $\boldsymbol{\xi}'$ is varied. Finally, we increased the connectivity of the network by including additional fixed strengths, ϵ_{ij} (red edges in the graph), to the network. The same previous analysis was performed again by varying the strengths of the blue links and the corresponding results are shown in red in the panels on the right. By randomly sampling the location and strengths of the added links, we investigate if the explorability and dynamical robustness statistically increase or diminish for higher values of the connectivity.

explorability as the volume of feasible and stable fixed points spanned by modifying the link weights, while all other model parameters are kept fixed. The explorability resembles the concepts of robustness and adaptability in the context of evolutionary dynamics, which make up the number of 'phenotypes' (attractors of the dynamics) that can be reached by mutations in the space of 'genotypes' (interaction networks) [130, 131]. Nevertheless, in our case the system has only one stable and feasible fixed point ('phenotype') once the weights w_{ij} are fixed (w is invertible). Therefore, for any change of a link weight (a 'mutation' of w) we have a different fixed point ('phenotype'), i.e.

in our setting there are not 'neutral' mutations.

More specifically, we can define the explorability for interacting systems described by a GLV dynamics (Eq. (277)) and for a given topology (i.e., an ensemble of interaction networks having the same adjacency matrix A, but in general different links weights w_{ij}) of the interaction network. The explorability V_E is the volume in $\mathbb{R}^S$ spanned by all the feasible and stable fixed points as one varies w_{ij} while keeping all other parameters fixed (see Fig. 14). Notice that, with such a definition, the fully connected network has the largest possible explorability, since any other topology is attainable by making some of the matrix entries arbitrarily close to zero. However, might the optimal or quasi-optimal solutions indeed be the ones where most of the interactions are turned off, as suggested by the observational data? Moreover, in the fully connected case, many interaction parameters have to be specified (there are S^2 matrix elements that can be varied), and then spanning all the possible fixed points becomes a complicated, fine-tuning problem, which does not seem to be feasible in biological systems [132]. Therefore, we pose the following questions: what is the relationship between explorability and the interaction network topology? Is there an optimal network structure that maximises explorability? To answer these questions, we started by analysing the extreme case of a sparse topology with just S links, i.e. a tree-like network with connectivity $C = 2/S$ (see Fig. 14) (the factor 2 comes from the fact that we also count the self-interactions). However, even in this simple case, measuring the explorability requires us to scrutinise an S-dimensional space of parameters (corresponding to the S entries of the interaction matrix). Furthermore, one still has to choose the values of α_i, which are intrinsic parameters of the dynamics (e.g. species growth rates) and should be set *a priori* (in contrast to the interactions w_{ij}, which are tuning parameters in our approach). For this reason, we introduced various degrees of approximations in our setting. We first considered the simplest uni-parametric case, $\alpha_i = \alpha$, that we can fix without a loss of generality to $\alpha = 1$ (we checked that our conclusions are still valid for other choices of α_i, see below). In addition, we first restricted the analysis to the subspace of fixed points with homogeneous components, i.e. $x_i^* = x^*$. Under these approximations, computing the explorability becomes a much simpler task and we were able to develop an analytical solution to this problem (see the proper section below). This approach, although *a priori* seems too drastic, leads to rather reasonable estimates of the explorability. As a second step, we enlarged the region explored by introducing some heterogeneity into the components of $\mathbf{x}^*$.

Most probably, the volume of feasible and stable fixed points may become infinite. However, we are always interested in comparing such volumes for different topologies. Indeed, in the simple homogeneous situation, we observed that in almost all the cases (100 per cent for tree-like networks and, e.g., more than 98 per cent for $C = 0.5$), we can identify two regions along $x_i^* = x^*$: fixed points become unstable for small x^* and stable for large x^*, with a marginally stable fixed point intersecting at a single value x_c^*, for which $\Re(\lambda)_{\max} = \max_{i=1,..,S} \Re(\lambda_i) = 0$, where λ_i are the eigenvalues of the Jacobian matrix J (see Supplementary section for more details). Therefore, we can take $V_E = V_0 - x_c^*$ as a proxy for the explorability, where V_0 is a sufficiently large constant ($V_0 = 1$ in our analysis), which allows for comparison between different topologies. With this definition, we can compute analytically the explorability of a tree-like network with S links (see Supplementary section), finding that, among all the possible tree-like topologies, the one with just a loop composed of three nodes leads to the optimal explorability, $V_E = 2/3$. This structure (which we refer to as the optimal tree-like network) constitutes our reference network when increasing the connectivity.

As a third step, we analysed the explorability of networks with higher connectivities. This enormously increases the number of matrix entries that have to be modified when computing the spanned volume of feasible and stable fixed points. For this reason, we adopted the following approach (see Fig. 14): starting from the tree-like topology, we introduced *additional* links to the tree-like topology of weights ϵ_{ij} for any extra links between nodes i and j, and then computed the explorability, fixing the values of all ϵ_{ij} and tuning the other matrix elements. Sampling different values of the added link weights (but not their locations), we can construct a histogram of the explorabilities, $P(V_E|\{\epsilon_{ij}\})$. In addition, we are not interested in distinguishing different topologies with the same connectivity C, so we also sampled over different locations of the added links, leading to $P(V_E|C)$ (see the subsection below for technical details). For numerical reasons, we have tested that our results are robust for network sizes $S < 100$. However, it is important to mention that network size is a significant factor in the spectrum of fixed points [133] and that more complex phenomenology could be found in very large systems.

Numerical results are represented in Fig. 15 (left panel), illustrating that the explorability of the optimal tree-like network is indeed statistically higher than the one for denser networks. Furthermore, the average explorability decreases as the connectivity of the interaction network increases (Fig. 15, cen-

tral panel). We were able to prove this result for some particular topologies of small networks, for which the explorability can be calculated analytically (see Supplementary section). In conclusion, our results suggest that, on average, explorability decays with the connectivity of the system, and therefore, sparse networks generally lead to higher values of explorability.

A.3.1 Measuring explorablity

The explorability of a tree-like network with S links ($C = 2/S$) can be found by studying the following inverse problem: by fixing the parameters α_i and moving along the space of fixed points, one can retrieve the non-zero S values of w_{ij} according to the fixed point equation $\sum_j w_{ij} x_j^* = -\alpha_i$ and this can then be used to check the stability of the associated fixed point $\mathbf{x}^*$. The solution exists if for each node, i, there is at least a node j, such that $w_{ij} \neq 0$ (see Supplementary section). The same procedure can be applied to the more general case where extra links are added to the network, each one with a given fixed strength ϵ_{ij} (see Supplementary section for more detail).

A.4 Dynamical robustness

Another crucial property of complex interacting systems is their robustness to perturbations [134, 135]. Understanding the role of network architecture in the stability of a system with many degrees of freedom is an important challenge, since it impacts on our capacity both to prevent system failures and to design more robust networks to tolerate perturbations to the system dynamics.

The standard measure of stability (known as asymptotic resilience in ecology [136, 137]) is defined as the capacity of the system to return to the original stationary state after a perturbation of it, $\mathbf{x}^*+\delta\mathbf{x}$, while the dynamics is kept fixed. Let us note that our definition of explorability already takes into account this kind of stability, i.e. explorability is defined only for stable system dynamics.

Alternatively, we can study how the stability of the system is modified as a result of a perturbed dynamics, $\dot{\mathbf{x}} = (G + \delta G)(F + \delta F)(\mathbf{x})$, where δG and δF represent the perturbations with respect to the original dynamics. This can be understood as including further non-linear effects that were not present before. As a consequence of this kind of perturbation, *both the original stationary states and their degree of stability are modified*. We then

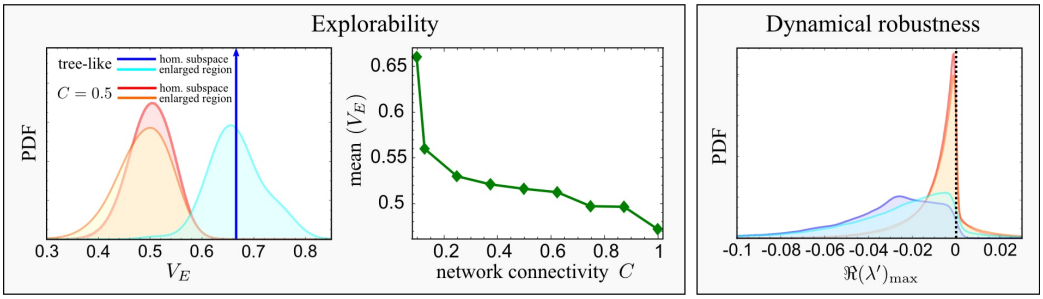

Figure 15: **Explorability and dynamical robustness for different connectivities (Left panel)** Probability distribution functions (PDF) of the explorability V_E for the optimal tree-like graphs and networks with $C = 0.5$ obtained by adding extra links with random (uniformly distributed) locations and weights ϵ_{ij} taken from a zero-mean Gaussian distribution with the standard deviation $\sigma_\epsilon = 0.1$, for a network size $S = 20$. First, we computed V_E in the simple setting of uniform concentrations and growth rates, i.e. $x_i^* = x^*$ independent of i and $\alpha_i = 1$. The explorability $V_E = 2/3$ of the tree-like network (calculated analytically - solid blue line) is larger than the one corresponding to graphs with higher density (red curves were computed by taking 10^3 independent realizations of the added links). Similar results hold also in the more general setting of non-uniform concentrations and growth rates (sampled from Gaussian distributions with zero mean and standard deviation $\sigma_x = \sigma_\alpha = 0.1$, see the subsection below). Even with such a variability, the tree-like network (cyan curve) generally exhibits higher values of the explorability than more dense networks (orange curve for $C = 0.5$). **(Center panel)** Mean value of the explorability (computed from the PDF of V_E) as a function of the connectivity in the homogeneous case ($x_i^* = x^*$ and $\alpha_i = 1$). **(Right panel)** Given $w_{ij}^{\rm edge}$ (see Fig. 14C), we calculated the Jacobian matrix of the perturbed dynamics $J'_{ij} = \xi'_i w_{ij}^{\rm edge}$. The corresponding eigenvalue with the largest real part ($\Re(\lambda')_{\max}$) gave the degree of stability for the new fixed point, from which we measured the dynamical robustness of the system (see the proper section in the text). We generated 10^3 configurations of ϵ_{ij}'s as done for the left panel ($\epsilon_{ij} = 0$ corresponds to a tree-like network), and for each one, 10^3 values of $\boldsymbol{\xi}'$ (encoding the perturbation of the dynamics) from a uniform distribution in $[0, 1]$, and then computed the system response through the distribution $P(\Re(\lambda')_{\max}|C)$. Both homogeneous and non-homogeneous settings were analyzed for the tree-like network and $C = 0.5$ (same color code as for the left panel). In all cases, we found that increasing the network connectivity shifted the distribution of $\Re(\lambda'_{\max})$ towards the less stable region. Qualitatively similar results were obtained for larger values of σ_ϵ, σ_x and σ_α (see Supplementary section).

quantify the capacity of the system to re-organize after a perturbation of the dynamics such that the new stationary state of the system is close to the original one and still stable. We refer to this as the *dynamical robustness* of the system (to avoid confusing this new measure of stability with the standard resilience).

We found the pleasing result that the Jacobian matrix evaluated at the new stationary state, J'_{ij}, retained a similar form than for the original dynamics, i.e. $J'_{ij} = \xi'_i w_{ij}$, where $\boldsymbol{\xi}'$ depends on the specific details of the perturbed dynamics (see Supplementary section). Focusing on the worst case, which corresponds to marginally stable fixed points for which $\Re(\lambda)_{\max} = 0$ (denoted by $w^{\rm edge}$), we perturbed the dynamics and computed the maximum real part of the eigenvalues of J'_{ij} at the new stationary point, $\Re(\lambda')_{\max}$. For a given

deterministic perturbation of the dynamics $\boldsymbol{\xi}'$ and topology, $\Re(\lambda')_{\max}$ can be taken as a measure of the dynamical robustness (see Fig. 14, panel C). Since we wanted to keep the analysis as general as possible, we studied the dynamical robustness against random perturbations of the dynamics (generated from a distribution $P(\boldsymbol{\xi}')$). In particular, for each connectivity C, we fixed the additional links to ϵ_{ij} and then looked for the set of matrices $w^{\text{edge}}(\{\epsilon_{ij}\})$ at the edge of stability (for which, by definition, $\Re(\lambda)_{\max} = 0$). Taking different realisations of ϵ_{ij} and ξ'_i, we compared the distributions $P(\Re(\lambda')_{\max}|C)$ (see Fig. 14). We can then define a statistical measure R of the dynamical robustness by taking the value of $-\Re(\lambda')_{\max}$ located at the fifth percentile, $R = -\Re(\lambda')^{5th}_{\max}$. In this way, we have an indicator of how much stability could be gained under random perturbations of the dynamics. Other choices of this measure can be taken, e.g. based on the 10th, 20th and 50th percentiles, leading qualitatively to the same conclusion. However, lower percentile values generally enhance the differences between topologies (see Supplementary section).

The right panel of Fig. 15 shows the histogram of $\Re(\lambda')_{\max}$ for different connectivities. Again, it can be seen that the case of a tree-like network leads to the best performance, whereby the fixed point of the perturbed dynamics generally becomes stable, i.e. $\Re(\lambda')_{\max}$ is negative, and the modulus reaches larger values than in the corresponding case of networks with higher connectivity. Therefore, our analysis shows that sparse tree-like networks have both a larger explorability and a larger dynamical robustness than random networks with higher connectivity.

A.4.1 Increasing heterogeneity

We also calculated the explorability increasing the heterogeneity in both the dynamics parameter (α_i) and the fixed points (x_i^*) that were sampled: we took random realizations of $\alpha_i = \alpha + q_i$, where the q_i's were independent Gaussian random variables with zero mean and standard deviation σ_α (as for the simple case, we set $\alpha = 1$); for each realization, we also enlarged the region explored around the homogeneous state by taking different realizations of $x_i^* = x^* + p_i$ (where the p_i's are distributed as the q_i's with standard deviation σ_x). Varying the value of x^*, we counted *all* the fixed points at the edge of stability (within a small error $|\Re(\lambda)_{\max}| < 10^{-2}$), and for each one we evaluated $V_E = 1 - \sum_i x_i^*/S$ as the most straightforward generalization of our previous definition of V_E; then, we constructed the histogram of V_E.

The curves in Fig. 15 for the case with heterogeneity were obtained using 10^2 independent realizations of ϵ_{ij}, and, for each one, 10 realizations of p_i and q_i, respectively.

A.5 Optimisation approach

We then went one step further and compared the explorability and dynamical robustness of tree-like networks with graphs constructed via an optimisation process rather than randomly generated.

In the optimisation, weight values ϵ_{ij} were changed accordingly to a stochastic hill climbing algorithm [138], whereas their locations were kept fixed. Introducing a random Gaussian perturbation with zero mean and standard deviation $\delta\epsilon$ in all ϵ_{ij}, the new configuration was accepted if the quantity to optimise (either V_E or R) increased, and the process was iterated for T time steps. Our results are robust for different choices of $\delta\epsilon$ in the range $[10^{-3}, 10^{-1}]$. We restricted our analysis to the homogeneous case ($x_i^* = x^*, \alpha_i = \alpha$), using network sizes of $S = 10$ to facilitate the convergence of the optimisation algorithms. Still, the landscape of $V_E(\epsilon_{ij})$ and $R(\epsilon_{ij})$ appeared to be highly irregular with many local minima when increasing the connectivity.

Fig. 16 represents the initial random-generated networks with connectivities in the range $C \in [0.25, 0.75]$ (blue dots) and the corresponding optimised values for the explorability and the dynamical robustness (green and magenta dots, respectively). Qualitatively similar results are found using different schedules of the simulated annealing algorithm [139]. The explorability reached for networks with connectivities larger than the one for tree-like networks turned out to be very close to the corresponding value for the optimal tree-like topology. However, in general, such networks exhibited low values of dynamical robustness. Similarly, when optimising the dynamical robustness we ended up with values very close to that of the optimal tree-like network, but remarkably, without improving the explorability.

We also implemented a multi-objective optimisation algorithm, in which a perturbation in ϵ_{ij} was only accepted if it increased simultaneously both the explorability and the dynamical robustness of the network. However, this method worked only for tree-like networks with one or two additional links (see red dot in Fig. 16), while it was totally inefficient for more dense structures. Slightly better (but still suboptimal) results were obtained when both tasks were optimised one at a time in alternating periods.

In conclusion, sparse networks provide quasi-optimal values for both the explorability and dynamical robustness without fine-tuning many of the interaction strengths.

A.6 Self-similarity

Finally, we proved that the property of sparsity is self-similar, since on aggregating sparse interacting communities, we obtained larger sparse communities (see Supplementary section for details). For example, joining two networks with a tree-like topology using a single link led again to a network with a tree-like topology. Similarly, if sparse networks with S nodes have $aS - b$ links, with a and b integer constants, then joining two such networks with S and S' nodes using b links leads again to a sparse network with $a(S + S') - b$ links. Therefore, the optimal features of sparsity are conserved on assembling or disassembling processes, thereby avoiding any drastic change in the stability [140].

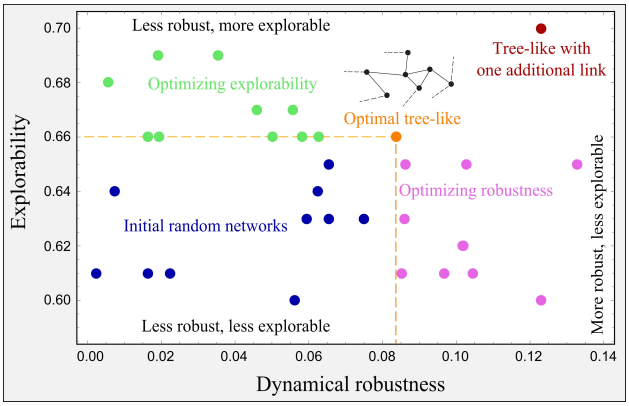

Figure 16: Optimisation of random generated networks of size $S = 10$ and with different connectivities in the range $[0.25, 0.75]$ (blue dots) in the explorability (green dots) and dynamical robustness (magenta dots). The optimal tree-like network is represented by the orange dot. The red dot in the right top corner represents a tree-like network with one additional link, obtained using a multi-objective optimization for both the explorability and the dynamical robustness; such a method appeared to be inefficient for higher values of the connectivity. Each network was optimized using a stochastic hill climbing algorithm [138] with parameters $T = 200$ and $\delta\epsilon = 0.01$.

A.7 Discussion

Our approach provides a theoretical insight into why sparsity is an observed common feature in living interacting systems. Sparse networks generally of-

fer optimal values of both explorability and dynamical robustness, whereas denser networks can only perform better if interactions are selectively tuned. Nevertheless, we observed that finding dense optimal networks with higher values of both explorability and dynamical robustness was barely feasible due to the multiplicity of the parameters that must be simultaneously tuned. Moreover, typically, the final networks have values of explorability and dynamical robustness comparable to those achievable for tree-like networks structures without the need to tune any parameters.

The results presented support the idea that sparsity is an emergent pattern of living interaction networks and this has implications for the understanding of the relationship between stability and complexity in real ecosystems. Indeed, sparsity may play a key role in the resolution of the so-called complexity-stability paradox [74, 76], in which highly biodiverse ecosystems will probably be unstable. The essence of the argument [74, 76] can be summarised as follows. The linearised dynamics for the population density around a stationary state depends on what is known as the community matrix, M. If all the eigenvalues of M have negative real parts, then the stationary point is also stable against small perturbations of the stationary populations. A null model corresponds to assume that M is a random matrix with diagonal elements (the self-interactions) equal to $-d < 0$, whereas the off-diagonal elements are zero with probability $1 - C$ and with probability C are drawn from a probability distribution with zero mean and variance σ^2. Under this null hypothesis, one finds (see [74, 76] and references therein for rigorous results) that the stationary point is unstable with probability 1 if $\sigma\sqrt{CS} > d$, where S is the number of species in the ecosystem (a measure of its biodiversity). This result holds if S is assumed to be large enough. Thus if σ and d do not have a peculiar scaling with the network size, highly complex ecosystems (i.e. with high CS) are not stable: a prediction in contradiction to empirical data [140, 115, 141]. However if the interaction network is sparse, i.e. $C \sim 1/S$, the above inequality becomes independent of S and the stability of the ecosystem is not threatened by high biodiversities: sparsity in ecological interaction networks allows for stable large living interacting systems [140, 115, 122]. As a matter of fact, such a scaling relationship is supported by the empirical observation (see Fig. 13).

Recent theoretical findings show that an increase in the interconnectivity between multiple systems composed themselves of interacting units can have a strong impact on the vulnerability of the whole system [142]. In the same vein, our results provide a theoretical understanding of this feature. We

suggest that sparsity is a key feature allowing living systems to be poised in a state that confers both robustness and adaptability (explorability) to best cope with an ever-changing environment and to promptly react to a wide range of external stimuli and to resist to perturbations.

Our ideas could be applied to understand the emergence of sparsity in some non-biological systems, as it has been empirically observed in human-built networks [143]. The underlying hypothesis of our approach is that living system interactions, unlike physical interactions (e.g. electromagnetic interactions among charged particles), can evolve/adapt to turn themselves on or off. The same idea holds for many non-biological networks, i.e. interactions can be selective and change in time, although the equations governing the underlying dynamics can be unknown.

Finally, we stress that our results do not depend on the specific details of the system and thus can be applied in many other fields. For example, a possible application might be in the design of artificial learning machines, such as deep neural networks [144, 145]. There is mounting evidence that deep learning often finds solutions with good generalisation properties [146, 144] and it has been shown recently [147] that to achieve such a good performance, it is crucial to have regions of the optimisation landscape that are both robust and accessible, independent of the particular task or of the training data set. On the other hand, maximisation of computation efficiency is a crucial point when designing learning machines: deep networks are very dense as each node is connected to all other nodes of the adjacent layers [145], which makes multilayer neural networks computationally hard to train. Our solution suggests that designing sparse neural networks will increase the explorability of the system while improving the convergence and robustness properties of the existing optimisation algorithms.

A.8 Supplementary to the Appendix

In this section we present some supplementary analytical and numerical results on the Appendix, in order to give a complete picture of our theoretical approach to explain the sparsity of living systems.

A.8.1 Experimental data

The following table lists all experimental datasets used in Figure 1 of the text, indicating details of the corresponding networks.

Type of network	Name	Nodes	Edges	Connectivity
Neural network	Brain C.Elegans [148]	252	509	0.00805
Gene-regulation	TRN Yeast-1 [148]	4441	12873	0.000653
	TRN Yeast-2 [148]	688	1079	0.00228
	TRN E.Coli-1 [148]	1550	3340	0.00139
	TRN E.Coli-2 [148]	418	519	0.00298
	TRN S.Cerevisiae [106]	723	2158	0.00413
Trust	College student [148]	32	96	0.0968
	Prison inmate [148]	67	182	0.0411
Protein interaction	Drugs-Targets [106]	1282	3186	0.00194
	ncRNA human [106]	188	498	0.0142
	ncRNA 6-organisms [106]	523	1294	0.00474
Metabolic	E.Coli [148]	2275	5763	0.00111
	S.Cerevisiae [148]	1511	3833	0.00168
	C.Elegans [148]	1173	2864	0.00208
FW Host-Parasite	Altuda 1979 [149]	47	122	0.0564
	Marathon 1979 [149]	78	346	0.0576
	Britain 1991 [150]	94	232	0.0265
	Finland 1991 [150]	69	190	0.0405
FW Plants-Herbivors	Cold lake [151]	50	182	0.0743
	Lake of the woods [152]	175	768	0.0252
	Lake Huron [153]	130	632	0.0377
	Smallwood reservoir [154]	31	106	0.114
	Parsnip river [155]	66	228	0.0531
	McGregor river [155]	70	316	0.0654
Mutualistic	Cordn del Cepo [115]	185	722	0.0212
	Cordn del Cepo [115]	107	392	0.0346
	Cordn del Cepo [115]	61	162	0.0443
	Central New Brunswick [115]	114	334	0.0259
	Princeton [115]	26	62	0.0954
	Mount Missim [115]	38	204	0.145
	Caguana [115]	39	128	0.0864
	Cialitos [115]	52	174	0.0656
	Cordillera [115]	36	94	0.0746

	Fronton [115]	34	96	0.0856
	Pikes Peak [115]	371	1846	0.0134
	Tropical rainforest [115]	77	268	0.0458
	Hickling [115]	78	292	0.0486
	Shelfanger [115]	52	170	0.0641
	Tenerife [115]	49	212	0.0901
	Latnjajaure [115]	142	484	0.0242
	Zackenberg [115]	107	912	0.0804
	Mauritius Island [115]	27	104	0.148
	Mtunzini [115]	24	182	0.330
	Santa Genebra Reserve [115]	23	62	0.122
	Santa Genebra Reserve [115]	62	238	0.0629
	North Negros Forest Reserve [115]	63	394	0.101
	Doñana National Park [115]	205	824	0.0197
	Hazen Camp [115]	110	358	0.0299
	Hato Ratn [115]	31	182	0.196
	Snowy Mountains [115]	127	538	0.0336
	Campeche State [115]	30	84	0.0965
	Hazen Camp [115]	111	380	0.0311
	Ashu [115]	770	2386	0.00403
	Kuala Lompat [115]	84	890	0.128
	Gabon [115]	25	122	0.203
	CMBRS [115]	62	124	0.0328
	Laguna Diamante [115]	66	166	0.0387
	Rio Bianco [115]	95	250	0.0280
	Bristol [115]	104	598	0.0558
	Melville Island [115]	29	76	0.0936
	Monteverde [115]	208	1322	0.0307
	North Carolina [115]	57	286	0.0896
	Galapagos [115]	159	408	0.0162
	Nava Correhuelas [115]	56	214	0.0695
	Nava Noguera [115]	44	174	0.0920
	Flores [115]	22	60	0.130
	Hestehaven [115]	49	124	0.0527
	Garajonay [115]	84	290	0.0415
	KwaZulu-Natal region [115]	64	198	0.0491
	Jamaica [115]	97	356	0.0382
	Arhur's pass [115]	78	240	0.0400
	Cass [115]	180	748	0.0232
	Craigieburn [115]	167	692	0.0250
	Daphn [115]	797	5866	0.00925
	Guarico State [115]	86	218	0.0298
	Canaima National Park [115]	97	312	0.0335
	Yakushima Island [115]	33	52	0.0492
	Brownfield [115]	40	130	0.0833

	Ottawa [115]	47	282	0.130
	Chilo [115]	156	624	0.0258
	Tropical rainforest [115]	62	414	0.109
	Intervales and Saibadela [115]	315	2106	0.0213
	Great Britain [115]	23	60	0.118

A.8.2 Measuring explorability

We detail the method developed in the text to estimate the explorability of a given topology. The section is organized as follows: *i)* We solve analytically the uniparametric case $\alpha_i = \alpha$, computing the volume of feasible and stale fixed points as a function of the threshold of stability, moving along the bisector $x_i^* = x^*$. By investigating the tree-like structures, we find an optimal tolopology that maximizes the explorability. *ii)* We increase the connectivity by including additional links to the optimal tree-like network, whose weights are fixed. In the case in which we add a few edges, we are able to find some particular interaction matrices which enlarge the value of explorability respect to the sparsest tree-like case. *iii)* We increase the explored region around the bisector and study the stability of the attractors as a function of the variability introduced. *iv)* We analyze the explorability for a more generic case of non-linear dynamics.

Analytical solution for a tree-like network in the uniparametric case

We start considering the simplest case of a $S \times S$ matrix w with S off-diagonal links, fixing the diagonal elements to $w_{ii} = -1$ [74, 156]. For a given value of x_i^* and α_i for each i, edges weights can be determined by solving the fixed point equation:

$$\sum_j w_{ij} x_j^* = -\alpha_i. \tag{278}$$

Eq. (278) has a unique solution if w has one non-diagonal entry per row, which means that the network must have one single loop, beyond the S self loops due to the diagonal entries. In this situation the interaction matrix is sparse, and its connectivity C is equal to:

$$C = \frac{number\ of\ links}{matrix\ dimension} = \frac{2}{S} \tag{279}$$

In order to evaluate the explorability of this network, we first investigate the bisector of the attractor space, setting all the components of a fixed point equal to x^*. We also fix model parameters to $\alpha_i = \alpha$ for sake of simplicity. In this case, the weights w of the S off-diagonal links in the interaction matrix are:

$$w = \frac{x^* - \alpha}{x^*} \tag{280}$$

Eq. (280) does not depend on the specific position of the S links. In order to analyze the stability of a fixed point $\mathbf{x}^*$, we have to write the characteristic polynomial of the Jacobian matrix J and seek for the real part of its principal eigenvalue, $\Re(\lambda)_{\max}$. Note that J has the same topology of w, with $-x^*$ as diagonal elements and wx^* as off-diagonal elements. One can express the determinant of $J^{(\lambda)} = J - \lambda\mathbf{1}$ using the Grassmann variables $\{\chi_i, \chi_i^*\}_{i=1}^S$ [157] in terms of the following Gaussian integral:

$$\det J^{(\lambda)} = \int d\chi_1 ... d\chi_S d\chi_1^* ... d\chi_S^* \exp\left(\chi_k J_{kl}^{(\lambda)} \chi_l^*\right) \tag{281}$$

Using the properties of the Grassmann variables [157], from Eq. (281) we can state the following operative rules to derive the characteristic polynomial of $J^{(\lambda)}$:

1. Represent the interaction matrix as a graph with a fixed number of loops.
2. Associate to each self-loop a weight $-x^* - \lambda$ and to the links a weight $x^* - \alpha$.
3. Consider all possible combinations of links forming loops reaching once every node in the graph.
4. The weight of each of these combinations is obtained by multiplying the weights associated to the links and a factor-1 for each loop in the combination under consideration.
5. Sum up each of these contributions to obtain the characteristic polynomial.

Using this method, it is easy to demonstrate that, for the simple uniparametric case of a tree-like network with one single loop, the characteristic polynomial is:

$$\det J^{(\lambda)} = (x^* + \lambda)^{S-l}[(x^* + \lambda)^l - (x^* - \alpha)^l], \tag{282}$$

where $l > 1$ is the number of links of the loop. The real part of the corresponding roots are:

$$\Re(\lambda_k) = -x^* + (x^* - \alpha)\cos\left(\frac{2k\pi}{l}\right) \qquad k = 1, ...l. \tag{283}$$

By imposing that the maximum of these values to be negative, which guarantees that $\mathbf{x}^* = (x^*, \ldots, x^*)$ is a stable fixed point, we obtain the following inequalities:

$$\begin{aligned} x^* > x_c^* = \frac{\alpha}{2} \qquad & \textit{if} \;\; l \;\; = \;\; 2n \\ x^* > x_c^* = \frac{\alpha}{3} \qquad & \textit{if} \;\; l \;\; = \;\; 3 \\ x^* > x_c^* = \frac{\alpha}{1+\phi(n)} \qquad & \textit{if} \;\; l \;\; = \;\; 2n+3 \end{aligned} \tag{284}$$

where n is a positive integer and $\phi(n) = -\left(\cos\left(\frac{2(n+1)\pi}{2n+3}\right)\right)^{-1}$. From equation (284) we find that a network with one loop of length 3 provides the lowest x_c^*, and therefore maximizes the volume of feasible and stable attractors.

The threshold of stability x_c^* can be used as a proxy for the volume of explorability; the larger the value of x_c^*, the smaller the explorability V_E. As we are only interested in comparing the explorability of different networks, one possibility is to take $V_E = V_0 - x_c^*$, with V_0 a constant value that has to be large enough to avoid negative values of V_E. With this definition, $V_E = V_0 - \frac{1}{3}\alpha$ for the tree-like network.

On the other hand, α is a parameter of the dynamics (e.g. the species growth rates), that can be set to $\alpha = 1$ without loss of generality (this only sets a time-scale, although rescaling α without rescaling the weights w_{ij} changes the location of the attractors).

Unless otherwise specified, in what follows we set $V_0 = \alpha = 1$, which leads to $V_E = \frac{2}{3}$ for the optimal tree-like network.

Numerical results increasing the number of links

Starting from the solution just found, i.e. the optimal tree-like network with a single loop of length 3, we introduce additional weighted links. If in the tree-like network, the link leaving node i and ending at node j is missing, we may add it with its weight denoted by ϵ_{ij}. Following the method

described in the previous section, we derive analytically the characteristic polynomial of the Jacobian matrix. Because this expression clearly depends on the positions and weights of the additional links, an exhaustive search of solutions that improve the explorability of the optimal tree-like network cannot be performed. However, in Fig. 17 we show two particular topologies with $V_E > \frac{2}{3}$.

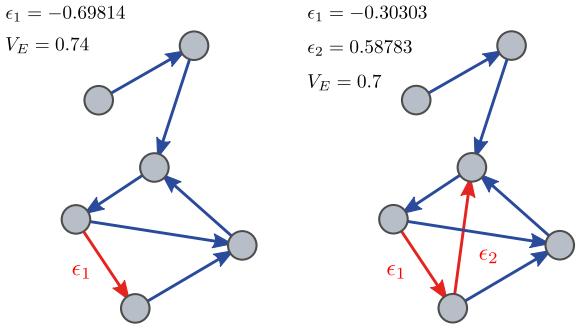

Figure 17: Topologies improving the explorability of the optimal tree-like network: *left)* 2-loop interaction matrix, *right)* 3-loop interaction matrix. We have set $\alpha = 1$ as well as $V_0 = 1$ in the definition of the explorability in terms of the threshold of stability, which leads to $V_E = 2/3$ for the optimal tree-like network.

Although it is possible to improve the explorability of the optimal tree-like network, this becomes harder and harder as the connectivity, C, increases. Indeed, as illustrated in Fig. 3 in the text, taking random realizations of the added links ϵ_{ij} from a Gaussian distribution with zero mean and standard deviation σ_ϵ and their positions uniformly distributed, we obtain a histogram $P(V_E|C)$ which is shifted to lower values of V_E than the optimal one for a tree-like network. Similar results are shown in Fig. 18 for different values of the σ_ϵ.

Defining a threshold of stability

In the simplest situation in which $x_i^* = x^*$ and $\alpha_i = \alpha$, we observed that, in most cases, $\Re(\lambda)_{\max}$ is positive for small x^* and negative for large x^*, intersecting $\Re(\lambda)_{\max} = 0$ at a single value x_c^*. However, we have observed some singular cases: some of them (less than 1% for $C = 0.5$ and $\sigma_\epsilon = 0.1$) lead to multiple solutions for $\Re(\lambda)_{\max} = 0$ (see Fig. 19). For these cases taking the threshold as the minimum value among all the possible solutions

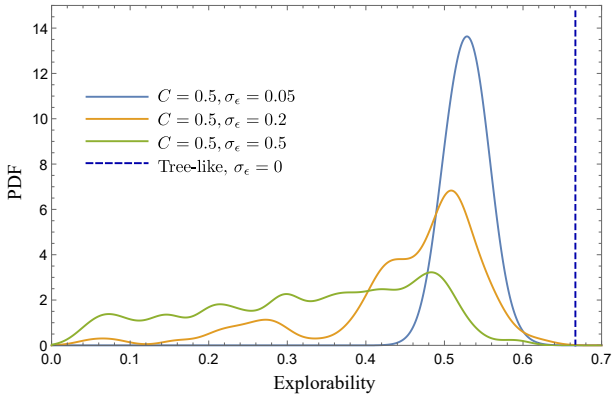

Figure 18: Probability distribution functions (PDF) of the explorability V_E for the optimal tree-like graph and networks with $C = 0.5$ obtained by adding extra links with random (uniformly distributed) locations and weights ϵ_{ij} taken from a zero-mean Gaussian distribution with standard deviation σ_ϵ, for a network size $S = 20$ and $\alpha = 1$, using 10^3 independent realizations of the added links. Increasing the variability of the weights of the added links the explorability generally decreases. We have set $V_0 = 1$ in the definition of the explorability.

lead to an overestimate of the explorability. As these cases only appear for dense topologies, such an overestimate does not affect our conclusions.

In addition, only for dense networks, we could find some cases (less than 1% for $C = 0.5$ and $\sigma_\epsilon = 0.1$) with no feasible and stable attractors (i.e. with $\Re(\lambda)_{\max}$ always positive), which are not admissible cases in our analysis.

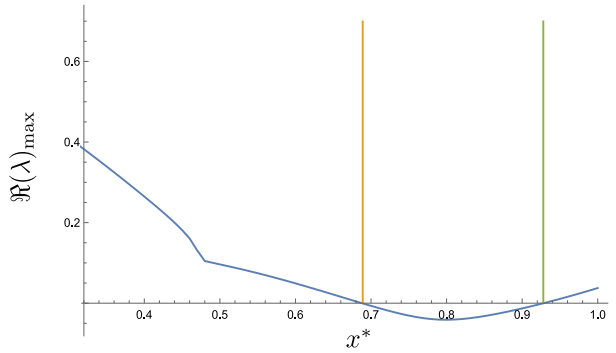

Figure 19: $\Re(\lambda)_{\max}$ as a function of x^* for a particular network with $C = 0.5$ generated using $\sigma_\epsilon = 0.5$ ($\alpha = 1$, $S = 20$). The curve exhibits two solutions for $\Re(\lambda)_{\max} = 0$.

Introducing variability in the explored region

In the previous sections we carried out an analysis for x_i^* and α_i independent of i, i.e. moving along the bisector of the attractor space in a uniparametric subspace. Here we enlarge the explored region of attractors, by introducing a variability in the fixed point and in the model parameters, as follows:

$$x_i^* = x^* + p_i$$
$$\alpha_i^* = \alpha + q_i$$

for $i = 1, ...S$, where p_i and q_i are independent Gaussian random variables with zero mean and standard deviation σ_x and σ_α, respectively. In this case, we counted all the sampled attractors at the edge of stability (within a small error $|\Re(\lambda)_{\max}| < 10^{-2}$), and for each one we evaluated $V_E = 1 - \sum_i x_i^*/S$ as the most straightforward generalization of the measure of explorability.

Fig. 20 shows, for the case $\sigma_x = \sigma_\alpha$, how the probability of being stable changes for the optimal tree-like network and for the topologies shown in Fig. 17. Notice that such curves become smoother and smoother as the heterogeneity increases. In this case, simulations have been done with $S = 4$, as only links forming loops contribute to the Jacobian (see Section 2.1), and consequently similar results can be expected using larger networks with only 1, 2 and 3 loops.

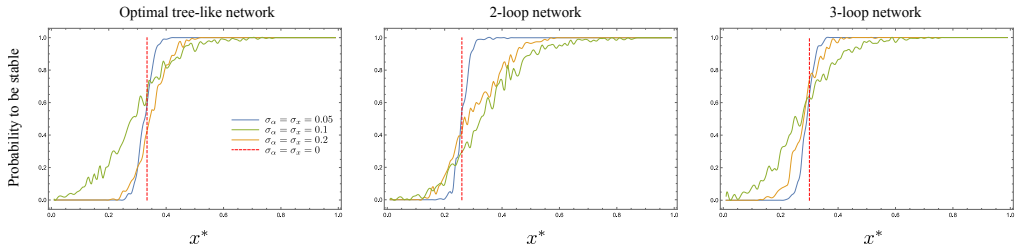

Figure 20: Probability to be stable around the bisector for different network structures and values of heterogeneity. Moving along the bisector $x_i^* = x^*$, we generate 200 independent realization of $(x^* + p_i, \alpha + q_i)$, where p_i and q_i are independent Gaussian variables with zero mean and standard deviation σ_x and σ_α, respectively. We represent the probability of these attractors to be stable as a function of $\bar{x}^* = \sum_i x_i^*/S$ for: *left)* the optimal tree-like network with $S = 4$; *middle)* the 2-loop interaction matrix in Fig. 17 and *right)* the 3-loop network in Fig. 17. Red-dashed line represents the homogeneous case for comparison.

Finally, similarly to Fig. 3 of the text, Fig. 21 illustrates the histogram of explorability, $P(V_E|C)$, for different values of $\sigma_x = \sigma_\alpha$, for the tree-like network and for a more dense topology with $C = 0.5$. These results show

that the introduction of variability does not change our conclusion, that is sparse networks generally provide larger values of explorability.

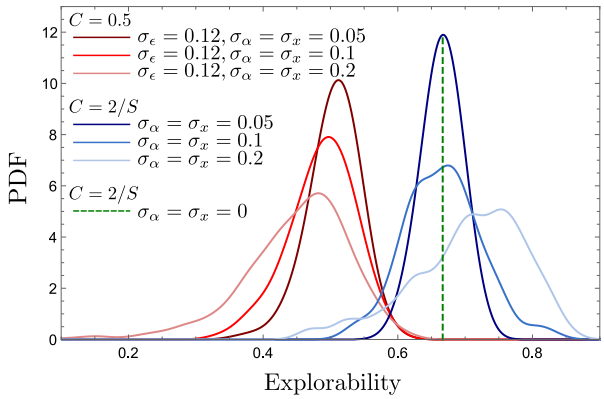

Figure 21: Probability distribution functions (PDF) of the explorability V_E for the optimal tree-like graph and networks with $C = 0.5$. We performed 10^2 independent realizations of the added links ($\epsilon_{ij} = 0$ for the tree-like network), and for each one sampling 10 different choices (p_i, q_i). Network size $S = 20$ and $\alpha = 1$. Variability does not qualitatively influence our main results.

From a Lotka-Volterra model to a more general dynamics

The results presented in the previous sections implicitly refer to a generalized Lotka-Volterra dynamical model [127, 125, 129, 158, 159, 160, 126]. We can also generalize the dynamics to the form:

$$\dot{x}_i = G_i\left(x_i\right) F_i\left(\sum_j w_{ij} x_j\right) \tag{285}$$

whose fixed point is determined by $F_i(-\alpha_i) = 0$ leading to Eq. (278) (see text). The Jacobian matrix of such a dynamics is $J_{ij} = G_i\left(x_i^*\right) \left.\frac{dF_i}{dz_i}\right|_{-\alpha_i} w_{ij}$, where $z_i = \sum_j w_{ij} x_j$. Since we have no available information of the particular form of $\mathbf{G}$ and $\mathbf{F}$, in the same spirit of May's original contribution [74, 156], we can write the Jacobian matrix as $J_{ij} = \xi_i w_{ij}$, where ξ_i is a random number uniformly distributed between 0 and 1, in analogy with the Lotka-Volterra simple case. Fig. 22 represents the histogram of the explorability for a tree-like matrix and $C = 0.5$, sampling different values of $\boldsymbol{\xi}$.

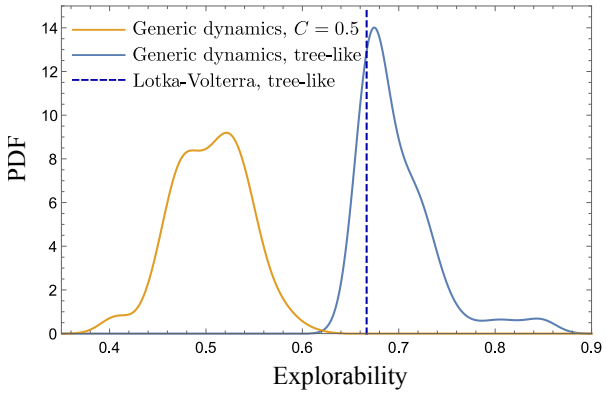

Figure 22: Probability distribution functions (PDF) of the explorability V_E for a generic form of the dynamics, Eq. (285), for the optimal tree-like network (blue solid curve) and $C = 0.5$ (orange curve). Dashed-blue line indicates the explorability of the optimal tree-like network in the case of the Lotka-Volterra dynamics for comparison. Still for such a generic form of the dynamics, more dense networks customarily lead to lower values of the explorability. We performed 10^2 independent realizations of the added links ($\epsilon_{ij} = 0$ for the tree-like network), and for each one 10 different dynamics encoded in $\boldsymbol{\xi}$, extracted from a uniform distribution in $[0, 1]^S$. Parameters are set to $S = 20$, $\alpha = 1$, $\sigma_\epsilon = 0.12$ and $\sigma_x = \sigma_\alpha = 0$.

A.8.3 Dynamical robustness

In this section we derive the explicit expression of the perturbed dynamics Jacobian (see text). In addition, we discuss how to include additional information on the dynamics rather than performing a simple random-matrix approach, and include several numerical simulations to support this method.

Perturbing the dynamics

We introduce a perturbation of the dynamics, Eq. (285), in the form $\dot{x}_i = (G_i + \delta G_i)(F_i + \delta F_i)(z_i)$ where $z_i = \sum_j w_{ij} x_j$. Up to the first order in the perturbation the dynamical equation becomes:

$$\dot{x}_i = G_i\left(x_i\right) F_i\left(z_i\right) + \delta G_i\left(x_i\right) F_i\left(z_i\right) + G_i\left(x_i\right) \delta F_i\left(z_i\right). \tag{286}$$

The new fixed point equation becomes $(F_i + \delta F_i)(z_i'^*) = 0$. Now we suppose that the new fixed point $x_i^{*\prime}$ of (286) differs only by a little amount δ_i from the original fixed point of the unperturbed dynamics, i.e. $x_i^{*\prime} = x_i^* + \delta_i$. In this case $z_i^{*\prime} \equiv \sum_j w_{ij} x_i^{*\prime} = z_i^* + \Delta_i$, with $\Delta_i \equiv \sum_j w_{ij}\delta_j$. Thus to the first

order in δF we get

$$\delta_i = -\sum_j w_{ij}^{-1} \frac{\delta F_j(z_j)}{dF_j(z_j)/dz_j}\bigg|_{z_j=z_j^*} \tag{287}$$

We are now interested in calculating the Jacobian matrix evaluated at the fixed point. Reminding that, by definition, $F_i(z_i) = 0$ at $\mathbf{x}^*$, and that $\frac{dF_i(z_i)}{dx_j} = \frac{dF_i(z_i)}{dz_i}\frac{dz_i}{dx_j} = \frac{dF_i(z_i)}{dz_i}w_{ij}$. As $\frac{dG_i(x_i)}{dx_j} = \frac{dG_i(x_i)}{dx_i}\delta_{ij}$ and $\frac{d\delta G_i(x_i)}{dx_j} = \frac{d\delta G_i(x_i)}{dx_i}\delta_{ij}$, the Jacobian matrix evaluated at the new fixed point can be written as:

$$J'_{ij} = \xi'_i w_{ij}, \tag{288}$$

where

$$\xi'_i = \left[G_i(x_i)\left(\frac{dF_i(z_i)}{dz_i} + \frac{d\delta F_i(z_i)}{dz_i} + \frac{d^2F_i(z_i)}{{dz_i}^2}\Delta_i\right) + \frac{dF_i(z_i)}{dz_i}\left(\frac{dG_i(x_i)}{dx_i}\delta_i + \delta G_i(x_i)\right)\right]. \tag{289}$$

Adopting a random matrix approach (i.e. without further information about the dynamics), ξ'_i can be set to be a random variable, that, in analogy with a Lotka-Volterra dynamics, we take uniformly distributed between 0 and 1 (see text).

Including additional information in the perturbed Jacobian matrix

For the Lotka-Volterra dynamics, $\boldsymbol{\xi} = \mathbf{x}^*$. In general, we can suppose that there exists a correlation between the vectors $\boldsymbol{\xi}$ and its perturbed version $\boldsymbol{\xi'}$ with the fixed point $\mathbf{x}^*$. A simple way to introduce such a correlation is:

$$\xi_i = \gamma r_i + (1-\gamma)x_i^* \tag{290}$$

$$\xi'_i = \gamma' r'_i + (1-\gamma')x_i^* \tag{291}$$

where r_i and r'_i are random variables uniformly distributed between 0 and 1, and γ and γ' are parameters (between 0 and 1) controlling the correlation for the non-perturbed and the perturbed dynamics, respectively.

Fig. 23 illustrates numerical results for the explorability when the unperturbed and the perturbed dynamics are respectively characterized by $\gamma = 0.1$ and $\gamma' = 0.5$ (with this choice, the unperturbed dynamics is "closer" to a Lotka-Volterra dynamics than the perturbed one). Analogously in Fig. 24

we show the probability distribution of the maximum real part of the eigenvalue of the Jacobian for the perturbed dynamics for the same choice of parameters. As it can be seen, our conclusions are still valid in this more general situation: tree-like networks generally offer the best performance. Qualitatively similar results are obtained for other values of γ and γ'.

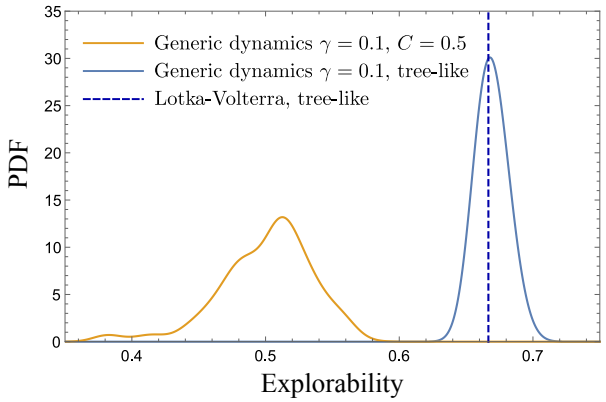

Figure 23: Probability distribution functions (PDF) of the explorability V_E for generic dynamics characterized by $\gamma = 0.1$ (Eq. (290)). Solid blue and orange curves represent the optimal tree-like network and $C = 0.5$, respectively. Dashed blue line indicates the value of V_E for the optimal tree-like network in the case $\gamma = 0$. We performed 10^2 independent realizations of the added links ($\epsilon_{ij} = 0$ for the tree-like network), and for each one 10 different dynamics $\boldsymbol{\xi}$ as given by Eq. (290). Parameters are set to $S = 20$, $\alpha = 1$, $\sigma_\epsilon = 0.12$ and $\sigma_x = \sigma_\alpha = 0$.

Measuring dynamical robustness

When analyzing the dynamical robustness, we qualitatively compare the PDF of $\Re(\lambda')_{\max}$ for different connectivities. Based on such distribution, we can give a quantitative measure R of "how dynamically robust" is a certain topology, that will be useful when implementing the optimization algorithm.

In the text we refer to the 5th percentile (with a minus sign) of the distribution of $\Re(\lambda')_{\max}$ as a measure of dynamical robustness, $R = -\Re(\lambda')^{5th}_{\max}$ (with the minus sign, more robust topologies lead to larger values of R). Naively speaking, this is a quantification of "how stable" can be the system for such perturbed dynamics that makes the system as stable as possible. Certainly, it is possible to define other measures of this property (e.g. the 10th, 20th and 50th percentiles) that lead, qualitatively, to the same conclusion, as illustrated in Fig. 25. However, lower percentile values generally enhance the differences between topologies.

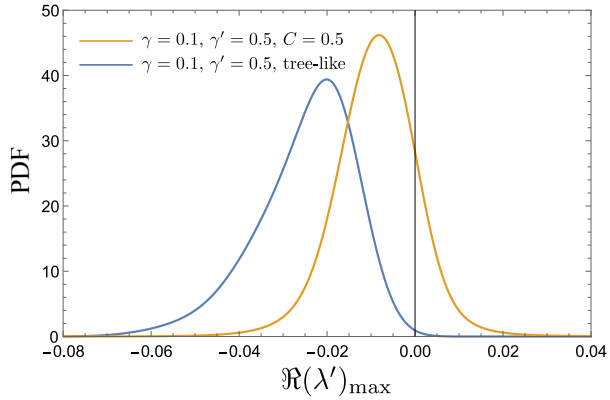

Figure 24: Probability distribution functions (PDF) of the real part of the maximum eigenvalue of the Jacobian matrix of the perturbed dynamics with $\gamma' = 0.5$ whereas the non-perturbed dynamics is characterized by $\gamma = 0.1$ (see Equations (290) and (291)). We performed 10^2 independent realizations of the added links ($\epsilon_{ij} = 0$ for the tree-like network), and for each one 10 different dynamics $\boldsymbol{\xi}$. For each matrix at the edge of instability (within an error $|\Re(\lambda')_{\max}| < 10^{-2}$), we sampled over 10^3 perturbed dynamics $\boldsymbol{\xi'}$. Parameters are set to $S = 20$, $\alpha = 1$, $\sigma_\epsilon = 0.12$ and $\sigma_x = \sigma_\alpha = 0$.

A.8.4 From sparse interaction matrices to community structures

An important characteristic of sparse tree-like is their ability to remain sparse after aggregation of many of them. Therefore, sparse systems will preserve their optimal features after aggregation. More specifically, the characteristic polynomial only depends on the loops of the network (see Section A.8.2), and therefore an aggregation of sparse structures through a few links will not dramatically change its explorability. In Fig. 26 we represent a simple example of two tree-like topologies that can be assembled, preserving the optimality feature.

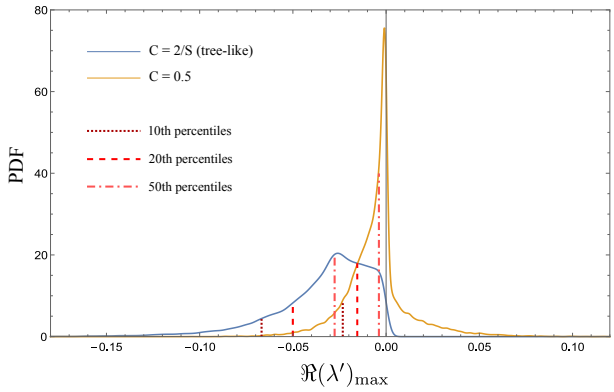

Figure 25: Comparison between different measures of dynamical robustness (10th, 20th and 50th percentiles of the distribution $P(\Re(\lambda')_{\max})$) in the case of $\sigma_\alpha = \sigma_x = 0.1$ for the optimal tree-like network and graphs of $S = 20$ with $C = 0.5$ (for which $\sigma_\epsilon = 0.12$). We have set $\alpha = 1$. All the curves are obtained as explained in Fig. 3 of the text. In all cases, the corresponding measure of dynamical robustness decreases when increasing the connectivity.

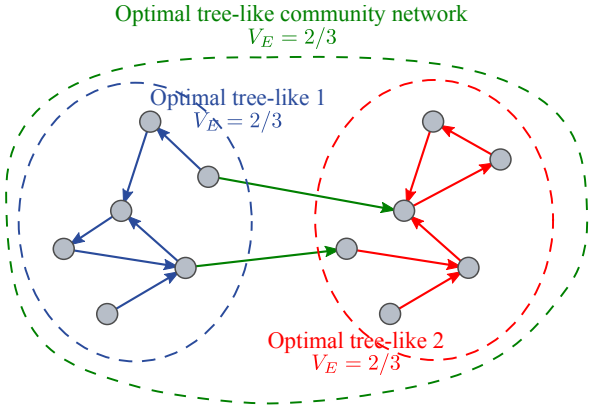

Figure 26: Example of two tree-like networks that can be assembled obtaining a larger community with the same explorability as each single component.

References

[1] D. Kondepudi and I. Prigogine, *Modern thermodynamics: from heat engines to dissipative structures*. John Wiley & Sons, 2014.

[2] C. Van den Broeck *et al.*, "Stochastic thermodynamics: a brief introduction," *Physics of Complex Colloids*, vol. 184, pp. 155–193, 2013.

[3] R. Clausius, "Über verschiedene für die anwendung bequeme formen der hauptgleichungen der mechanischen wärmetheorie," *Annalen der Physik*, vol. 201, no. 7, pp. 353–400, 1865.

[4] E. T. Jaynes, "Gibbs vs boltzmann entropies," *American Journal of Physics*, vol. 33, no. 5, pp. 391–398, 1965.

[5] E. T. Jaynes, "Information theory and statistical mechanics," *Physical review*, vol. 106, no. 4, p. 620, 1957.

[6] E. T. Jaynes, "Information theory and statistical mechanics. ii," *Physical review*, vol. 108, no. 2, p. 171, 1957.

[7] M. A. Nielsen and I. Chuang, "Quantum computation and quantum information," 2002.

[8] C. E. Shannon, "A mathematical theory of communication, part i, part ii," *Bell Syst. Tech. J.*, vol. 27, pp. 623–656, 1948.

[9] T. Speck, V. Blickle, C. Bechinger, and U. Seifert, "Distribution of entropy production for a colloidal particle in a nonequilibrium steady state," *EPL (Europhysics Letters)*, vol. 79, no. 3, p. 30002, 2007.

[10] S. Toyabe, T. Sagawa, M. Ueda, E. Muneyuki, and M. Sano, "Experimental demonstration of information-to-energy conversion and validation of the generalized jarzynski equality," *Nature physics*, vol. 6, no. 12, pp. 988–992, 2010.

[11] J. M. Horowitz and J. M. Parrondo, "Designing optimal discrete-feedback thermodynamic engines," *New Journal of Physics*, vol. 13, no. 12, p. 123019, 2011.

[12] R. D. Astumian, "Thermodynamics and kinetics of a brownian motor," *science*, vol. 276, no. 5314, pp. 917–922, 1997.

[13] P. Romanczuk, M. Bär, W. Ebeling, B. Lindner, and L. Schimansky-Geier, "Active brownian particles," *The European Physical Journal Special Topics*, vol. 202, no. 1, pp. 1–162, 2012.

[14] C. Ganguly and D. Chaudhuri, "Stochastic thermodynamics of active brownian particles," *Physical Review E*, vol. 88, no. 3, p. 032102, 2013.

[15] J. Howard, "Molecular motors: structural adaptations to cellular functions," *Nature*, vol. 389, no. 6651, pp. 561–567, 1997.

[16] A. B. Kolomeisky and M. E. Fisher, "Molecular motors: a theorist's perspective," *Annu. Rev. Phys. Chem.*, vol. 58, pp. 675–695, 2007.

[17] S. Ciliberto, S. Joubaud, and A. Petrosyan, "Fluctuations in out-of-equilibrium systems: from theory to experiment," *Journal of Statistical Mechanics: Theory and Experiment*, vol. 2010, no. 12, p. P12003, 2010.

[18] U. Seifert, "Stochastic thermodynamics, fluctuation theorems and molecular machines," *Reports on Progress in Physics*, vol. 75, no. 12, p. 126001, 2012.

[19] K. Sekimoto, "Langevin equation and thermodynamics," *Progress of Theoretical Physics Supplement*, vol. 130, pp. 17–27, 1998.

[20] J. Kurchan, "Fluctuation theorem for stochastic dynamics," *Journal of Physics A: Mathematical and General*, vol. 31, no. 16, p. 3719, 1998.

[21] J. L. Lebowitz and H. Spohn, "A gallavotti–cohen-type symmetry in the large deviation functional for stochastic dynamics," *Journal of Statistical Physics*, vol. 95, no. 1, pp. 333–365, 1999.

[22] C. Maes, "On the origin and the use of fluctuation relations for the entropy," *Séminaire Poincaré*, vol. 2, pp. 29–62, 2003.

[23] U. Seifert, "Entropy production along a stochastic trajectory and an integral fluctuation theorem," *Physical review letters*, vol. 95, no. 4, p. 040602, 2005.

[24] O. Penrose, *Foundations of statistical mechanics: a deductive treatment*. Courier Corporation, 2005.

[25] U. Seifert, "Stochastic thermodynamics of single enzymes and molecular motors," *The European Physical Journal E: Soft Matter and Biological Physics*, vol. 34, no. 3, pp. 1–11, 2011.

[26] R. Kubo, "The fluctuation-dissipation theorem," *Reports on progress in physics*, vol. 29, no. 1, p. 255, 1966.

[27] M. Baiesi, C. Maes, and B. Wynants, "Nonequilibrium linear response for markov dynamics, i: jump processes and overdamped diffusions," *Journal of statistical physics*, vol. 137, no. 5, pp. 1094–1116, 2009.

[28] J. B. Johnson, "Thermal agitation of electricity in conductors," *Physical review*, vol. 32, no. 1, p. 97, 1928.

[29] H. Nyquist, "Thermal agitation of electric charge in conductors," *Physical review*, vol. 32, no. 1, p. 110, 1928.

[30] L. Onsager, "Reciprocal relations in irreversible processes. i.," *Physical review*, vol. 37, no. 4, p. 405, 1931.

[31] C. Jarzynski, "Nonequilibrium equality for free energy differences," *Physical Review Letters*, vol. 78, no. 14, p. 2690, 1997.

[32] G. E. Crooks, "Entropy production fluctuation theorem and the nonequilibrium work relation for free energy differences," *Physical Review E*, vol. 60, no. 3, p. 2721, 1999.

[33] O. Raz, Y. Subaşı, and C. Jarzynski, "Mimicking nonequilibrium steady states with time-periodic driving," *Physical Review X*, vol. 6, no. 2, p. 021022, 2016.

[34] R. Landauer, "Irreversibility and heat generation in the computing process," *IBM journal of research and development*, vol. 5, no. 3, pp. 183–191, 1961.

[35] C. H. Bennett, "The thermodynamics of computationa review," *International Journal of Theoretical Physics*, vol. 21, no. 12, pp. 905–940, 1982.

[36] C. H. Bennett, "Notes on landauer's principle, reversible computation, and maxwell's demon," *Studies In History and Philosophy of Science*

Part B: Studies In History and Philosophy of Modern Physics, vol. 34, no. 3, pp. 501–510, 2003.

[37] L. Szilard, "Über die entropieverminderung in einem thermodynamischen system bei eingriffen intelligenter wesen," *Zeitschrift für Physik A Hadrons and Nuclei*, vol. 53, no. 11, pp. 840–856, 1929.

[38] S. R. De Groot and P. Mazur, *Non-equilibrium thermodynamics*. Courier Corporation, 2013.

[39] T. Hatano and S.-i. Sasa, "Steady-state thermodynamics of langevin systems," *Physical review letters*, vol. 86, no. 16, p. 3463, 2001.

[40] C. Pérez-Espigares, A. B. Kolton, and J. Kurchan, "Infinite family of second-law-like inequalities," *Physical Review E*, vol. 85, no. 3, p. 031135, 2012.

[41] E. Trepagnier, C. Jarzynski, F. Ritort, G. E. Crooks, C. Bustamante, and J. Liphardt, "Experimental test of hatano and sasa's nonequilibrium steady-state equality," *Proceedings of the National Academy of Sciences of the United States of America*, vol. 101, no. 42, pp. 15038–15041, 2004.

[42] G. Gallavotti and E. G. D. Cohen, "Dynamical ensembles in nonequilibrium statistical mechanics," *Physical Review Letters*, vol. 74, no. 14, p. 2694, 1995.

[43] I. Neri, É. Roldán, and F. Jülicher, "Statistics of infima and stopping times of entropy production and applications to active molecular processes," *Physical Review X*, vol. 7, no. 1, p. 011019, 2017.

[44] J. M. Parrondo, C. Van den Broeck, and R. Kawai, "Entropy production and the arrow of time," *New Journal of Physics*, vol. 11, no. 7, p. 073008, 2009.

[45] P. Pietzonka, A. C. Barato, and U. Seifert, "Universal bounds on current fluctuations," *Physical Review E*, vol. 93, no. 5, p. 052145, 2016.

[46] T. R. Gingrich and J. M. Horowitz, "Fundamental bounds on first passage time fluctuations for currents," *arXiv preprint arXiv:1706.09027*, 2017.

[47] J. Mehl, T. Speck, and U. Seifert, "Large deviation function for entropy production in driven one-dimensional systems," *Physical Review E*, vol. 78, no. 1, p. 011123, 2008.

[48] W. R. Browne and B. L. Feringa, "Making molecular machines work," *Nature nanotechnology*, vol. 1, no. 1, pp. 25–35, 2006.

[49] J. V. Hernández, E. R. Kay, and D. A. Leigh, "A reversible synthetic rotary molecular motor," *Science*, vol. 306, no. 5701, pp. 1532–1537, 2004.

[50] R. Ziener, A. Maritan, and H. Hinrichsen, "On entropy production in nonequilibrium systems," *Journal of Statistical Mechanics: Theory and Experiment*, vol. 2015, no. 8, p. P08014, 2015.

[51] M. Esposito, "Stochastic thermodynamics under coarse graining," *Physical Review E*, vol. 85, no. 4, p. 041125, 2012.

[52] A. Puglisi, S. Pigolotti, L. Rondoni, and A. Vulpiani, "Entropy production and coarse graining in markov processes," *Journal of Statistical Mechanics: Theory and Experiment*, vol. 2010, no. 05, p. P05015, 2010.

[53] S. Bo and A. Celani, "Entropy production in stochastic systems with fast and slow time-scales," *Journal of Statistical Physics*, vol. 154, no. 5, pp. 1325–1351, 2014.

[54] L. Martyushev and V. Seleznev, "Maximum entropy production principle in physics, chemistry and biology," *Physics reports*, vol. 426, no. 1, pp. 1–45, 2006.

[55] A. H. Reis, "Use and validity of principles of extremum of entropy production in the study of complex systems," *Annals of Physics*, vol. 346, pp. 22–27, 2014.

[56] R. Dewar, "Information theory explanation of the fluctuation theorem, maximum entropy production and self-organized criticality in non-equilibrium stationary states," *Journal of Physics A: Mathematical and General*, vol. 36, no. 3, p. 631, 2003.

[57] H. Ozawa, A. Ohmura, R. D. Lorenz, and T. Pujol, "The second law of thermodynamics and the global climate system: a review of the maximum entropy production principle," *Reviews of Geophysics*, vol. 41, no. 4, 2003.

[58] M. Polettini, "Fact-checking zieglers maximum entropy production principle beyond the linear regime and towards steady states," *Entropy*, vol. 15, no. 7, pp. 2570–2584, 2013.

[59] N. G. Van Kampen, *Stochastic processes in physics and chemistry*, vol. 1. Elsevier, 1992.

[60] C. Gardiner, "Stochastic methods," *Springer Series in Synergetics (Springer-Verlag, Berlin, 2009)*, 1985.

[61] J. Schnakenberg, "Network theory of microscopic and macroscopic behavior of master equation systems," *Reviews of Modern physics*, vol. 48, no. 4, p. 571, 1976.

[62] F. Schlögl, "On thermodynamics near a steady state," *Zeitschrift für Physik A Hadrons and nuclei*, vol. 248, no. 5, pp. 446–458, 1971.

[63] R. Zia and B. Schmittmann, "Probability currents as principal characteristics in the statistical mechanics of non-equilibrium steady states," *Journal of Statistical Mechanics: Theory and Experiment*, vol. 2007, no. 07, p. P07012, 2007.

[64] R. Clausius, "Über eine veränderte form des zweiten hauptsatzes der mechanischen wärmetheorie," *Annalen der Physik*, vol. 169, no. 12, pp. 481–506, 1854.

[65] A. Y. Khinchin, *Mathematical foundations of information theory*. Courier Corporation, 2013.

[66] K. Mallick, "Some recent developments in non-equilibrium statistical physics.," *Pramana: Journal of Physics*, vol. 73, no. 3, 2009.

[67] H. Hinrichsen, C. Gogolin, and P. Janotta, "Non-equilibrium dynamics, thermalization and entropy production," in *Journal of Physics: Conference Series*, vol. 297, p. 012011, IOP Publishing, 2011.

[68] B. Barzel and A.-L. Barabási, "Universality in network dynamics," *Nature physics*, vol. 9, p. 673, 2013.

[69] M. Asllani, D. M. Busiello, T. Carletti, D. Fanelli, and G. Planchon, "Turing patterns in multiplex networks," *Physical Review E*, vol. 90, no. 4, p. 042814, 2014.

[70] M. Asllani, D. M. Busiello, T. Carletti, D. Fanelli, and G. Planchon, "Turing instabilities on cartesian product networks," *Scientific reports*, vol. 5, 2015.

[71] D. M. Busiello, G. Planchon, M. Asllani, T. Carletti, and D. Fanelli, "Pattern formation for reactive species undergoing anisotropic diffusion," *arXiv preprint arXiv:1504.00797*, 2015.

[72] M. E. Newman, "The structure and function of complex networks," *SIAM review*, vol. 45, no. 2, pp. 167–256, 2003.

[73] S. Boccaletti, V. Latora, Y. Moreno, M. Chavez, and D.-U. Hwang, "Complex networks: Structure and dynamics," *Physics reports*, vol. 424, no. 4, pp. 175–308, 2006.

[74] R. M. May, "Will a large complex system be stable?," *Nature*, vol. 238, no. 5364, pp. 413–414, 1972.

[75] S. Suweis, F. Simini, J. R. Banavar, and A. Maritan, "Emergence of structural and dynamical properties of ecological mutualistic networks," *Nature*, vol. 500, pp. 449–452, 2013.

[76] S. Allesina and S. Tang, "Stability criteria for complex ecosystems," *Nature*, vol. 483, no. 7388, pp. 205–208, 2012.

[77] D. M. Busiello, S. Suweis, J. Hidalgo, and A. Maritan, "Explorability and the origin of network sparsity in living systems," *Scientific Reports*, vol. 7, 2017.

[78] T. L. Hill, "Studies in irreversible thermodynamics iv. diagrammatic representation of steady state fluxes for unimolecular systems," *Journal of theoretical biology*, vol. 10, no. 3, pp. 442–459, 1966.

[79] D. M. Busiello, J. Hidalgo, and A. Maritan, "Entropy production in systems with random transition rates," *arXiv preprint arXiv:1708.02262*, 2017.

[80] T. Tomé and M. J. de Oliveira, "Entropy production in nonequilibrium systems at stationary states," *Physical review letters*, vol. 108, no. 2, p. 020601, 2012.

[81] C. Mencuccini and V. Silvestrini, "Fisica ii," *Elettromagnetismo-Ottica. Corso di fisica per le facoltà scientifiche corredato di esempi ed esercizui, Nuova edizione accresciuta, Liguori editore*, 1998.

[82] L. D. Landau and E. M. Lifshitz, *Statistical Physics: V. 5: Course of Theoretical Physics*. Pergamon press, 1969.

[83] A. Kleidon, Y. Malhi, and P. M. Cox, "Maximum entropy production in environmental and ecological systems," 2010.

[84] J. Garcia-Palacios, "Introduction to the theory of stochastic processes and brownian motion problems," *arXiv preprint cond-mat/0701242*, 2007.

[85] H. Risken, "Fokker-planck equation," in *The Fokker-Planck Equation*, pp. 63–95, Springer, 1996.

[86] S. Kullback and R. A. Leibler, "On information and sufficiency," *The annals of mathematical statistics*, vol. 22, no. 1, pp. 79–86, 1951.

[87] K. Kawaguchi and Y. Nakayama, "Fluctuation theorem for hidden entropy production," *Physical Review E*, vol. 88, no. 2, p. 022147, 2013.

[88] H.-M. Chun and J. D. Noh, "Hidden entropy production by fast variables," *Physical Review E*, vol. 91, no. 5, p. 052128, 2015.

[89] M. Esposito and J. M. Parrondo, "Stochastic thermodynamics of hidden pumps," *Physical Review E*, vol. 91, no. 5, p. 052114, 2015.

[90] D. A. Leigh, J. K. Wong, F. Dehez, and F. Zerbetto, "Unidirectional rotation in a mechanically interlocked molecular rotor," *Nature*, vol. 424, no. 6945, pp. 174–179, 2003.

[91] R. D. Astumian, "Adiabatic operation of a molecular machine," *Proceedings of the National Academy of Sciences*, vol. 104, no. 50, pp. 19715–19718, 2007.

[92] N. Sinitsyn and I. Nemenman, "The berry phase and the pump flux in stochastic chemical kinetics," *EPL (Europhysics Letters)*, vol. 77, no. 5, p. 58001, 2007.

[93] I. Sokolov, "A perturbation approach to transport in discrete ratchet systems," *Journal of Physics A: Mathematical and General*, vol. 32, no. 13, p. 2541, 1999.

[94] D. Mandal and C. Jarzynski, "A proof by graphical construction of the no-pumping theorem of stochastic pumps," *Journal of Statistical Mechanics: Theory and Experiment*, vol. 2011, no. 10, p. P10006, 2011.

[95] S. Rahav, J. Horowitz, and C. Jarzynski, "Directed flow in nonadiabatic stochastic pumps," *Physical review letters*, vol. 101, no. 14, p. 140602, 2008.

[96] C. Maes, K. Netočnỳ, and S. R. Thomas, "General no-go condition for stochastic pumping," *The Journal of chemical physics*, vol. 132, no. 23, p. 06B612, 2010.

[97] D. Mandal, "Unification and new extensions of the no-pumping theorems of stochastic pumps," *EPL (Europhysics Letters)*, vol. 108, no. 5, p. 50001, 2014.

[98] V. Chernyak and N. Sinitsyn, "Pumping restriction theorem for stochastic networks," *Physical review letters*, vol. 101, no. 16, p. 160601, 2008.

[99] S. Asban and S. Rahav, "No-pumping theorem for many particle stochastic pumps," *Physical review letters*, vol. 112, no. 5, p. 050601, 2014.

[100] J. Ren, V. Chernyak, and N. Sinitsyn, "Duality and fluctuation relations for statistics of currents on cyclic graphs," *Journal of Statistical Mechanics: Theory and Experiment*, vol. 2011, no. 05, p. P05011, 2011.

[101] S. Rahav, "Extracting work from stochastic pumps," *Journal of Statistical Mechanics: Theory and Experiment*, vol. 2011, no. 09, p. P09020, 2011.

[102] G. Floquet, "Sur les equations differentielles lineaires," *Ann. ENS [2]*, vol. 12, no. 1883, pp. 47–88, 1883.

[103] J. M. Horowitz and C. Jarzynski, "Exact formula for currents in strongly pumped diffusive systems," *Journal of Statistical Physics*, vol. 136, no. 5, pp. 917–925, 2009.

[104] W. Rudin, *Real and complex analysis*. Tata McGraw-Hill Education, 1987.

[105] Y.-Y. Liu, J.-J. Slotine, and A.-L. Barabási, "Controllability of complex networks," *Nature*, vol. 473, no. 7346, pp. 167–173, 2011.

[106] J. C. Nacher and T. Akutsu, "Structural controllability of unidirectional bipartite networks," *Scientific reports*, vol. 3, 2013.

[107] M. M. Babu, N. M. Luscombe, L. Aravind, M. Gerstein, and S. A. Teichmann, "Structure and evolution of transcriptional regulatory networks," *Current opinion in structural biology*, vol. 14, no. 3, pp. 283–291, 2004.

[108] R. Milo, S. Shen-Orr, S. Itzkovitz, N. Kashtan, D. Chklovskii, and U. Alon, "Network motifs: simple building blocks of complex networks," *Science*, vol. 298, no. 5594, pp. 824–827, 2002.

[109] J. R. Banavar, J. Damuth, A. Maritan, and A. Rinaldo, "Ontogenetic growth (communication arising): modelling universality and scaling," *Nature*, vol. 420, no. 6916, pp. 626–626, 2002.

[110] J. R. Banavar, A. Maritan, and A. Rinaldo, "Size and form in efficient transportation networks," *Nature*, vol. 399, no. 6732, pp. 130–132, 1999.

[111] G. B. West and J. H. Brown, "Life's universal scaling laws," *Physics today*, vol. 57, no. 9, pp. 36–43, 2004.

[112] H. Stanley, L. Amaral, P. Gopikrishnan, P. C. Ivanov, T. Keitt, and V. Plerou, "Scale invariance and universality: organizing principles in complex systems," *Physica A: Statistical Mechanics and its Applications*, vol. 281, no. 1, pp. 60–68, 2000.

[113] H. Stanley, L. Amaral, S. Buldyrev, A. Goldberger, S. Havlin, H. Leschhorn, P. Maass, H. Makse, C.-K. Peng, M. Salinger, *et al.*, "Scaling and universality in animate and inanimate systems," *Physica A: Statistical Mechanics and its Applications*, vol. 231, no. 1, pp. 20–48, 1996.

[114] J. Bascompte, P. Jordano, C. J. Melián, and J. M. Olesen, "The nested assembly of plant–animal mutualistic networks," *Proceedings of the National Academy of Sciences*, vol. 100, no. 16, pp. 9383–9387, 2003.

[115] S. Suweis, F. Simini, J. R. Banavar, and A. Maritan, "Emergence of structural and dynamical properties of ecological mutualistic networks," *Nature*, vol. 500, no. 7463, pp. 449–452, 2013.

[116] J. A. Dunne, R. J. Williams, and N. D. Martinez, "Food-web structure and network theory: the role of connectance and size," *Proceedings of the National Academy of Sciences*, vol. 99, no. 20, pp. 12917–12922, 2002.

[117] L. H. Fraser, J. Pither, A. Jentsch, M. Sternberg, M. Zobel, D. Askarizadeh, S. Bartha, C. Beierkuhnlein, J. A. Bennett, A. Bittel, *et al.*, "Worldwide evidence of a unimodal relationship between productivity and plant species richness," *Science*, vol. 349, no. 6245, pp. 302–305, 2015.

[118] M. Pascual and J. A. Dunne, *Ecological networks: linking structure to dynamics in food webs*. Oxford University Press, 2006.

[119] W. E. Kunin and K. J. Gaston, "The biology of rarity: patterns, causes and consequences," *Trends in Ecology & Evolution*, vol. 8, no. 8, pp. 298–301, 1993.

[120] D. Garlaschelli, G. Caldarelli, and L. Pietronero, "Universal scaling relations in food webs," *Nature*, vol. 423, no. 6936, pp. 165–168, 2003.

[121] S. Suweis, J. Grilli, J. R. Banavar, S. Allesina, and A. Maritan, "Effect of localization on the stability of mutualistic ecological networks," *Nature communications*, vol. 6, 2015.

[122] J. Grilli, M. Adorisio, S. Suweis, G. Barabás, J. R. Banavar, S. Allesina, and A. Maritan, "Feasibility and coexistence of large ecological communities," *Nature Communications*, vol. 8, 2017.

[123] B. Bollobás, *Modern graph theory*, vol. 184. Springer Science & Business Media, 2013.

[124] W. Bialek, *Biophysics: searching for principles*. Princeton University Press, 2012.

[125] L. Stone, "The google matrix controls the stability of structured ecological and biological networks," *Nature Communications*, vol. 7, 2016.

[126] G. Ackland and I. Gallagher, "Stabilization of large generalized Lotka-Volterra foodwebs by evolutionary feedback," *Physical review letters*, vol. 93, no. 15, p. 158701, 2004.

[127] K. Z. Coyte, J. Schluter, and K. R. Foster, "The ecology of the microbiome: Networks, competition, and stability," *Science*, vol. 350, no. 6261, pp. 663–666, 2015.

[128] A. Bashan, T. E. Gibson, J. Friedman, V. J. Carey, S. T. Weiss, E. L. Hohmann, and Y.-Y. Liu, "Universality of human microbial dynamics," *Nature*, vol. 534, no. 7606, pp. 259–262, 2016.

[129] M. Hirafuji, K. Tanaka, and S. Hagan, "Lotka-volterra machine for a general model of complex biological systems," in *Computer Aided Control System Design, 1999. Proceedings of the 1999 IEEE International Symposium on*, pp. 516–521, IEEE, 1999.

[130] J. A. Draghi, T. L. Parsons, G. P. Wagner, and J. B. Plotkin, "Mutational robustness can facilitate adaptation," *Nature*, vol. 463, no. 7279, pp. 353–355, 2010.

[131] A. Wagner, "The role of robustness in phenotypic adaptation and innovation," *Proceedings of the Royal Society of London B: Biological Sciences*, vol. 279, no. 1732, pp. 1249–1258, 2012.

[132] H. Schreier, Y. Soen, and N. Brenner, "Exploratory adaptation in large random networks," *arXiv preprint arXiv:1606.00101*, 2016.

[133] R. Pinho, E. Borenstein, and M. W. Feldman, "Most networks in wagner's model are cycling," *PloS one*, vol. 7, no. 4, p. e34285, 2012.

[134] D. R. Nelson, W. N. Adger, and K. Brown, "Adaptation to environmental change: contributions of a resilience framework," *Annual review of Environment and Resources*, vol. 32, no. 1, p. 395, 2007.

[135] S. Suweis, J. A. Carr, A. Maritan, A. Rinaldo, and P. DOdorico, "Resilience and reactivity of global food security," *Proceedings of the National Academy of Sciences*, vol. 112, no. 22, pp. 6902–6907, 2015.

[136] J.-F. Arnoldi, M. Loreau, and B. Haegeman, "Resilience, reactivity and variability: A mathematical comparison of ecological stability measures," *Journal of theoretical biology*, vol. 389, pp. 47–59, 2016.

[137] J. Gao, B. Barzel, and A.-L. Barabási, "Universal resilience patterns in complex networks," *Nature*, vol. 530, no. 7590, pp. 307–312, 2016.

[138] S. J. Russell, P. Norvig, J. F. Canny, J. M. Malik, and D. D. Edwards, *Artificial intelligence: a modern approach*, vol. 2. Prentice hall Upper Saddle River, 2003.

[139] S. Kirkpatrick, C. D. Gelatt, M. P. Vecchi, *et al.*, "Optimization by simmulated annealing," *science*, vol. 220, no. 4598, pp. 671–680, 1983.

[140] K. S. McCann, "The diversity–stability debate," *Nature*, vol. 405, no. 6783, pp. 228–233, 2000.

[141] S. Azaele, S. Suweis, J. Grilli, I. Volkov, J. R. Banavar, and A. Maritan, "Statistical mechanics of ecological systems: Neutral theory and beyond," *Reviews of Modern Physics*, vol. 88, no. 3, p. 035003, 2016.

[142] A. Vespignani, "Complex networks: The fragility of interdependency," *Nature*, vol. 464, no. 7291, pp. 984–985, 2010.

[143] N. Blagus, L. Šubelj, and M. Bajec, "Self-similar scaling of density in complex real-world networks," *Physica A: Statistical Mechanics and its Applications*, vol. 391, no. 8, pp. 2794–2802, 2012.

[144] Y. LeCun, Y. Bengio, and G. Hinton, "Deep learning," *Nature*, vol. 521, no. 7553, pp. 436–444, 2015.

[145] I. Goodfellow, Y. Bengio, and A. Courville, *Deep Learning*. MIT Press, 2016.

[146] N. Kashtan and U. Alon, "Spontaneous evolution of modularity and network motifs," *Proceedings of the National Academy of Sciences of the United States of America*, vol. 102, no. 39, pp. 13773–13778, 2005.

[147] C. Baldassi, C. Borgs, J. T. Chayes, A. Ingrosso, C. Lucibello, L. Saglietti, and R. Zecchina, "Unreasonable effectiveness of learning neural networks: From accessible states and robust ensembles to basic algorithmic schemes," *Proceedings of the National Academy of Sciences*, vol. 113, no. 48, pp. E7655–E7662, 2016.

[148] Y.-Y. Liu, J.-J. Slotine, and A.-L. Barabási, "Controllability of complex networks," *Nature*, vol. 473, no. 7346, pp. 167–173, 2011.

[149] A. Joern, "Feeding patterns in grasshoppers (orthoptera: Acrididae): factors influencing diet specialization," *Oecologia*, vol. 38, no. 3, pp. 325–347, 1979.

[150] S. R. Leather, "Feeding specialisation and host distribution of british and finnish prunus feeding macrolepidoptera," *Oikos*, pp. 40–48, 1991.

[151] T. Leong and J. Holmest, "Communities of metazoan parasites in open water fishes of cold lake, alberta," *Journal of Fish Biology*, vol. 18, no. 6, pp. 693–713, 1981.

[152] A. O. Dechtiar, "Parasites of fish from lake of the woods, ontario," *Journal of the Fisheries Board of Canada*, vol. 29, no. 3, pp. 275–283, 1972.

[153] R. V. Bangham, "Studies on fish parasites of lake huron and manitoulin island," *American Midland Naturalist*, pp. 184–194, 1955.

[154] V. Chinniah and W. Threlfall, "Metazoan arasites of fish from the smallwood reservoir, labrador, canada," *Journal of Fish Biology*, vol. 13, no. 2, pp. 203–213, 1978.

[155] H. P. Arai and D. R. Mudry, "Protozoan and metazoan parasites of fishes from the headwaters of the parsnip and mcgregor rivers, british columbia: a study of possible parasite transfaunations," *Canadian Journal of Fisheries and Aquatic Sciences*, vol. 40, no. 10, pp. 1676–1684, 1983.

[156] A. Roberts, "The stability of a feasible random ecosystem," *Nature*, vol. 251, pp. 607–608, 1974.

[157] F. Berezin, *The method of second quantization*, vol. 24. Elsevier, 2012.

[158] F. L. Tobin, V. Damian-Iordache, and L. D. Greller, "Towards the reconstruction of gene regulatory networks," in *Technical Proc. 1999 International Conference on Modeling and Simulation of Microsystems*, Citeseer, 1999.

[159] I. M. Bomze, "Lotka-volterra equation and replicator dynamics: a two-dimensional classification," *Biological cybernetics*, vol. 48, no. 3, pp. 201–211, 1983.

[160] V. Bucci and J. B. Xavier, "Towards predictive models of the human gut microbiome," *Journal of molecular biology*, vol. 426, no. 23, pp. 3907–3916, 2014.